MODULATION OF IN VIVO NEURAL NETWORK ACTIVITY WITH ELECTROCHEMICALLY CONTROLLED DELIVERY OF NEUROACTIVE MOLECULES

by

Zhanhong Du

Bachelor of Science, University of Science and Technology of China, 2009

Submitted to the Graduate Faculty of

Swanson School of Engineering in partial fulfillment

of the requirements for the degree of

Doctor of Philosophy

University of Pittsburgh

2015

UNIVERSITY OF PITTSBURGH

SWANSON SCHOOL OF ENGINEERING

This dissertation was presented

by

Zhanhong Du

It was defended on

October 22nd, 2015

and approved by

Daniel J. Simons, PhD., Professor, Department of Neurobiology

Aaron P. Batista, PhD., Associate Professor, Department of Bioengineering

Guo-Qiang Bi, PhD., Professor, School of Life Sciences, University of Science and Technology of China

Douglas J. Weber, PhD., Associate Professor, Department of Physical Medicine and Rehabilitation and Bioengineering

Dissertation Director: Xinyan Tracy Cui, PhD., Professor, Department of Bioengineering

MODULATION OF IN VIVO NEURAL NETWORK ACTIVITY WITH ELECTROCHEMICALLY CONTROLLED DELIVERY OF NEUROACTIVE MOLECULES

Zhanhong Du, PhD.

University of Pittsburgh, 2015

Neural interface technologies with implantable microelectrode arrays hold great promise for treating neural injuries or disorders. On neural electrode surfaces, conducting polymers can be electropolymerization with negatively charged molecules incorporated. When the polymer is reduced with negative current, dopant molecules are released from the polymer. This feature can be utilized to deliver neural transmitters and modulators from the electrodes to alter neural network activity. Previously, release of CNQX (6-cyano-7-nitroquinoxaline-2,3-dione), an AMPA (2-amino-3-(5-methyl-3-oxo-1,2- oxazol-4-yl)propanoic acid) receptor antagonist in hippocampal neuron culture effectively suppressed local neural activity in a transient manner. In this study, we further advance this technology by characterizing the drug loading and release capacity from microelectrodes, expanding the range of candidate dopants, and demonstrating *in vivo* effectiveness in rat somatosensory (S1) barrel cortex.

Firstly, to quantify the concentration of released drug, fluorescent model molecule was used and quantitatively assessed in a real time imaging system. Stimulation amplitude was varied to determine the amount of released drug from microelectrodes. Secondly, only negatively charged drugs have been effectively released in the past. In this study, zwitterionic transmitter γ-Aminobutyric acid (GABA) was successfully delivered with the technique, greatly expanding the

applicable range for the technique. Finally, we used evoked response from barrel cortex to evaluate the release of DNQX (6,7-dinitroquinoxaline-2,3-dione), an analog of CNQX. The neural activity of barrel cortex reliably represents sensory stimuli from whiskers, hence provides an excellent *in vivo* network model for evaluating our neurochemical release system. Neural activity from multi-whisker stimulation was immediately and locally suppressed by released DNQX for one to six seconds, demonstrating the high spatial-temporal resolution of the technique. Furthermore, weaker activities were nearly abolished by released DNQX whilst stronger activities were less influenced, because the strong over-saturated neural input can only be partially antagonized. The system demonstrates successful modulation of neural network activity in a highly controllable manner. With the ease of being incorporated in existing neural implants without increasing the volume or complexity, this technology may find use in a wide range of neuroscience studies and potentially therapeutic devices.

TABLE OF CONTENTS

LIST OF FIGURES

PREFACE

This dissertation would not have been possible without the guidance, encouragement, and support of many individuals. A huge acknowledgement goes to my advisor, Dr. X. Tracy Cui, who supported me in countless ways during the past years. Throughout the years, her patience and encouragement have been the most important factor to help me through my difficult times of graduate school. The lessons she taught me will not only help me in my career of becoming a researcher, but will also serve me in other numerous ways, in which I found extremely helpful is the ability to talk and collaborate with many different researchers in any field. After accepting me into her laboratory six years ago, she has been the unlimited source of knowledge and support. She taught me how to establish an academic mindset and be always thinking ahead of and be prepared for the future challenges. All the NTE lab members, past and present, have helped me throughout the graduate school. Prof. Xiliang Luo provided many in-depth discussions to turn my original knowledge of chemistry into preparations for utilizing conducting polymer materials on neural electrodes. Without the guidance he gave, none of this work would have been possible. Drs. Bill Stauffer and Cassandra Weaver's work on modulating *in vitro* neural network activity have been the foundation of this study. The continuous help from Prof. Dan Simons' lab and Dr. Erdrin Azemi was my first experience to practice *in vivo* neurophysiology. Trevor Sleight helped me establish all the earliest recording and stimulation systems as well as neural data analysis techniques. Dr. Takashi Kozai has always demonstrated

great knowledge and patience when I need helpful discussion with literatures, experiments or career advices. I have also learned a great deal from Dr. Christi Kolarcik about immunohistochemistry; from Dr. Mitch Taylor about analytical chemistry and from Dr. Bin Cao about materials synthesis and functionality. I want to thank Ms. Xia Li helped me a lot with animal and immunohistochemistry experiments, and Dr. Yang Shen for the helpful discussions about nanoparticles and cell culture. In the course of graduate school, I learned many important lessons about materials, electrochemistry and analytical techniques together with Noah Snyder and Kasey Catt. James Eles was always helping by listening and discussing about my frustrations with experiments, which was very important for the last few years of my graduate school. Me, Noah, Kasey and James also shared many great experience and cherishable memories together working on the translation project "Oxi-dent" in 2015 Randall's Family Big Idea Competition together with Andy Glowacki from ChemE Department. I also got a tremendous amount of help from a number of great undergraduate students who were willing to help me collect data for several projects: Sanjeev Khanna, Ali Aneizi, Andrew Macgregor, Gabriel Szczepanek and Livia Cabral. I would also like to thank all the committee members for helping me through different phases of my study to form a complete work on this project: Dr. Guo-Qiang Bi, for first inspiring me with all the important neuroscience lessons and ideas ever since I was an undergraduate student at USTC. He is always a great mentor who not only helps me look for the best professors in different fields and let me use his lab instruments, but also tremendously helped me during my biggest life transition from an undergraduate in China to a graduate student in the United States; Dr. Dan Simons for helping me learn all the important techniques and knowledge about barrel cortex and for the numerous times of discussion when I'm uncertain about interpreting any *in vivo* electrophysiology or other result; Dr. Doug Weber for helping me with the Multi-Electrode

Array recording, simultaneously recording and stimulation as well as the knowledge for analyzing the data while letting me borrow his laboratory instruments; Dr. Aaron Batista for guiding me during my graduate studies, helping me with presentation and writing skills and for all the exciting new knowledge about brain computer interface and neural signal processing techniques, as well as the equipment I borrowed from his lab.

I would like to thank the Department of Bioengineering at the University of Pittsburgh for providing such a great training program with so much research diversity and providing me the resources and opportunities to realize my research plans. The Center for the Neural Basis of Cognition for offering me financial supports and opportunity to interact with such a great neuroscience community around Pittsburgh area. Center for Biological Imaging for the valuable instruments, resources, trainings and experiences. McGowan Institute of Regenerative Medicine for the opportunity to learn from so many different Bioengineering related medical fields.

I want to thank all my friends for being there during my graduate school. Thank you for the support and encouragement in my difficult times. And I will always cherish the good memories we had together.

I want to particularly thank my parents, Junkai Du and Fenxia He, who have always been the source of unlimited, unconditioned love, support and encouragement ever since I was born. I could never thank my parents enough for supporting my ideas of pursuing a PhD in neural engineering field abroad. Hoping to make you feel proud of me has always been one of my biggest motivations of learning the best Bioengineering knowledge to help the others.

1.0 INTRODUCTION

The application of implantable microelectrode arrays to directly interface the neural tissue and restore lost functions or treat neural disorders have demonstrated great promises in recent years. Brain computer interface technology to enable the movement computer controlled devices with the intention of decoded neural signal is a broadly known successful application of the *in vivo* MEA implantations. Another important application of MEAs are the simultaneous recording and stimulation of functional neural networks to understand the spatial temporal pattern of a large population of neurons. Both the neuroscience research and clinical application of MEA benefit from the capability to modulate the neural activity of the recorded neural network to dissect the functions of various network components in a complex behavior. However, the manufacture of MEAs requires highly delicate and complex micro fabrication techniques and the addition of fluidic channels or fiber optics for the neural modulation often tremendously increase the fabrication difficulty and the failure rate during the process. The utilization of electrochemically synthesized conducting polymers can bypass these difficulties by directly modify the recording or stimulation electrode and delivery neuroactive molecules to the local neural network without impeding the extracellular recording of MEAs.

1.1 NEURAL RECORDING AND STIMULATION ON MICROELECTRODE ARRAY

Multi-electrode array (MEA) provide the unique benefit of simultaneous recording and stimulation from a large number of neurons. MEAs for both *in vitro* and *in vivo* applications have been developed for interfacing with neural networks. The *in vitro* MEAs are developed for the purpose of high throughput test bed for drug selection[1] or the understanding of theories about spatial temporal firing patterns[2] of neural networks, due to the relative low cost and high channel count to utilize this technology. In comparison, *in vivo* MEAs are often used for decoding intention of neural network activity[3] or modulate disease affected abnormal neural firing patterns[4] because *in vivo* MEAs can directly interface with neural networks underlying various cognitive process.

1.1.1 *In vitro* MEA

The advantage of *in vivo* MEA implantation lies in the direct investigation of neural network in an intact animal with the context of neural functionality. But the technique is restricted to relatively small number of trials due to multiple reasons, including the difficulty in surgically implanting the MEA[5, 6], the chronic failure of the device[7, 8], the highly complex process to manufacture *in vivo* MEA in large quantities[9-11] lead to high cost of the device with limited channel numbers. The *in vitro* preparation serves as a simplified alternative to study the property of neurons and isolated neural networks by electrophysiology techniques. The earliest work on isolated *Loligo* giant axons [12-16] lay the foundation of our understanding towards the membrane dynamics mechanism of action potentials as well as the active channel conductance

change during neural signaling process. The study of isolated neurons are ideal for basic neural electrophysiology research because the simplified system is essentially free from random variabilities from unknown source during complex *in vivo* neural processes. Additionally, the traditional single cell recording technologies such as patch clamp are limited to a very small number of neurons to be investigated simultaneously, but the *in vitro* MEA allow high throughput recording of neurons thus benefit drug selection and toxicity study as well as possible big data analysis of neural properties and classifications. First *in vitro* MEA application [17]instantly increased the number of simultaneously recordable neurons and allow the study of spatial temporal neural dynamics generated by a simplified neural network. The use of MEAs have also expanded to the understanding of generation mechanisms underlying spontaneous neural network firing patterns[2] as well as electrical stimulation parameter optimization for direct and highly efficient modulation of neural activities [18]. Another intriguing application of *in vitro* MEAs is the generation of a simplified brain mimicking neural network culture for controlling external device based on specific input information transduced by electrically stimulate the neural networks in spatial temporal patterns [19-21]. These works are still preliminary but create an exciting outlook for the future use of neural technologies.

1.1.2 *In vivo* MEA

One of the most promising use of *in vivo* MEA for brain computer interface technology is the control of external devices with intentions decoded from motor cortex recordings [22-24]. The neural signal extracted from motor cortex allows the direct control of robotic arms[25-27] or virtual cursor[28, 29]. The application of this technology will not only benefit our understanding in motor planning process, but also restore the lost motor function of patients with full or partial

paralysis [30-32]. The device to interface with neural tissue directly and obtain useful neural signal for decoding brain intention is the implantable multi-electrode array [22, 31, 33]. Efforts have also been made to create less invasive recording techniques with electroencephalogram (EEG) [29]or electrocorticography (ECoG)[34] recording capabilities. To decode precise information for better controllability over the device, high density and high channel count MEAs are usually preferred.

Many types of micro wire arrays and silicon based micro fabricated arrays have been developed as *in vivo* MEAs. Micro fabrication technology can produce MEAs with very high reproducibility and precisely controlled electrode distributions, while the traditional micro wire arrays require less complicated device and procedures during the manufacture yet capable of providing good signals [8, 35]. Among silicon based microelectrode arrays, Both the tip recording Utah arrays[36] and the shank recording Michigan probes[37, 38] have demonstrated high quality single unit recording capabilities.

A major hindrance to the application of BCI device for treatment of any paralysis patient is the chronic degradation of unit recording performance [8, 22, 36, 39, 40]. Various mechanisms have been linked to the device failure including both biological[41, 42] and abiological source such as mechanical[43] or material[39].

With the complex fabrication process and difficulties in recording meaningful neural signals of implantable MEAs, it is critical to develop neural modulation techniques with simplicity to adapt without interfering with neural recording function kept in mind. Because real time modulation of recorded neurons one of the most important techniques to successfully study of neural network functions underlying various neural network firing mechanisms[44-47].

1.2 LOCAL PHARMACOLOGICAL INTERVENTIONS FOR NEUROSCIENCE RESAERCHER

1.2.1 Benefit of local neural network modulation

Bi-direction BCI with capability to adjust motor control by sensory feedback input[48] or the close-loop neural stimulation devices[49, 50] for precise treatment of epilepsy have been of interest due to the capability to optimize device output based on the real time information from the modulation target. Besides the translational studies for restoration of lost neural function or treatment of neural disorders, simultaneous modulation of recorded neural networks also benefit the understanding of various receptors and subpopulation of neurons underlying particular neural activities[51-53]. The introduction of dopamine, 5-HT and GABA receptor modulation by iontophoresis[45, 54-56] and microinjection[57] helped elucidate the involvement of these receptors in the working memory process. Antagonizing different glutamate receptor species during the rat somatosensory processing with iontophoresis also helped understanding the contribution of various glutamate receptors during a whisker sensation event [47].

1.2.2 Local neural modulation techniques and limitations

Conventional neural modulation techniques include systemic perfusion [58] or localized cannula injection in a local area [57, 59]. However many study requires the use of pharmacological

perturbation to neural networks with high spatial and temporal resolutions beyond the limitation of these methods [53, 60-63]. Techniques such as pressurized injection [64-66], micro iontophoresis [47, 54, 55, 67], and microfluidics devices [68, 69]have been developed for more precisely controllable delivery of chemicals to local neural networks. The previous two techniques require additional positioning of fluidic channels without interfering with the fragile implantable MEA, and the microfluidics device remarkably increase the difficulty of device fabrication due to additional microfabrication steps. Furthermore all these local neural modulation techniques requires additional pump, valve, fluidic channels, and they often suffer from drug leakage or tip clogging due to the formation of glial scar around the foreign device. The development of optogenetics provide the capability of modulating a subpopulation of genetically modified neurons with high temporal resolution[70-74], and the devices implemented with optogenetics technology have demonstrated the capability to simultaneously record neural activity and optically control the firing of neural networks[75, 76]. However the device also yield a bulky size and require complex fabrication process due to the incorporation of fiber optics next to the recording microelectrode array. Additionally, the genetic modification of neurons for clinical applications require very cautious considerations thus add further steps before the product can be utilized, and the use of optical manipulation requires additional light generating device as well as fiber optics.

1.3 CONDUCTIONG POLYMRES

1.3.1 Synthesis and properties of conducting polymers

The first development of conducting polymer occurred in mid-19th century when Henry Letheby first polymerized polyaniline and conducted research on the unique properties[77]. Conducting polymer had since found use in many fields including electronics[78], energy storage[79], sensors [80-82], biointerfacing [83] and tissue engineering [84]. Because conducting polymers are intrinsically conductive for both electrons and chemicals, they resembles the properties of neural tissue to a certain extent, because neural signaling involves the process of conversion between electrical and chemical signals [85-87]. The conducting polymers Polypyrrole (PPy) and poly(3,4-ethylenedioxythiophene) (PEDOT) are among the most commonly utilized conducting polymers for neural interface[88-93]. PPy and PEDOT are the main material for this thesis due to their unique beneficial properties for improving neural interface and delivery neurochemicals [93-96]. The polymerization process of PPy with incorporated dopant molecule A is illustrated in Fig 1, in which the polymer is deposited onto electrode surface with 0.8 V oxidation potential.

The synthesis of conducting polymer can be realized by electrochemical deposition[92] as illustrated in Fig. 1-1, or can be achieved via chemical reactions such as free radical polymerization[97]. The polymer generated by potentiostat or galvanostat electrochemical deposition can only form on conductive surface while chemical synthesis can generate conducting polymer on any surface[98]. The chemically synthesized conducting polymer is best suitable for scaling up product in large quantities, but the homogeneity of the internal structure is usually hard to control and requires careful optimization[99]. In contrast the electrochemically

synthesized conducting polymer usually form a thin layer of film and modulate the surface property of the electrodes[89]. The electrochemically synthesized conducting polymer film [96, 100] lays out the foundation of the drug delivery study in this thesis.

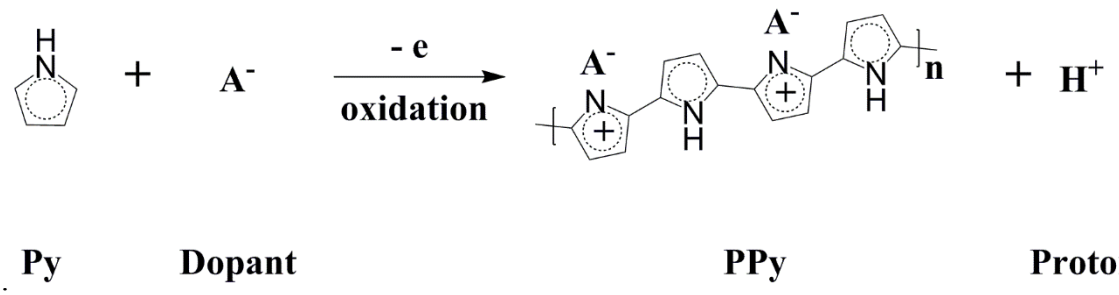

Figure 1-1 Electrochemical synthesis of PPy with Chronoamperometry technique. The solution of Py monomer can form conducting polymer on working electrode of electrochemical cell with oxidation potential around 0.8 V. The conjugated polymer chain maintain positive charged and the negatively charged ions A in the solution was electrostatically incorporated into the polymer. The synthesis of PPy result in pH change due to the formation of protons.

1.3.2 Redox property of conducting polymers

One unique property of the conducting polymer is the capability to switch the redox state after polymerization. As illustrated in Fig. 1-1. Conducting polymer exist in oxidized state after the electrochemical synthesis, with positive charges on the backbone of the polymer chain. The oxidized state is essential for the conductivity of the polymer, meanwhile small charged anion dopant A^- is electrostatically bond to the backbone of the polymer, restricting the diffusion of these dopants via any contact with external environment. Once sufficient reduction potential is applied to the polymer matrix, the polymer can be reduced to lose the positive charge on the

backbone. The equivalent effect of this reduction reaction towards the mobile anion dopant A^- is an electrostatic force to push the molecule A^- out of the polymer film, because the polymer exist in neutral state[101]. This intriguing feature of conducting polymer have been utilized to release bioactive molecules in the past. The delivery of Dexamethasone was one of the most popular applications due to the appealing idea of suppressing the inflammatory response to the neural electrode in a precise manner may improve the longevity of the high quality neural recording on MEAs[102, 103]. Releasing neurotrophic proteins to support the survival of neurons and possibly restore damaged axonal connections also received significant amount of investigation [104-107]. An interesting idea of molecularly imprinted conductive polymers with the capability of delivering an intrinsically exist neurotransmitter molecule and subsequently allow the polymer to be replenished by this specific neurotransmitter in the surrounding extracellular space also brings about the appealing possibility of unlimited number of drug release with single implanted device[108].

1.3.3 Use of conducting polymer in neural engineering

One approach for improving the performance of implanted MEAs by altering the surface properties of the microelectrodes is the electrochemical deposition of conducting polymers[109]. The conducting polymer can benefit the MEAs by decrease the electrical impedance [109, 110], promote specific cell attachment [88, 90, 111], or release anti-inflammatory drug like Dexamethasone [102, 112]. The modification of microelectrode with the conducting polymer coating can drastically increase the surface roughness and lead to large effective surface area for charge transfer and molecular adhesion [22]. Recently, developing ultra-small MEAs have gained wide popularity due to the beneficial properties for alleviating tissue response caused by

the implant [86, 113, 114]. The smaller penetration profile of such devices also remarkably reduce the probability of severing the axonal connections of the target neural population thus preserve the quality of the extracellular signal even for high density recordings [115]. The surface impedance, however, were noticeably increased by the reduction of Geometric Surface Area (GSA) of these devices, and the impairment to impedance cannot be corrected by any electrode conductor material itself. Deposition of metal oxide (e.g. IrO2) or fuzzy metal (e.g. Pt-Black) have been investigated as possible solution, but the they pose the threat of releasing heavy metal ions or even micro particles that will harm the implanted tissue [33], especially during mechanical agitation or electrical stimulation. The electrochemically synthesized conducting polymer PEDOT is known for good conductivity, tunable morphology as well as outstanding biocompatibility, thus is ideal for lowering the impedance of such small GSA electrodes [86, 114]. Among the widely investigated PEDOT polymers for improving the performance of neural implants, polystyrenesulfonate (PSS) doped PEDOT demonstrated high performance for chronic neural recordings [116]. The benefit of incorporating large molecule dopants relies on the immobility of such molecules. With the multi-site electrostatic bond between PEDOT and PSS, the polymers remains in very stable structure for long period. Functionalized CNTs with large amount of negative net charge on the surface have demonstrated beneficial recording performance, extending the success of PEDOT to even larger increase of surface area by the morphology with nano features[95]. These benefits can be replicated with polymerizing PEDOT with small ionic molecules in a highly conducting ionic liquid environment as well. The ultrahigh surface area with hollow structures allow the high mobility small anion dopants to be quickly exchanged with any PBS or saline solutions thus pose no threat to the biocompatibility of the polymer[110].

1.3.4 Conducting polymer and functional carbon nanomaterials

Carbon nanotubes[117] and graphene[118] materials have been widely investigated for various applications including electronics, optics and medical engineering due to their unique mechanical, electrical and optical properties. Graphene is known to be the thinnest material composed of single sheet of tightly packed carbon atoms in honeycomb structure. The large two dimensional structure of graphene create unique physical properties not known to any other material. Carbon nanotubes (CNTs) are long wire structure of carbon items that can be viewed as rolled up graphene in single- or multi-layer structure[119]. CNTs are broadly known for the outstanding mechanical strength, electrical conductivity as well as chemical stability[120]. The application of CNTs have been recently expanded into the neural interface field[121]. The incorporation of CNTs into conducting polymers PPy [122-125] and PEDOT [94, 95, 126-128] have been demonstrated in previous literature and shown improved polymer properties such as electrical conductivity and stability. The CNTs can be utilized in neural engineering field for improve neural stimulation [94], recording[95], stimulation neurite outgrowth[129], promote stem cell neuron differentiation [130] and serve as substrate for neuronal attachment and growth[131, 132]. One of the most intriguing applications of CNTs as blending material during conducting polymer synthesis is the capability of incorporating high concentration drug molecules in the inner cavities as serve as a reservoir for replenishing polymers during controlled drug delivery, as demonstrated in Fig. 1-2.

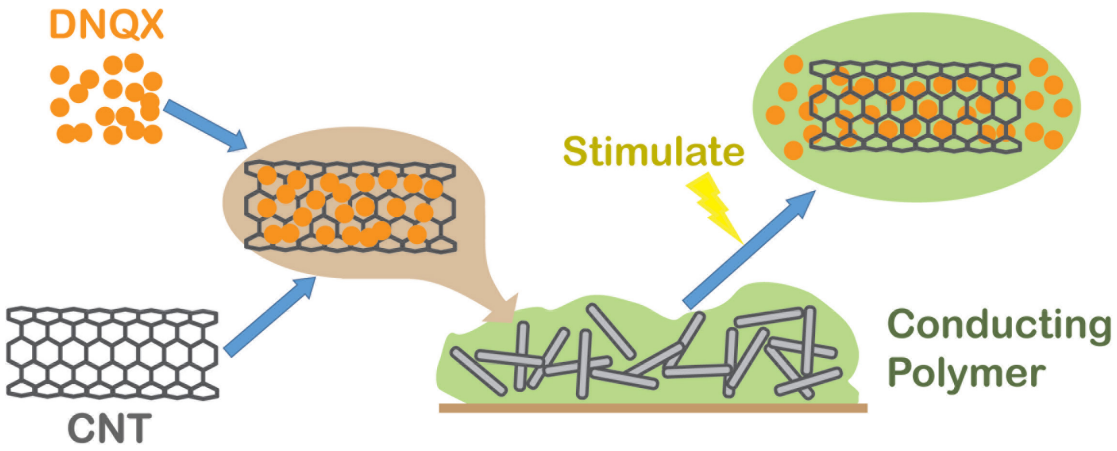

Figure 1-2 Electrochemical synthesis of PPy conducting polymer with Chronoamperometry technique. High concentration drug solution is first loaded into the inner cavity of functionalized multi-walled CNTs. The CNTs are then incorporated into the conducting polymer matrix as dopant during electrochemical polymerization. The drug molecules in the CNTs are sealed by the polymer to prevent leakage. Once the redox state of the conducting polymer is changed to delivery drug from the polymer, the drug molecules in the conducting CNTs immediately diffuse out and replenish the polymer for further drug delivery trials.

1.4 EXTRACELLULAR STIMULATION AND BARREL CORTEX RECORDING

Deep brain stimulation (DBS) for the treatment of Parkinson's disease[133-136], epilepsy[50, 137, 138], essential tremor[139, 140] and dystonia[141, 142] have been extensively investigated due to the therapeutic potential and the effectiveness of the technique in treating patients. More recently, DBS have also demonstrated promising treatment effect for emotional disorders like depression[143, 144], obsessive compulsive disorder (OCD)[145, 146] and anxiety. The electrical stimulation depolarizes the membrane potential of adjacent neurons to cause generation of action potentials[33]. Recent *in vivo* two photon recording of large

population of neurons distributed in a broad spatial range also revealed the activated neurons are distributed sparsely [147]. This is possibly due to the activation of axons traveling near the stimulation electrodes are activated preferentially by the stimulation[148]. Theoretical model studies have revealed the importance of capacitive current in activating neurons[149]. So we chose prolonged cosine waveform with very low rising slope for the trigger of drug release to minimize directly generated action potentials. The simultaneous recording and stimulation or sequential switch between recording and stimulation also require delicate electrical circuit as well as algorithms to reduce the artifact and noise during switch as well as ensure the safety of recording [18, 150]. In this study, a simultaneous recording and stimulation paradigm with completely different grounding skull screws to isolate the stimulation and recording circuits was utilized to deliver the drug while recording. The artefact evoked by drug release trigger was in reasonable range without impacting the neural recording performance after the stimulation is terminated.

The Layer IV of barrel cortex is the input layer of neural information from the thalamus to the cortex for further processing[151]. Direct mechanical stimulation of facial whiskers of rats generated reliable neural response in specific barrels that topographically represent the facial whiskers [152, 153]. Iontophoresis studies with NMDA and AMPA receptor blockers in the barrel cortex successfully elucidate the various contributions of NMDA and AMPA receptor to the different temporal component of the barrel cortex response [47]. However, due to the limitation of iontophoresis device on single channel or few channel recording at same location. The multi-channel simultaneous recording and pharmacological intervention with electrochemically controlled drug release may provide new insight to the neural network dynamics affected by different receptor agonist or antagonists.

1.5 OUTLINE OF THESIS

Chapter one of the thesis focus on the quantitative analysis of drug release from PPy/CNT conducting polymer matrix with a double layer polymer preparation on PEDOT/CNT coating. Previous work had demonstrated the use of electrochemically released AMPA receptor antagonist CNQX to precisely modulate neural network activity pattern in hippocampal neuron culture [154]. But because of the extreme difficulty to directly quantify the target molecule, CNQX, or its analog molecule DNQX, the precise concentration of released drug molecule was mimicked by fluorescein molecule and the dynamics of fluorescein release was carefully characterized. The fluorescent microscopy technique provide the real time diffusion profile and the semi-quantitative information about the detailed trend of fluorescein release over 90 trials. With carefully selected drug release trigger parameters, the concentration of delivered fluorescein can be fitted by a two term exponential decay function. The further spectrometry measurement of fluorescein and DNQX release directly from the polymer film on a novel microelectrode array was combined with the model prediction of fluorescein concentration and yield a precise quantitative model of DNQX concentration from the conducting polymer matrix.

Chapter two expand the scope of releasable drug molecules to another important class of neurotransmitters, zwitterionic charged molecules like GABA. GABA not only serve as the primary inhibitory neurotransmitter in the brain, but also plays critical role in neuron development. And GABA neuron abnormality underlies various neural network mechanisms of disorders such as schizophrenia [155, 156]. Electrochemically synthesized PEDOT/CNT/GABA film successfully delivered GABA molecules upon receiving drug release triggers and the released GABA molecule maintained its bioactivity for inhibiting neural networks. The incorporation of GABA molecules on the surface of PEDOT polymer not only remarkably

improved the survival of neural stem cells and differentiation ratio into neurons, but also facilitated the neuronal survival and neurite extension on the polymer. The precise concentration of released GABA molecule from microelectrodes was quantified with custom build microelectrode arrays. Quantification result indicate the GABA doped PEDOT film can spontaneously leach out GABA to possibly facilitate neural development and can be triggered to release higher concentration of GABA upon demand.

Chapter three extended the application of electrochemically controlled release of DNQX to the *in vivo* neural network in layer IV of barrel cortex. Simultaneous application of electrical trigger signal and collection of neural recording on 4 x 4 acute Michigan probe was conducted with carefully designed experiment paradigm. Barrel cortex neural activity was topographically evoked with air puff to facial whisker with high precision and reliability [157, 158]. The application of DNQX molecule abolished the neural network firing for one to six seconds while the control triggers without doped DNQX did not alter the neural network activity. The electrochemically controlled release can modulate barrel cortex activity for more than 25 trials and the spatial extent of the drug effect is about 400 μm radius according to a well fit second order polynomial function of drug effectiveness index.

2.0 QUANTIFICATION OF ELECTROCHEMICALLY CONTROLLED DELIVERY OF NEUROCHEMICALS FROM MICROELECTRODE USING A FLUORESCEIN RELEASE MODEL

2.1 ABSTRACT

Conducting polymers can be formed electrochemically on neural microelectrodes with negatively charged molecules incorporated in the process. When reductive potential is applied onto the conducting polymer film, the polymer backbone loses some positive charge but still maintain conductivity while dopant molecules can be precisely released from the film. The electrical-chemical coupling of signal on microelectrode mimic the synaptic transmission of neurons, during which action potentials trigger the release of neurochemicals in a precise manner. Conducting polymers on microelectrode arrays can delivery neural transmitters and modulators for neural activity modulation which can be simultaneously recorded with co-existing neurophysiology recording channels. To elucidate the application conditions of this novel drug delivery technique, concentration and effective range of released drug molecule is mimicked by fluorescein and quantitatively assessed in a real time imaging system. Drug delivery parameters were carefully evaluated to precisely determine the amount of released drug from neural electrodes. AMPA receptor antagonist DNQX (6,7-dinitroquinoxaline-2,3-dione) was selected to represent a class of negatively charged neuromolecules due to its direct impact

on the fast excitatory neural transmission. This system demonstrates a possible foundation for feedback suppression of neural network activity in a localized manner beyond traditional fluidic and neural stimulation techniques. With the ease of being incorporated in existing neural electrode arrays and the controllable spatial and temporal dynamics pattern of drug diffusion, this technology may find use in a wide range of research and therapeutic devices.

2.2 INTRODUCTION

Fundamental brain functions such as cognition, learning, and memory are executed by activities of many neurons that form intricate circuits [159, 160]. Multielectrode Arrays (MEAs) with the capability of recording from ensembles of neurons *in vivo* or *in vitro* have been developed to extract information from such neural activity [37, 161]. To aid the study of neural networks and examine the response of networks to external perturbations, neural modulation are often necessary to change the networks. The ideal bi-directional neural interface systems require highly localized precise neural modulation[48]. Such attempts include electrical stimulation[162], drug infusion cannulas[57], iontophoresis[54] and more recently, optogenetics[74]. However, limitations are observed with each class of neural modulation techniques including selectivity, types and precision of neural modulation. And in some cases, the ongoing neural modulation treatments abolish the capability of MEAs to record from targeted neural tissue in real time.

To solve some of these problems, a technique has been developed by Simon et al. in which the conducting polymer PEDOT doped with polystyrene sulfonate (PSS) has been

fabricated into a micro device that functions as an ion pump[163, 164]. The device has demonstrated controllability to precisely delivery neurochemicals for certain applications. Unfortunately, the device requires complicated fabrication and is not capable of neural recording or stimulation. Thus, it is very difficult to integrate the device onto *in vivo* MEAs.

The redox property of conducting polymers is utilized in this work as the basis of our method development. Conducting polymers can be electrochemically polymerized directly on surface of neural micro electrodes [88]. Negatively charged dopants can be reliably incorporated into the polymer matrix through electrostatic force because the synthesized conducting polymers possesses positive charges[125]. These dopant molecules can be immobile or releasable to encourage specific cell/surface interaction or regulate the local biochemical environment [88, 89, 165-167]. Only when negative current is injected into the conducting polymer matrix, the positively charged polymer backbone is reduced and less positive charges remain on polymer backbone to maintain the dopant molecules, thus the dopants are released when the redox reaction is triggered by electrical stimuli[101]. This polymer based electrochemical release of drug molecules have been utilized in several prototypic systems in which chemical agents such as anionic salicylate, adenosine triphosphate (ATP), 2-ethylhexylphosphate (EHP), and naproxen have been incorporated into different polymers and subsequently released in a controlled fashion [168-171]. *In vitro* utilization of this technique on releasing neuro-chemical CNQX (6-cyano-7-nitroquinoxaline-2,3-dione), an AMPA (2-amino-3-(5-methyl-3-oxo-1,2- oxazol-4-yl)propanoic acid) receptor antagonist from Polypyrrole (PPy) has been demonstrated to suppress action potential generation in hippocampal neural cultures in a localized and transient manner [154]. In this work, 6,7-dinitroquinoxaline-2,3-dione (DNQX) molecule, a very similar chemical analog of CNQX to antagonize AMPA receptor, was utilized as the bioactive drug molecule to release.

However, the loading and release capacity of DNQX releasing PPy coating is limited. One important feature of CNQX or the similar DNQX molecule as dopant molecule is the drastic increase of synthesized polymer impedance, resulting in very low deposition current because the voltage of reaction must be limited to prevent over oxidize. With CNQX or DNQX doped PPy film, the polymer can only form a very thin layer on electrode surface and almost act as an insulation layer. To solve this problem, previous work in our lab have demonstrated the remarkable property of functionalized CNT to serve as reservoir for drug release and significantly improve the drug loading capacity[125]. The incorporation of CNTs in conducting polymers can also improve both the strength and conductivity of the conducting polymers [172], which is important to develop stable and long-lasting conducting polymer based drug release systems. The high conductivity can reduce the threshold of the drug release stimuli and the mechanical strength may prevent the cracking and delamination of the polymer film [173]. CNTs serving as structural supplement in the polymers are large in size and essentially immobile inside the polymer, this allows the negative current stimulation to deliver the small drug molecules without unbinding CNTs from polymer matrix[125]. However, even with the facilitation of functionalized CNTs, the PPy/CNT/DNQX polymer still can only form a thin layer structure due to the hindrance of DNQX on the polymer electrical conductivity. So a novel approach was developed in this work where PEDOT/CNT layer is first synthesized on microelectrodes due to the mechanical stability, expanded three dimensional surface area and low impedance of this polymer. The CNT network inside PEDOT polymer provide excellent mechanical property, expanded surface area as well as decreased surface impedance compare to the Pt/Ir microelectrode. PEDOT on its own also demonstrated excellent electrical conductivity and

stability. Polypyrrole/CNT/DNQX film is synthesized on top of PEDOT/CNT film to maximize the capacity of releasable neural molecules.

The precise concentration of molecules delivered has proven difficult to quantify due to the difficulty in determining the quantity of polymer redox reaction and the small molarity of molecules that can be delivered on microelectrodes. In this work, the PEDOT/CNT and PPy/CNT/Drug polymer composite for releasing negatively charged neural molecules has been developed and carefully characterized. PPy/CNT/Fluorescein film on PEDOT/CNT polymer is synthesized on microelectrode to model DNQX release quantity. The release profile and diffusion pattern of Fluorescein model molecule was visualized and semi-quantitatively assessed by fluorescent microscopy at very low concentration. A two term exponential decay function fitted the release trend of fluorescein with very high fidelity. Next double layer Fluorescein and DNQX release was quantified with spectroscopy technique and the result was applied to semi-quantitative model fitting to precisely determine the release dynamics for both molecules.

With the development and characterization of this conducting polymer based drug release method *in vitro*, our novel technique can be readily implemented on either neural recording or stimulation sites of MEAs and multi-modal modulation of neural networks with various species of neural modulators can be easily achieved. Manipulation of *in vivo* neural networks without interrupting extracellular recording of adjacent electrodes demonstrates the working range and efficacy of the system.

2.3 MATERIALS AND METHODS

2.3.1 Materials and Electrodes

2.3.1.1 Materials

DNQX disodium salt was acquired from Abcam (MA) or Alomone Labs (Israel), Multi-walled carbon nanotubes (mwCNT) was purchased from Nanoamor (TX) and was chemically functionalized with –COOH with previously reported method [125]. UV-curing fluorescent transparent optical adhesives NOA 63 was obtained from Norland Products Inc. (NV) 127um diameter Platinum/Iridium (Pt/Ir 9:1) wires were purchased from A-M Systems (WA). All other chemicals were obtained from Sigma-Aldrich (MO).

16 channel microelectrode arrays for *in vivo* neural recording and drug delivery was obtained from Neuronexus (MI). The GSA of electrode sites on the probe was 704 μm^2. The electrodes are arranged on 4 shanks with 4 electrodes on each shank. The site spacing on each shank is 100 μm and the shanks are 125 μm apart from each other. The sites expand a depth of 300 μm, allowing all recordings to be performed within layer IV of barrel cortex.

CNT were first sonicated in acid solution (1:3 HNO_3 and H_2SO_4) for 2 hours rendering the inner and outer walls of CNTs hydrophilic [174, 175]. This treatment also opens the CNT ends and removes the heavy metal, consequently eliminates the toxicity of CNTs. Ultracentrifuge (Sorvall RC 6 plus, Thermo Scientific, PA) at 12k-19k rpm was employed to remove the residual acid from the CNT. After the pH of CNT solution is pH neutral, the CNT were first dried with a rotovap then completely heated and dried in oven at 50 ^oC. The CNT was stored in a vacuum freezer at -20 ^oC with desiccants.

2.3.1.2 Epoxy multielectrode array for drug delivery

Custom build microelectrode arrays were fabricated with three Pt/Ir wires and UV-curing epoxy. The fabrication process is summarized as follows: three Pt/Ir wires were carefully aligned inside a 200uL pipette tip submerged in epoxy. The epoxy was first cured with UV light source for 5 minutes. Then the array was further consolidated by 5 minutes UV exposure on the side. Next, a razor blade was utilized to slice open the side and remove the pipette tip, exposing the epoxy embedded Pt/Ir array. The array was sawed to 1.5cm length followed by alumina particle electrode polishing kit (CH Instruments, Inc., TX) with particle diameter of 1 μm and 0.3 μm. During fluorescein release experiment, a layer of black non-fluorescent liquid electrical tape (Mcmaster-Carr, IL) was applied onto the surface of the epoxy array to absorb non-specific reflection light.

2.3.2 Electrochemical synthesis and characterization

2.3.2.1 Electrochemical deposition

PEDOT/CNT films were first potentiostatic deposited using a FAS 2 Femtostat (Gamry, PA) onto electrodes. The deposition solution was consisted of 0.015 M EDOT monomer and 1 mg/μL CNT dissolved in 1mL de-ionized water (DI H_2O). The concentration of EDOT monomer was slightly higher than the soluble amount of EDOT monomer in water because CNT surface is capable of absorbing EDOT monomers, allowing higher concentration of monomer to be dissolved. 15 minutes of sonication with a probe sonicator (Q500, Qsonica, CT) was applied to the mixed solution in order to homogenize the CNT and EDOT monomers. The polymerizations were carried out in a three-electrode cell consisting of a platinum sheet counter electrode and Ag/AgCl reference electrode, 0.95 V was applied to the working electrode for 15 s to form the

film. After the synthesis of PEDOT/CNT, the electrode arrays were removed from the deposition solution with EDOT monomer and CNT, followed by complete DI H_2O rinse to remove any leftover monomer or CNT, then carefully dried for at least 5 minutes the PEDOT/CNT film to stabilize and to prevent dilution of the second layer polymerization solution.

Fluorescein or DNQX molecules were loaded into the inner cavity of functionalized CNT (1 mg/mL) by mixing CNT and drug for 10 minutes. Pyrrole monomers were added to the CNT suspension with drug and further sonicated for 5 minutes. Electropolymerization was carried out during which PPy film grew on the microelectrode array sites and the drug-loaded CNT were sealed by the polymer. Chronoamperometry was utilized to synthesize the PPy/CNT/fluorescein film on top of PEDOT/CNT substrate film. Chronoamperometry was selected for synthesizing PPy/CNT/fluorescein film to prevent possible over-oxidation of the conducting polymer. The deposition potential was carefully controlled at 0.75 V and the duration was 15 seconds. After the electrodeposition was complete, the array was rinsed with DI H_2O to remove the residual deposition solution. Then the array was washed in 1X PBS solution with stirring for 30 minutes before the drug delivery quantification experiment was carried out.

2.3.2.2 Film characterization

The impedance spectrum from 10 Hz to 32 kHz and cyclic voltammetry measurements with a scan rate of 1 V/s and a scan range of -0.9 V to 0.6 V were obtained using an Autolab N128 (Metrohm Autolab B.V., The Netherlands) in 10 mM phosphate buffered solution (1X PBS). The characterization was carried out in a three electrode electrochemical cell including a platinum sheet as counter electrode and Ag/AgCl reference electrode.

Microscopy images of the polished microelectrodes and the polymer coated electrodes were examined under a Zeiss fluorescent microscope (Germany). Scanning electron microscopy

(SEM) images of polymer deposition on microelectrodes were taken using a JSM 6330F SEM (Joel, Japan). A 5 nm layer of Pd was sputtered onto the electrode to improve the conductivity before the SEM and 5 kV was used for the SEM imaging.

2.3.3 Quantitative analysis of drug delivery

2.3.3.1 Semi-quantitative fluorescent imaging for fluorescein release

The setup for semi-quantitative characterization of Fluorescein release is illustrated in Fig. 2-1B. PEDOT/CNT and PPy/CNT/Fluorescein coated microelectrode arrays were mounted onto an electrode holder controlled by a motorized three-axis micromanipulator (Siskiyou Instruments, OR) for fluorescent imaging. A fluorescent microscope (Leica, Germany) with a 488 nm excitation light and a 510 nm emission light because Fluorescein molecules with this excitation and emission wavelength was utilized for the fluorescent imaging. A Uniblitz shutter was inserted between the lamp and microscope to precisely control the duration of fluorescent excitation light, in order to prevent possible excessive photo bleach of the fluorescein. A solenoid fluidic controller was used to switch on and off the 1X PBS perfusion and vacuum suction simultaneously. The DAC output of a Digidata digitizer (Molecular Devices, CA) was utilized to generate the cathodic leading cosine waveform with an amplitude of 1 V, 1.5 V and 2 V to trigger the release of fluorescein from the film. The duration of the cosine waveform is 100 ms, followed by a 200 ms, half amplitude reverse polar charge balancing phase, accommodating for the conventional *in vivo* neural stimulation scheme to prevent tissue damage from injecting net charge. A fast CCD camera was used to record a series of tiff images at 10Hz for semi-quantitative characterization of the Fluorescein release dynamics. The synchronization TTL

signals in the system is generated by a master 8 (A.M.P.I., Israel). The timing schematics of quantifying Fluorescein release is illustrated in Fig 2-1A. The PBS perfusion for 15 seconds is executed at the beginning of each drug delivery trial, ensuring the precision of the 5 seconds baseline fluorescent intensity imaging immediately following PBS perfusion. Then the fluorescent shutter is turned on and the camera imaging start at the same time. The PBS flow is completely stopped at 15 seconds to ensure a natural diffusion pattern of the Fluorescein molecule after the electrical trigger. Drug release electrode is stimulated with the drug delivery trigger 5 seconds after the camera start to take baseline measurement. Another 10 seconds of drug releasing electrode were captured to quantify the Fluorescein release and diffuse pattern. The microscope light source is controlled by a remotely switchable shutter to minimize the duration of applying fluorescent excitation light. Each drug release experiment is 30 seconds long in total duration. The fluorescent shutter is then turned off and 5 seconds inter-trial interval is used to save the fluorescent image series and clear the memory for the imaging software. The process to save image files and control the start of fluorescent image capture is automatic by a custom written Visual Basic (Microsoft, WA) script for directly interfacing with mouse, keyboard and software control. 90 Fluorescein release trials were conducted for each PEDOT/CNT PPy/CNT/Fluorescein coated microelectrode, in order to capture the full trend for the drug release dynamics.

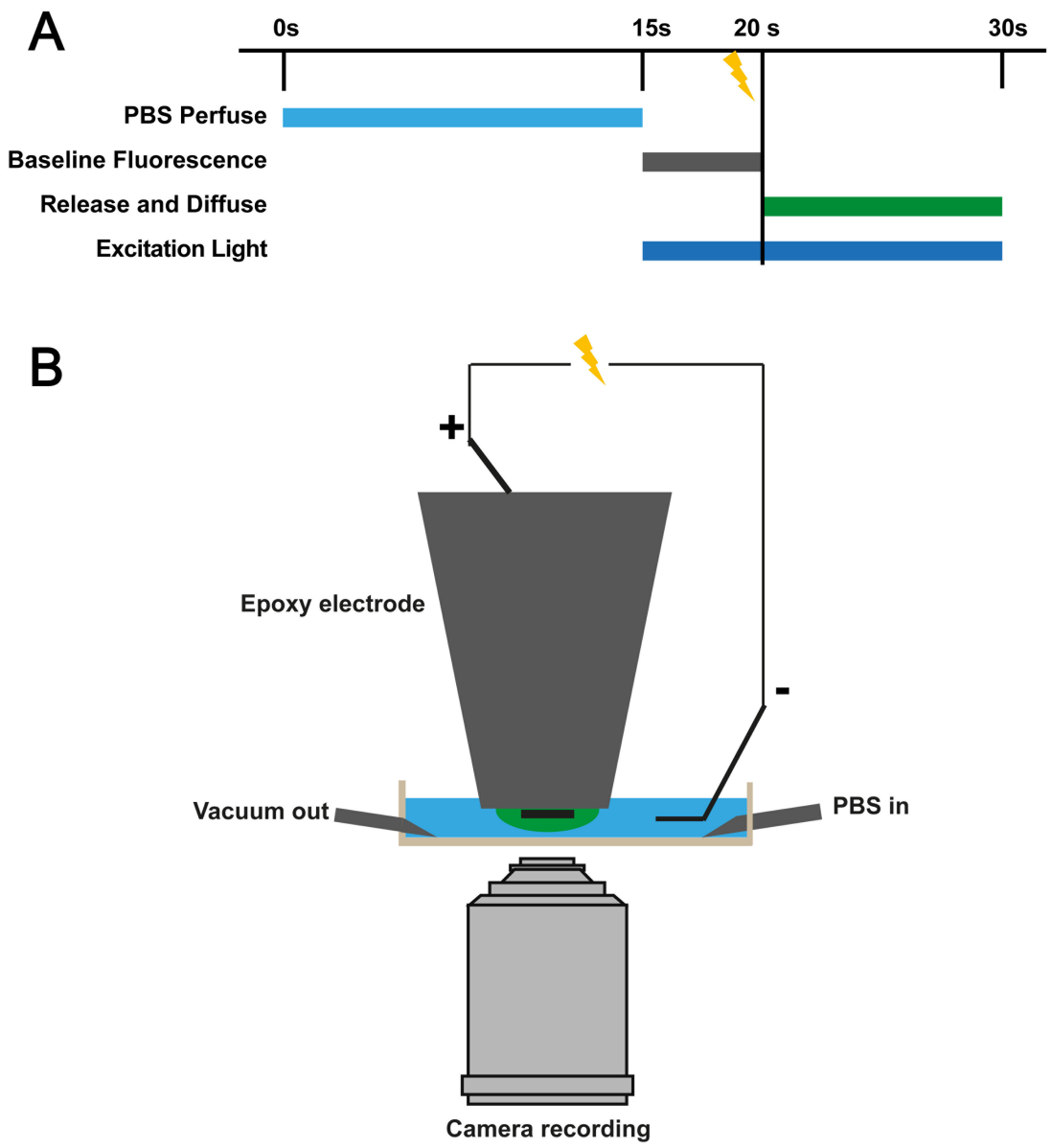

Figure 2-1 Fluorescence imaging scheme for semi-quantitative measure of Fluorescein concentration. (A) Timing schematics of the Fluorescein release experiment. The drug release trigger is delivered at 20 s time point. (B) Setup schematics for Fluorescein release experiment, the green semi-ellipse represent the diffusion pattern of Fluorescein after been release. After PBS perfusion to remove excess Fluorescein, the drug release trigger is applied to release Fluorescein from the electrode on Epoxy array, the black dish represent the conducting polymer coated on the cross section of the Pt/Ir electrode. The counter electrode on the right side of dish is an uninsulated Platinum wire with sufficiently large surface area compare to the working electrode.

2.3.3.2 Spectrometry quantification of Fluorescein and DNQX release

The drug release setup for spectrometry quantification of drug delivery was illustrated in Fig 2-2A. The setup allow most of the released drug to be accumulated in a very small volume thus a high concentration for the spectrometer measurement. A small Petri dish filled with DI H2O served as a moisture chamber to prevent excessive evaporation of drug release solution. A glass slide with hydrophobic surface was utilized as the substrate for drug release quantification. After the moisture maintaining petri dish, the slide and the platinum wire counter electrodes are positioned, 60 μL of PBS is added on top of the slide covering the platinum wire and form a liquid bubble under the surface tension. The drug release electrode is carefully positioned with a helping hand or micromanipulator to be submerged in the liquid bubble without touching counter electrode or the slide surface. 1.5 V drug release waveform was applied to the electrode for 45 times to replicate the exact same amount of Fluorescein release observed by fluorescent microscope quantification experiment. The cosine drug release stimulation was carried out by FAS2 Femtostat (Gamry, PA). After the drug release trigger was applied, repetitive pipette was utilized for gently homogenizing the drug release solution. 50 μL of release solution was then extracted from the liquid bubble and measured in a 96 well fluorescent plate for the quantification of analyte. The quantity of Fluorescein in this solution is used as the basis to calculate the total Fluorescein release in the 60 μL solution. Fluorescent spectrometry with excitation wavelength of 488 nm and emission wavelength of 510 nm was utilized to quantify the amount of released Fluorescein in the solution.

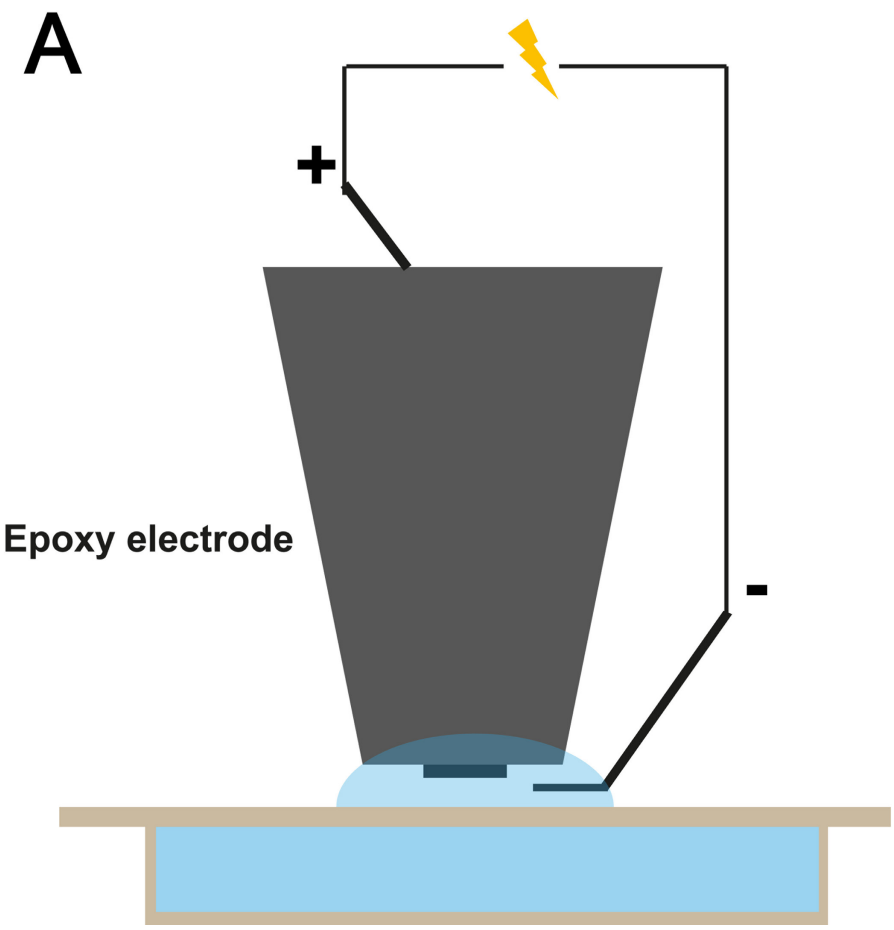

Figure 2-2 Quantify accumulated drug release amount with small volume drug delivery. (A) The drug release setup to precisely measure the drug release quantity in a very small volume PBS liquid bubble preparation. The PBS liquid bubble is maintained on the surface of a hydrophobic slide so the surface tension maintain a sufficient height of liquid bubble that enough distance is kept between the working electrode and the slide. The slide is placed directly on top of a petri dish so the local environment humidity around drug release PBS bubble is maintained at a high level. During the drug release experiment minimal amount of evaporation volume loss is observed from the liquid bubble. The custom build microelectrode array and the counter electrode Platinum wire are both positioned with a solder station.

The same drug release procedure was applied to DNQX coated bi-layer conducting polymer film and UV absorbance at 248 nm was utilized to quantify the amount of DNQX in the released solution.

Due to the extreme low quantity of Fluorescein molecules released by microelectrode during each trial, the 90 trial concentration of fluorescein was divided into two accumulative amount for quantify. Trial 1-45 consisted the first release amount and trial 46-90 consisted the second release amount. Despite the extremely small amount of analyte present in the release solution, a detectable concentration of Fluorescein or DNQX was observed in the solution.

2.3.4 Data analyses and statistics

All digital image analysis was done by custom written MATLAB (Mathworks, MA) scripts. The fluorescent image was first loaded into MATLAB memory, an average image intensity over the whole period of the drug delivery was calculated as the static baseline image and subtracted from the whole image series. At the peak drug release intensity, a two-dimensional Gaussian function is fitted to the image intensity in order to estimate the center of the Fluorescein release. Only the fluorescent intensity change within 100 μm diameter from the center of release was calculated for quantification purpose in order to better mimic the semi-sphere diffusion profile of the Fluorescein.

The fluorescent intensity of the image before the drug release trigger was subtracted from the maximum fluorescent intensity of the image series in order to calculate the fluorescence change. The change represent the semi-quantitative amount of Fluorescein released during this trial. For each release electrode, 1 V, 1.5 V or 2 V cosine stimulation was applied for 90 Fluorescein release trials in order to monitor the drug release dynamics at this particular voltage.

A two term exponential function was fitted to the drug release intensity change over trials to directly compare the underlying redox quantity of each voltage condition.

2.4 RESULTS

2.4.1 Synthesis and characterization of bilayer drug loaded coating

2.4.1.1 Fabrication of photopolymer Pt/Ir array

To fabricate a low cost custom electrode array for electrochemical characterization and drug delivery quantification directly on top of a microelectrode, three 127um diameter Pt/Ir wires were embedded in a UV-curing optical adhesive photopolymer material. Pt/Ir wires were selected because of the wide acceptance of this class of inert metal alloy as the suitable neural stimulation and recording materials. Different types of epoxy materials were compared for the potential use of insulating the Pt/Ir wire, the most important limitation is the auto-fluorescence of the epoxy material itself when directly excited by 488 nm wavelength, the working wavelength of Fluorescein. The photopolymer employed in this study features a very low self-fluorescence and an outstanding light transmission performance in a very wide wavelength range. The one part UV-curing design of this photopolymer also avoid the gradual self-polymerization of multi-parts mixing epoxy materials, thus provide more controllability over the fabrication process just by UV exposure. The photopolymer exhibits minimal volume change and excellent adhesion to metal surface, providing a very tightly sealed insulating layer directly on top of the Pt/Ir conductors (Fig. 2-3B). Compared to the surface area of microelectrodes embedded in the photopolymer insulator, the insulation cross section area is hundreds of times larger. The

handling of fabricated array during the polishing procedure is thus very easy compare to other techniques of fabricating microelectrodes with consistent surface area. Microelectrodes fabricated with this method demonstrated an even cross section surface with very smooth morphology and reliable impedance performance (Fig. 2-3B).

2.4.1.2 Deposition and characterization of PEDOT/CNT

Functionalized CNT is incorporated beneath the PPy/CNT/Fluorescein film to maximize the amount of Fluorescein molecules been released according to previous study [125]. As demonstrated in Fig 2-3A, incorporating Fluorescein molecule decreased the conductivity of the polymer film and result in very low current and poor growth of the film. Because these, poor drug delivery performance was observed from these films in preliminary experiments.

In order to create an electrode substrate more suitable for coating Fluorescein or DNQX incorporated PPy/CNT film, PEDOT/CNT was first deposited onto the electrode surface. After the electrochemical synthesis of PEDOT/CNT, the electrode surface impedance amplitude decreased significantly from the original values in Fig. 2-3A, due to the expanded surface area and the excellent conductivity of PEDOT polymer. The biggest decrease of impedance amplitude occur in the low frequency range from 10Hz to roughly 1000Hz. The typical impedance of interest for neurophysiology applications because of the frequency of extracellular action potential waveform frequency, 1000Hz, was also greatly impacted by the surface functionalization of PEDOT/CNT. Because the PEDOT/CNT polymer can greatly reduce the impedance of electrode and the direct current (DC) resistance, the polymer synthesis on microelectrode accelerates significantly when the polymerization process begins. 15 seconds of electrodeposition yielded a thick and uniform conducting polymer surface coating (Fig. 2-3C) without significantly impacting the geometric range surface area of the microelectrode (Fig. 2-

3B). The edge of the conducting polymer matrix is as smooth as bare Pt/Ir electrode surface in Fig. 2-3B. Under SEM examination in Fig. 2-4B, an ultra-porous three-dimensional matrix of PEDOT-CNT is observed on the coated electrode, permitting the maximum amount of surface area to polymerize the subsequent PPy/CNT/Fluorescein film. The CNT outer diameter is 20-30 nm. The CNT diameter is not visibly affected by PEDOT polymer.

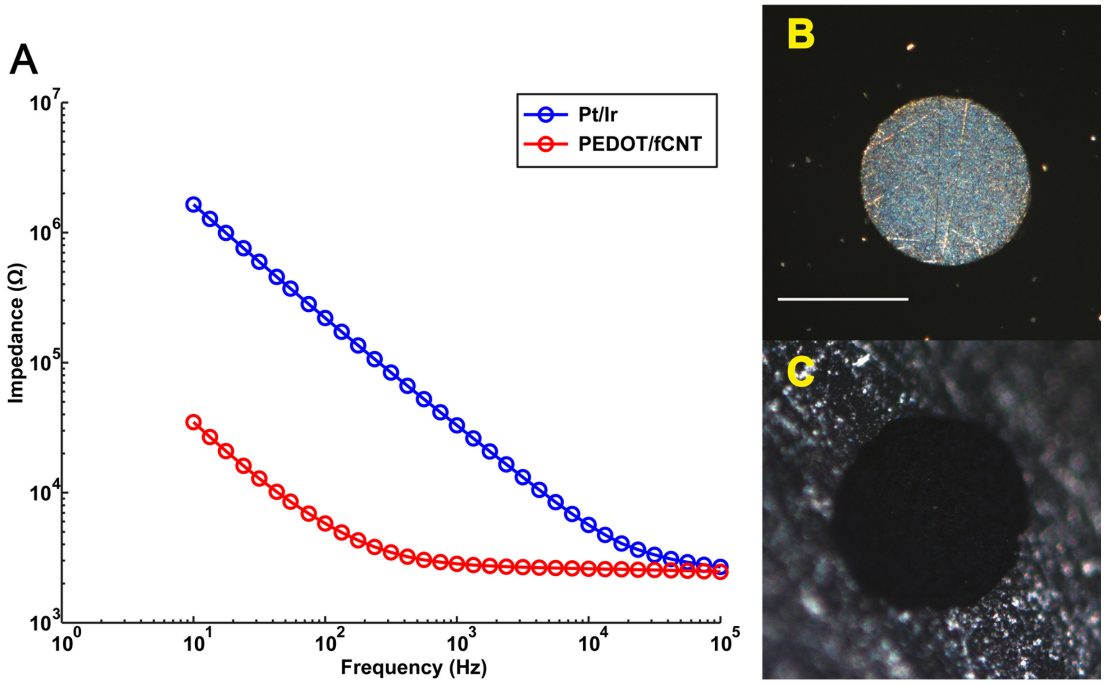

Figure 2-3 Characterization of PEDOT/CNT deposition on Pt/Ir microelectrode. (A) Comparison of impedance amplitude before and after PEDOT/CNT electrodeposition. (B) The smooth metallic surface texture of Pt/Ir wire cross section following the electrode polishing procedure. (C) The PEDOT/CNT polymer completely change the surface texture of the Pt/Ir electrode in comparison with the surrounding photopolymer insulation material. Scale bar=100um.

2.4.1.3 Synthesis and characterization of PPy/CNT/Fluorescein on PEDOT/CNT

The electrodeposition current of PPy/CNT/Fluorescein on top of PEDOT/CNT is markedly increased from the current of direct deposition on the surface Pt/Ir electrode (Fig. 2-4A). The total charge during the electrochemical synthesis is about 40 folds increase from the single layer deposition. In Fig. 2-4A, the coating current of single-layer PPy/CNT/Fluorescein film exhibit a decrease trend after a short spiking due to capacitive charging during Chronoamperometry deposition, but the double layer PPy/CNT/Fluorescein shows a very clear increasing trend as deposition time become longer. The possible reason behind this phenomenon is that when the PPy/CNT/Fluorescein film is synthesized on top of PEDOT/CNT film, the effective electrode surface area is much larger than the uncoated electrodes, allowing significantly more charge to be passed Although the poorly conducting PPy/CNT/Fluorescein slightly increase the electrode surface resistivity per area, the effective surface area of the conducting polymer increase quickly as more polymer is synthesized due to the roughened texture. The overall consequence of the two competitive mechanism is determined by the dominant one. As the result indicate, the effective area increase is remarkably stronger than the surface resistivity increase.

The solubility of EDOT in H_2O is relatively low compare to pyrrole, so the synthesized PEDOT will only form a very thin layer of polymer on the CNT surface due to the limited concentration of monomers. Fig. 2-4C demonstrated the surface morphology of PPy/CNT/Fluorescein film grown on PEDOT/CNT under SEM. Although the CNT morphology in the SEM image is slightly affected by the surface adhesion of PPy polymers in Fig. 2-4C, the PPy/CNT/Fluorescein film is still capable of maintaining a very porous structure with large surface area to volume ratio.

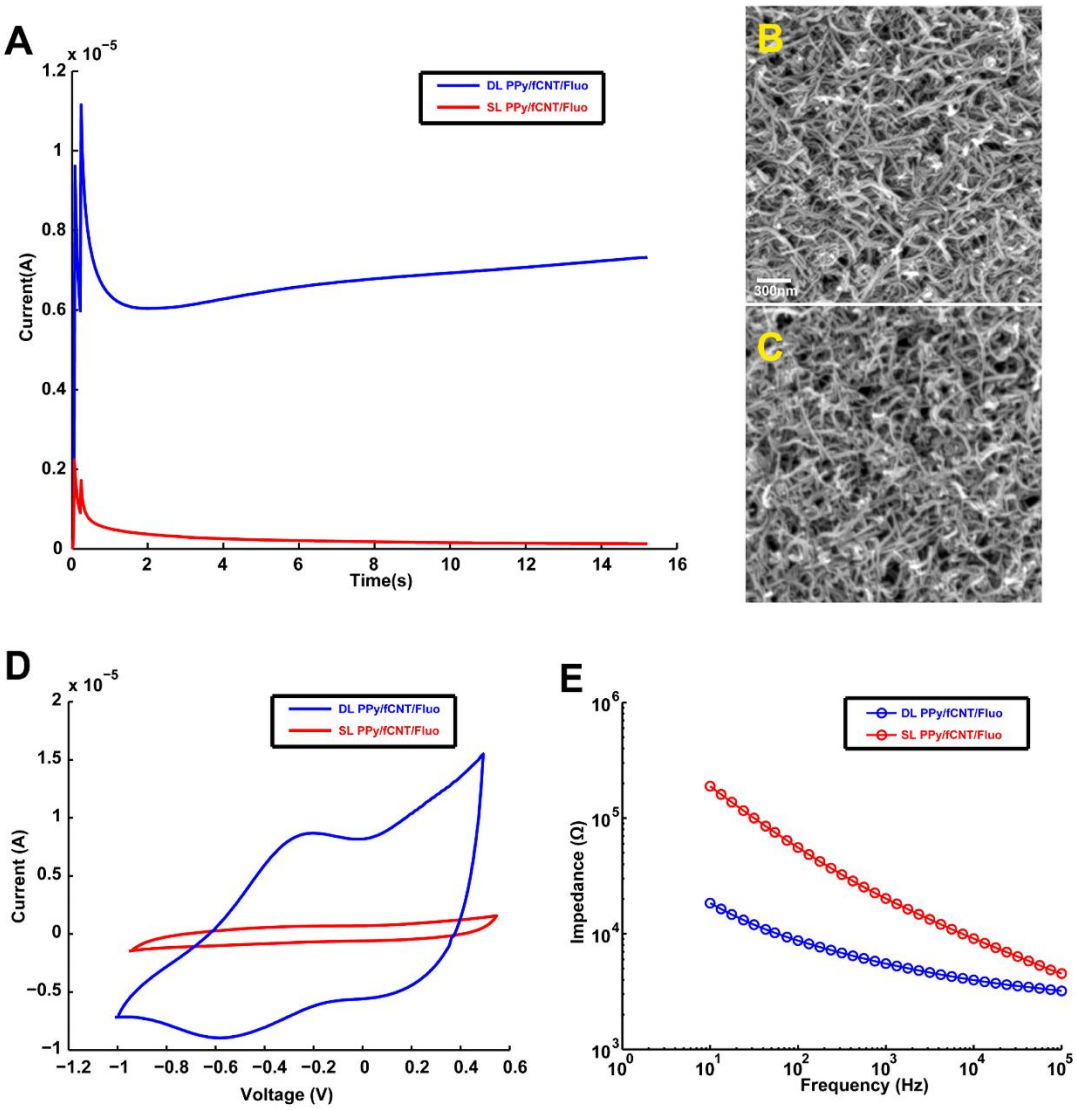

Figure 2-4 Synthesis and characterization of PPy/CNT/Fluorescein polymer on Pt/Ir and PEDOT/CNT surface. (A) Chronoamperometry deposition of PPy/CNT/Fluorescein on Pt/Ir and PEDOT/CNT, the current on top of PEDOT/CNT film is markedly increased from the direct synthesis current on Pt/Ir. (B) SEM image of PEDOT/CNT substrate layer demonstrated very expanded bird nest like structure with three dimensional structures to facilitate the growth and adhesion of PPy/CNT/Fluorescein polymer. (C) SEM image of PPy/CNT/Fluorescein bi-layer polymer composite. The surface texture of PEDOT/CNT is replaced with PPy/CNT/Fluorescein, indicated by the more visible polymer morphology on the surface of CNT. (D) Cyclic Voltammetry characterization of single layer and double layer PPy/CNT/Fluorescein coating. (E) Impedance

amplitude of PPy/CNT/Fluorescein on PEDOT/CNT and Pt/Ir measured in the frequency range between 10 Hz and 100000 Hz.

Cyclic voltammetry (CV) measurement of redox current on differently prepared single-layer and double-layer PPy/CNT/Fluorescein polymer also revealed very different performance of the polymer. The double layer conducting polymer exhibit a much larger current in the CV measurement, with prominent reduction peak around -0.6 V. The drug release trigger voltage was all designed to be much larger than the reduction voltage of PPy, allowing rapid shift of the PPy redox state during the drug release trigger. The cosine waveform for releasing drug is only 100 ms in duration in order to minimize the net charge and tendency of DC like tissue damage. But the high amplitude compensate for the short duration of the waveform as demonstrated by successful Fluorescein delivery. The low impedance demonstrated in Fig 2-4E is also a clear benefit for the double-layer polymer preparation. With the same driving voltage, the current on low impedance electrode is much higher than high impedance electrode. The double-layer polymer film impedance at 10 Hz is almost 10 times lower than the single-layer polymer. This impedance reduction effect of bi-layer approach is most prominent at low frequency range that is most suitable for the frequency of our drug delivery cosine waveform.

2.4.2 Fluorescein release quantification

2.4.2.1 Electrically controlled delivery of Fluorescein

The setup to quantify fluorescein release dynamics is illustrated in Fig 2-1. The flow of PBS can remove residual Fluorescein molecule from previous release trial and spontaneous diffusion, thus in the timing scheme of Fig 2-1A, the PBS flow was conducted immediately

before the imaging. The delivered drug quantity is related to the intensity difference before and after the drug delivery trigger. The drug release trigger is represented by the red vertical line 5 seconds after the camera start to record baseline image as represented by Fig. 2-5B. Then an immediate increase of fluorescent intensity is observed following the electrical trigger. The concentration of Fluorescein around the drug release electrode was highest immediately after the drug delivery trigger and gradually decrease. In Fig. 2-5A, the drug release quantity is represented by subtraction of frame 1 intensity from frame 2 intensity, and in Fig. 2-5B, the quantity is the maximum intensity after the red line subtracting the intensity before red line.

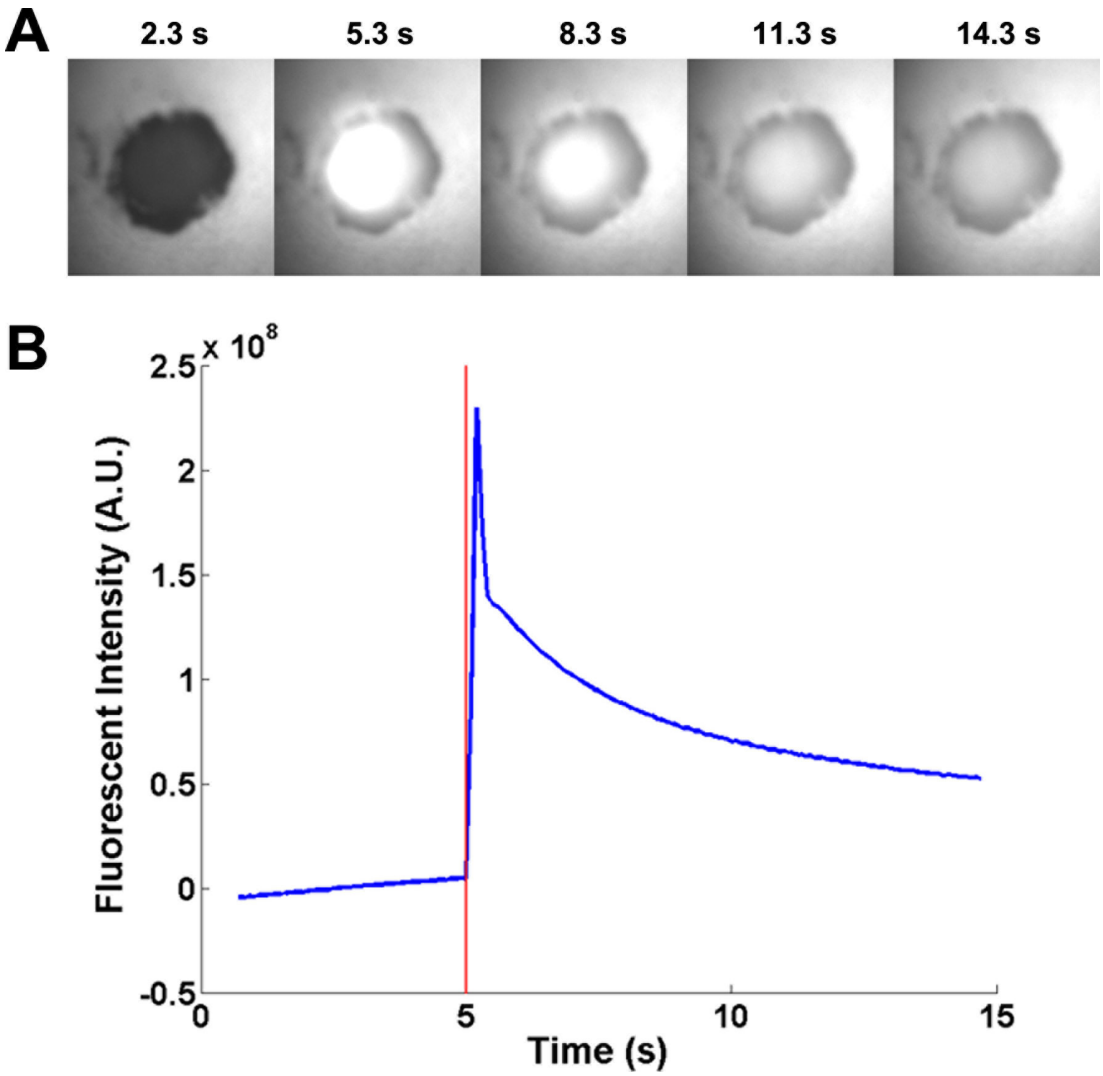

Figure 2-5 Fluorescent intensity in one Fluorescein delivery trial. (A1-5) Representative frames of the drug delivery and diffusion quantification process. The microscope was focused 20um below the electrode surface so the focal plane better represent the semi-sphere diffusion pattern of Fluorescein. In frame 1 the coated electrode is in black due to the optical absorption of CNT in the polymer matrix. Frame 2 represent the Fluorescein release process immediately after the drug delivery trigger. The Fluorescein was driven out from the conducting polymer due to the electrostatic force caused by polymer backbone reduction. From frame 3 to 5 the Fluorescein is clearly diffusing away gradually from the center of drug delivery. (B) The quantification of fluorescent intensity around the drug delivery electrode, with 100 μm radius from the center of a two-dimensional Gaussian function estimation of highest fluorescent intensity. The fluorescent intensity was highest following the drug release trigger and start to decay but maintained a relatively high concentration for a long period.

2.4.2.2 Exponential decay model of Fluorescein release quantity

The semi-quantitative measurement of Fluorescein release amount was conducted repeatedly for 1V, 1.5V and 2V. The result from different electrodes are illustrated in Fig. 2-6. In Fig. 2-6A, the drug delivery quantity trend for three voltages are summarized. The drug release quantity is positively correlated with the amplitude of the drug release stimulation. The drug release quantity at 1 V is significantly lower than 1.5 V and 2 V, indicating the amount of reduction reaction triggered by each stimulation amplitude is not linearly related to the applied potential.

$$C_{Fluo} = a * e^{b} + c * e^{d} \qquad \text{Eq. (1)}$$

The first 5 drug delivery trend is drastically different from the continuous trend afterwards, with much higher internal error as well. Physical adsorption of drug molecule contribute significantly to this phenomenon. Adherence force between the adsorbed molecule and the conducting polymer CNT matrix could vary drastically, so the PBS washing can only

partially remove the excess molecules. The drug release trigger is capable of removing the majority of these molecules in the first few release trials so the following quantity is only affected by the drug release reduction reaction and the drug molecule diffusion gradient in the matrix. In this experiment, the 1 V drug release quantity and the 2 V drug release quantity have very different dynamic range for the imaging requirement. For 1 V characterization the camera was set at higher multiplication gain to reduce the systemic error from internal thermal noise. The 2 V experiment was conducted with lower multiplication gain in order to prevent the camera from saturation. The inter group error between different electrodes is very low and was maintained across the trials. Only 2 V group displayed a relatively high variance possibly due to water hydrolysis that distort the fluorescent intensity quantification process. In the modeling process the first 5 trials of each group was removed to reduce the random error caused by different physical adsorption of molecules, the drug release quantity of 1.5 V and 2 V group both demonstrated a slight increase in fluorescent intensity at the beginning of the release trials, possibly because the dopant anion for surface polymer was replaced with PBS molecules during previous washing step, and the stimulation can replenish the surface with higher concentration of fluorescein from internal reservoir than the initial surface fluorescein concentration diluted by PBS.

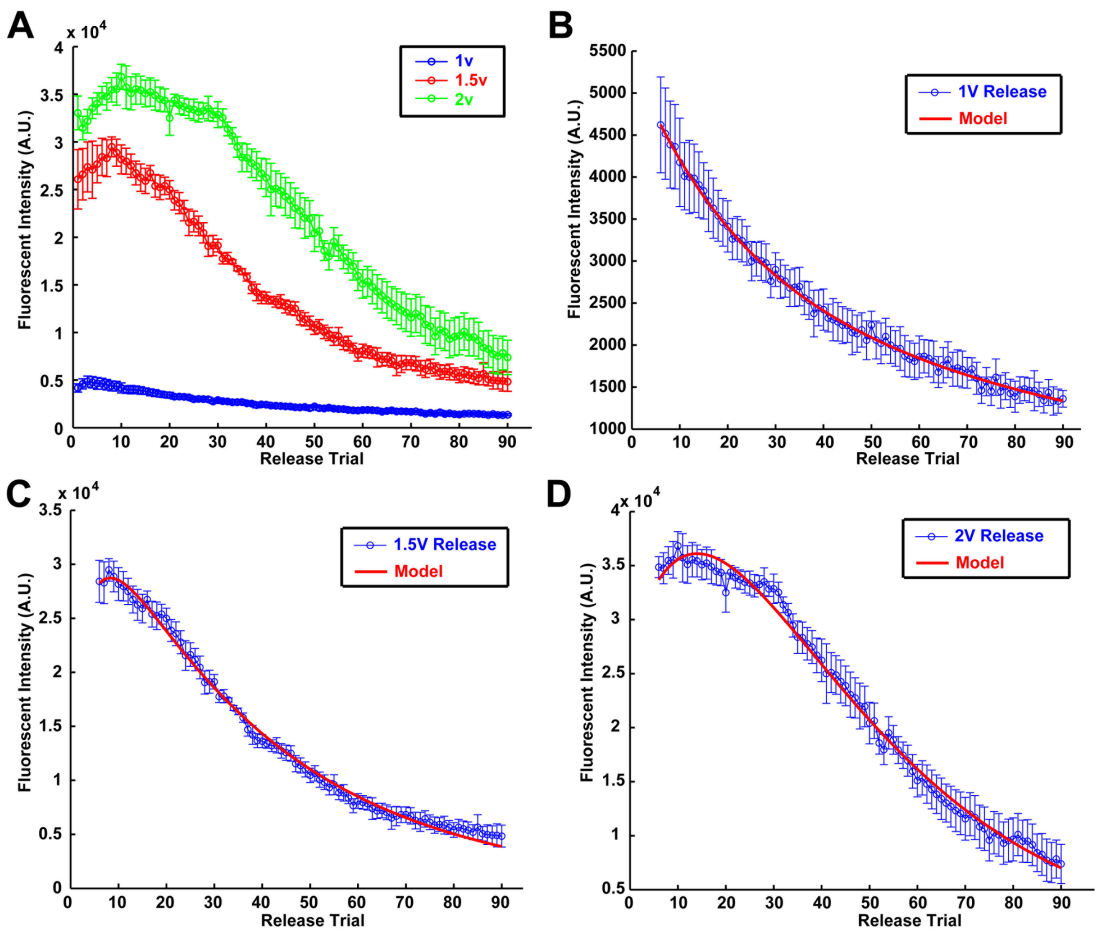

Figure 2-6 Fluorescent intensity trend for different release conditions can be modeled with two term exponential decay function (A) Fluorescent intensity change over trials for different drug delivery voltage groups, n=5 for 1 V group, n=5 for 1.5 V group, n=6 for 2 V group. The 2V group displayed larger variability during quantification possibly due to small amount of water hydrolysis formed air bubbles in some trials, interfering with the quantification. 2 V drug release trigger delivered the maximum amount of Fluorescein molecules, and the amount decrease with reduced voltage. (B) 1 V Fluorescein release group can be modeled by two term exponential decay function in Eq. (2). The goodness of fit is 0.99823. (C) 1.5 V drug release amount modeled by Eq. (2) function yield a goodness of fit value 0.99763. (D) 2 V drug release amount model yield a goodness of fit value 0.99702. All three groups are well modeled by two-term exponential functions.

2.4.3 Spectrometry quantification of Fluorescein and DNQX

2.4.3.1 Quantification of accumulative Fluorescein release

The semi quantitative assessment of drug release amount from fluorescence microscope follows a smooth and predictable pattern. However, the absolute quantity of Fluorescein molecules cannot be determined with this method because precise standard solution fluorescent intensity cannot be measured with the fluorescent microscope. The drug release process form a semi-sphere diffusion situation of Fluorescein with higher concentration in the center of diffusion. But a Fluorescein concentration function curve can only be drawn from a uniformly distributed concentration of molecules. So a spectrometry measurement of the Fluorescein concentration is preferred to quantify the amount of drug release and compare with known Fluorescein concentrations. Due the extremely small size of our microelectrode drug delivery setup, the amount of Fluorescein delivered with a single release trial is below the detection limit of spectrometer measurement. Instead the accumulative Fluorescein release amount was chosen to quantify. If the low concentration of Fluorescein is evenly distributed in a relatively large volume and we have to sample a small volume of solution for spectrum measurement, the result will approach the PBS baseline value and suffer from high systemic error. So a very small volume drug release system is designed, with a total release volume of 60 μL and a measurement volume of 50 μL. The accumulative Fluorescein release amount for released trial 1 to 45 and 46 to 90 are illustrated in Fig. 2-7A in comparison to the PBS baseline measurement. The fluorescent intensity emitted by the drug release solution clearly exceed the value of PBS, ensuring the relatively low contribution of systemic error from the spectrometer. To verify the trend predicted by the fluorescent microscope method, the quantity ratio from model predicted first and second 45 trials are calculated and compared to the measured ratio. The first 45 trials

were used as the basis of calculation because it yield a higher fluorescent intensity and was less affected by systemic error due to low analyte concentrations near detection limit. The single trial drug release quantity are not directly measureable with traditional drug delivery quantification techniques and can only be predicted by the back calculation from the accumulated release amount.

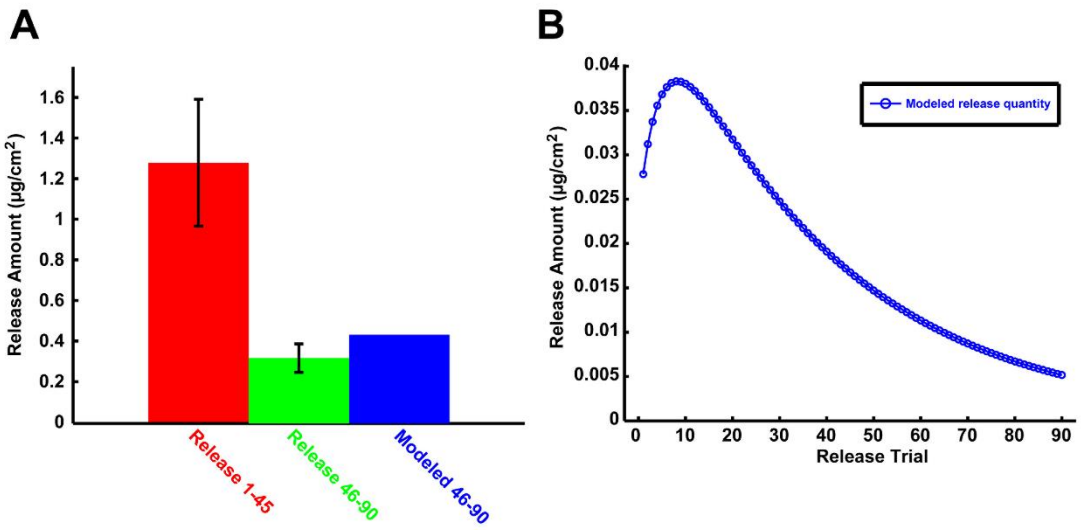

Figure 2-7 Spectrometry quantification of Fluorescein release amount in 45 accumulated trials. (A) The Fluorescein quantity is directly measured by a function curve of known Fluorescein concentration and then the unit of amount is converted to the drug release quantity per surface area of electrode. The Fluorescein intensity accumulated in the first and second 45 trials are both detectable with the spectrometer. For the second 45 trials, the accumulated Fluorescein quantity measurement is directly compared to the value predicted by the first 45 trails and the modelled drug release trend. The comparison yield a high similarity. This is a clear confirmation of the model prediction performance. (B) With the quantity measured in the first 45 accumulated trials, the model can predict drug release amount during every single drug release trial. The Fluorescein release quantity can reach maximum value of 0.04 μg/cm2. By the end of the 90 drug release trials, the Fluorescein release is only 0.005 μg/cm2.

2.4.3.2 Quantification of accumulative DNQX release

Another AMPA receptor antagonist, DNQX can directly affect neural network activity by suppressing the action potential generation mechanisms of neurons. The release of DNQX could be a valuable tool to control epileptic activity of local neural network or understand the spiking mechanism under the symptoms of other neural disorders. The trend for DNQX release quantity change is not measurable due to the low detection sensitivity of spectrometer to the UV absorption measurement. Only DNQX molecules with high concentration can be measured by the UV absorbance. So the release trend of DNQX molecules can only be predicted by the Fluorescein molecule. The model predicted a DNQX concentration very similar to the measured concentration for the second 45 drug release trials. Because Fluorescein quantification clearly confirm the model performance, this model and measurement similarity is a good indication that the drug release dynamics trend of Fluorescein molecules and the DNQX molecules are very similar to each other. Although the charge, molecular weight, solubility and other properties of the two molecules are very similar to each other, this is one of the first experiment result to justify the use of carefully selected fluorescent molecules for mimicking the drug release behavior of other molecules. It is important to note despite the similarity in the ratio of the first and second 45 accumulated drug release trials between the two different drug molecules, the absolute quantity of released drug is very different between the two. DNQX molecules can be released up to a very high concentration compared to Fluorescein molecules. This phenomenon indicates although the drug release polymer matrix may display similar release dynamic process with the same type of electrical stimulation triggers, the release quantity may heavily depend on other factors such as the dopant concentration in the polymer. The similar release dynamics indicate the mobility of drug molecule from internal structure to the surface release reservoir

may behave similarly between different molecules. This mobility of molecules from interior to the surface of polymer could be viewed as concentration gradient driven diffusion, fluorescein and DNQX displayed similar diffusion constant in the process.

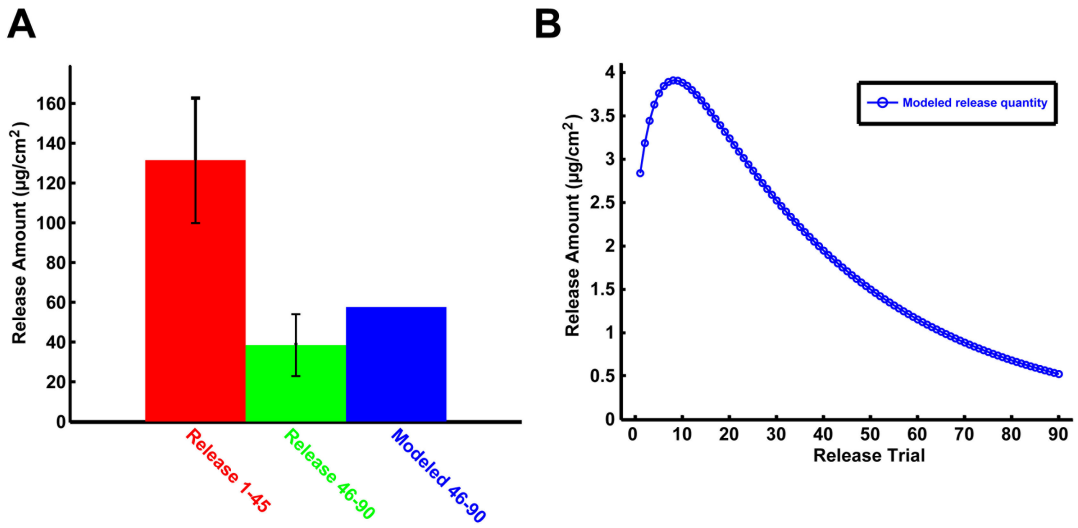

Figure 2-8 Spectrometry quantification of DNQX release amount in 45 accumulated trials. (A) The DNQX quantity is measured by UV absorption of known DNQX concentrations and then the unit of amount is converted to the drug release quantity per surface area. The DNQX quantity accumulated in the first and second 45 trials are both detectable with the spectrometer. The measured accumulated DNQX quantity in second 45 trials was compared to the modeled value. The high similarity in this comparison indicate the Fluorescein molecule is an ideal model system for mimicking the drug release behavior of DNQX. (B) Model prediction of the 90 drug release trial quantity estimated by the accumulated drug molecula amount over first 45 release trials, every single drug release trial quantity is indirectly calculated from the model. The DNQX release quantity can reach maximum value of 4 µg/cm2. By the end of the 90 drug release trials, the Fluorescein release is reduced to around 0.5 µg/cm2.

2.5 DISCUSSION

2.5.1.1 Benefit of double layer polymer on drug delivery

The Chronoamperometry polymerization current of single layer and double layer PPy/CNT/fluorescein clearly indicate the film is difficult to polymerize even with the facilitation of CNT. The deposition current kept a downward trend due to the increase of polymer surface resistivity. However, the double layer polymer on top of PEDOT/CNT completely reversed this trend and allow a much large deposition charge for PPy/CNT/fluorescein film. After polymerization, the inner cavity of CNTs is filled with high concentration fluorescein, which acts as a reservoir for PPy[125]. During the controlled release of fluorescein from PPy film, the CNT reservoir replenish the fluorescein near the outer surface of conducting polymer. The PEDOT/CNT coating increase the surface area for deposition, decrease the surface impedance, and improves the polymer stability under long term electrical stimulation[128]. Additionally, the porous surface of PEDOT facilitate the deposition of PPy and allow more fluorescein to be incorporated in the polymer[96].

When electrically stimulation is applied to the PPy/CNT/drug film, some drug in the PPy film is released via dedoping. The electrical stimulation also causes a porosity increase due to actuation effect that allow drug inside the CNTs to diffuse into the PPy films and be released by the subsequent stimulus. The CNT selected for our study has outer diameter between 10-20 nm and inner diameter between 5-10 nm. The distribution of CNT inner diameter is also shifted towards larger size of 10 nm according to the manufacture. With these parameters this type of CNT has one of the highest inner/outer diameter ratio among all mwCNT. The higher inner/outer diameter ratio is equivalent of larger internal cavity size, yielding a larger drug contain reservoir. This inner/outer diameter ratio is even higher than the mwCNT utilized as reservoir in previous

study for releasing larger quantity of Dexamethasone[125]. The selection of single-walled CNT (swCNT) may further increase the inner/outer diameter of the polymer[176], however the functionalization of swCNT may cause the tubes to become very short segments due to strong chemical etching and sonication in the process. The functionalization process with concentrated Sulfuric and Nitric acid under strong sonication condition can cut the 10-30 μm long mwCNT down to 2 μm or less, while opening the end of the CNT for drug loading.

For the second layer of conducting polymer film containing drug molecules, Polypyrrole is preferred compare to PEDOT. Another benefit brought about by PPy is the redox potential for PPy is much lower than PEDOT. Because the electrochemically triggered drug delivery requires reduction of conducting polymer backbone, PPy film can drive a large amount of drug delivery at low voltage amplitude around -0.34 V[102], but PEDOT can only be effectively reduced around -0.7 V[177]. The voltage measured by cyclic voltammetry in this work is not measured with saturated calomel electrode (SCE) so it is not a direct reflect of the PPy reduction peak. Baring the *in vivo* application of the technology in mind, the high reduction voltage amplitude of PEDOT endangers the neural tissue adjacent to the drug delivery electrode and may cause more side reactions such as water electrolysis when the polymer film is reduced for drug release. In the SEM image of PPy/CNT/Fluorescein, a porous structure of CNT and PPy is observed. The Fluorescein molecule release embedded in the conducting polymer matrix has a very large surface area to be released from. Furthermore, the hollow region between CNTs allows the polymers embedded deeper in the matrix to be released once the electrostatic force to hold the drug molecule is removed by the drug release trigger voltage.

2.5.1.2 Fluorescein model of DNQX release dynamics

The small fluorescent molecule Fluorescein was utilized as co-dopant for the synthesis of PPy/CNT/Fluorescein film, in order to mimic the drug release behavior of the neuroactive molecule DNQX. The Fluorescein molecule is suitable for several different reasons. Both types of molecules have two net charges per molecule in their disodium salt form. They have similar molecular weight (state what the weights are here) and good water solubility (state what the solubility is for each).

The spectrometry detection limit of DNQX can only reach 0.16 μM while for Fluorescein the detection limit is 0.44 nM. Direct measurement of DNQX release from microelectrode has proven to be difficult as the concentration is below the detection limit of UV absorbance measurement. On the other hand, Fluorescein can be detected with better sensitivity. Furthermore, direct visualization of Fluorescein release provides an excellent model system to visualize the diffusion profile of DNQX following the electrically triggered release from the conducting polymer film. The fluorescent imaging setup can detect fluorescent intensity to a very low concentration due to the sensitivity of the Charge-coupled device (CCD) camera. Although the imaging intensity of the recorded fluorescent strength cannot be directly viewed as linearly related to concentration of fluorescein in most cases, in our case the estimation of concentration from the fluorescent intensity is justifiable. In the illustration of our setup, the flow chamber has a thin layer of solution in between the working electrode array and the glass coverslip at the bottom of the PBS perfusion chamber. The representative size of the conducting polymer film on microelectrode is not drawn to ratio compare to the whole system but instead was exaggerated for the purpose of viewing. With the small size of the microelectrode, the glass coverslip and the surface of the epoxy array can both be viewed as infinite in size. In this type of system the

diffusion of Fluorescein is mostly constricted to horizontal direction rather than vertical direction, leading to reduced out of focus light intensity. Direct characterization of conducting polymer film on microelectrode and quantification of drug delivery are essential to future application of the drug delivery technique for several important reasons: first, the synthesis of the exact same conducting polymer film on macroelectrodes are more difficult than on microelectrodes, with a lower current density for electrochemical deposition; second, the uniformity of electrochemically synthesized conducting polymer on macroelectrodes is typically much worse than on microelectrodes; third, the polymer thickness to geometric surface area (GSA) ratio of conducting polymer on microelectrodes are much higher on microelectrodes even with the same thickness of polymer film, requiring the consideration of edge surface area expansion effect and the three-dimensional micro structure of the polymer; fourth, the direct impact of conducting polymer on the electrode surface morphology and impedance is drastically different on microelectrodes and macroelectrodes, leading to poor correlation between the drug delivery quantity of the two classes of electrodes.

2.5.1.3 Model prediction of Fluorescein release trend

The drug delivery process demonstrated a two phase dynamic process due to two different mechanisms determining the amount of released drug. The first phase occur on the outer surface of conducting polymer film, which is in direct contact with PBS solution for ion exchange. The releasable Fluorescein quantity of this phase is determined by the total Fluorescein near the surface of the polymer. The second phase involves the replenishment of this surface release amount. During each release, the Fluorescein near polymer surface is quickly depleted, generating a very high concentration gradient for internal Fluorescein molecules to diffuse outwards. Because the internal polymer matrix have much larger volume compare to

polymer surface. Internal Fluorescein molecules could be driven out by the concentration gradient with a small decrease to the internal Fluorescein reservoir and the next concentration gradient. Consequently, the final quantity of drug release after sufficient trials should reach a steady state, when the surface release rate of Fluorescein and the internal replenish rate of Fluorescein are roughly equal. The model prediction is substantiated by the decay function because the different between later drug release trials are much smaller compare to the early ones due to the exponential decay function.

2.5.1.4 Spectrometry quantification of accumulated Fluorescein and DNQX release

The small volume of 1X PBS was chosen for drug delivery quantification in order to obtain a detectable concentration of analyte. However small release volume is challenging for several reasons. First, care needs to be taken to position the microelectrode to avoid damaging the electrode and the drug releasing coatings. Another factor is the evaporation of liquid volume in the process. Because the PBS bubble has to form a semi-ellipsoid shape during the drug release process, the surface area to volume ratio of the PBS bubble is massive compared to solution in a chamber when the liquid form a cylindrical shape and only the cross section is exposed surface area for evaporation. The difficulty is overcome by maintaining high humidity around the PBS bubble.

The comparison of Fluorescein quantity during release trial 46-90 between modeled prediction and the spectrometry measurement confirmed the quality of the model. The DNQX release measurement and model prediction further consolidated this result. This is further consolidated by the similarity between the DNQX prediction and the measured concentration. Furthermore, due to the difficulty in direct quantification of DNQX quantity released from micro electrode with small surface area, our accumulative measurement of DNQX concentration is one

of the earliest result to directly measure the drug release quantity from microelectrodes. And the single trial release quantity predicted by the model is beyond the detection limitations of other quantification techniques for the same purpose.

2.6 CONCLUSIONS

PEDOT/CNT conducting polymer markedly improved the electrodeposition of PPy/CNT/Fluorescein polymer on microelectrodes. The double layer conducting polymer coating demonstrated excellent electrical property and stability and can be electrically triggered to precisely deliver Fluorescein molecule of specific concentration. Precise quantification of fluorescent intensity was achieved by a real time fast fluorescent imaging system and revealed a double-exponential decay trend for the delivered drug concentration at each stimulation amplitude. With 100 ms 1.5 V amplitude cosine waveform stimulation, the electrode can deliver Fluorescein up to 0.04 $\mu g/cm^2$ and DNQX up to 4 $\mu g/cm^2$. The quantification result indicate the releasable DNQX amount is sufficient to directly impact neural network activity *in vivo*.

2.7 ACKNOWLEDGEMENTS

We acknowledge the financial support by NIH R01NS062019, 7R43DA035545-02, 1R43DA036264-01 and 1R43AA022030-01.We thank the Center for Biological Imaging at the University of Pittsburgh for the use of the facility to perform microscopy experiments and image analysis.

3.0 MODULATING NEURAL NETWORK ACTIVITY AND NEURONAL STEM CELL DEVELOPMENT WITH POLY (3,4-ETHYLENEDIOXYTHIOPHENE)/CARBON NANOTUBE/ Γ-AMINOBUTYRIC ACID

3.1 ABSTRACT

Conducting polymers can be electrochemically polymerized on neural recording electrodes with charged molecules incorporated as co-dopant. Upon electrochemical stimulation, the dopant molecules can be released from the composite film. This property of conducting polymer can be utilized to deliver small charged neural active molecules from the neural electrodes in a controlled manner. Γ-Aminobutyric acid (GABA) is the predominant inhibitory neural transmitter in the central nervous system. It plays important roles in neural network activity and neural disorder mechanisms. Furthermore, neural stem cell development and neuronal cell survival are also greatly affected by GABA. GABA molecule represents a class of zwitterionic drugs that are difficult to incorporate and release by conducting polymers. In this study, a controlled, local release system to deliver GABA to neuron and neural stem cell cultures is developed. The impediment of utilizing GABA molecule with conducting polymer Poly(3,4-ethylenedioxythiophene) (PEDOT) is overcame by incorporating functionalized carbon nanotubes (fCNT) into the matrix. The resulting PEDOT/CNT/GABA film stability, drug loading capacity as well as electrical property were all enhanced by CNTs. The

PEDOT/CNT/GABA film supported neuron survival and promoted the neuronal differentiation of neural stem cells. Electrically reducing the polymer film released incorporated GABA molecules in a controlled manner. Neural network activity of *in vitro* neuron culture were abolished by released GABA from the PEDOT/CNT/GABA electrode.

3.2 INTRODUCTION

Agonist and antagonist molecules are frequently applied to *in vitro* and *in vivo* neural networks to elucidate the mechanisms of neural dynamics and the network basis of system behavior [178, 179]. For example, *in vivo* extracellular recordings was combined with micro-iontophoresis of specific receptor agonists and antagonists to reveal the role of different glutamate receptor subtypes in the neural network activity of rat barrel cortex[47]. Specific modulation of dopamine and norepinephrine receptors also revealed receptor subtypes differentially involved in neuronal firing tuning in the prefrontal cortex during working memory tasks [180]. Implantable neural probes and *in vitro* neuronal cell culture dishes that integrate pharmacological manipulation with electrophysiological recording could become a preferred tool to impact such field[181, 182].

Conventionally, systemic administration[183], global perfusion[58], and micro-cannula infusion[57] have been the most commonly utilized methods of drug delivery *in vitro* and *in vivo*. These methods are efficient and simple to apply in the cases that require low spatial and temporal resolution. Advanced research, however, requires controlled delivery or chemical stimulation at the scale of a small neural networks or even single neuron. Pressure puffing and iontophoresis have been employed for such control of neural activity [184]. However, these

methods are generally limited to very few targets. Micro-fluid channels equipped neural electrodes were also fabricated to achieve simultaneous chemical perturbation and electrical recording [185, 186]. The recent development in such technique eliminated the requirement of extra positioning devices and improved the spatial resolution and repeatability of local drug delivery. However, such complex fabrication with the addition of the channels, pumps, and valves for drug delivery can lead to lower yield, higher cost and higher failure rate. Furthermore, the size of the device were inevitably increased, which is undesirable for insertion injury and host tissue reaction *in vivo*. It has also been demonstrated that when a volume of liquid is injected to the host, physical disturbance or even separation to the nearby neural tissue could often be expected, adding difficulties to interpret the neurophysiological observations. A PEDOT PSS based ion pump micro device technique has been developed by Simon et al. to solve these problems [163]. Cationic species and neurotransmitters have been electrically pumped to the target cell or tissue without fluid flow [163, 164] in such cases. Unfortunately, the device requires complex fabrication, and is not compatible with simultaneous neural recording or stimulation studies. Our PEDOT/CNT based technique recruit a different mechanism to release neurochemicals from the polymer coated microelectrode arrays, bypassing the major hindrance of the previously discussed drug delivery methods.

Conducting polymers can be electrochemically synthesized directly on the surface of micro- or macro electrodes. The polymer backbones are oxidized in the process and have multiple positive charges, while the dopant molecules with negative charge are electrostatically bond to the polymer backbone to balance the net charge of the film. When reduction potential is applied to the polymer, a controllable amount of positive charges are removed by the reduction reaction, removing the electrostatic force holding dopant molecules. Thus the dopants are

delivered in the polymer reduction process. This redox property of conducting polymers serves as the foundation of our technique. The system has been widely explored to delivery negatively charged molecules for modulating biological processes. For example, Our lab has previously demonstrated the *in vitro* utilization of this technique to release CNQX (6-cyano-7-nitroquinoxaline-2,3-dione), an AMPA (2-amino-3-(5-methyl-3-oxo-1,2- oxazol-4-yl)propanoic acid) receptor antagonist to suppress action potential generation in hippocampal neural cultures in a precise manner [154]. And the delivery of anti-inflammatory drug Dexamethasone has also been used *in vitro* and *in vivo* to reduce inflammatory cell and tissue response [94]. On the other hand, loading and release of zwitterionic and cationic molecules has been largely limited. But some efforts have been made to delivery dopamine molecules with electrochemically controlled redox reaction of conducting polymers[187].[188-190]. The incorporation of cations requires the incorporation of large immobile anions as polymer dopant, and the cations could electrostatically bind to the large anion molecules. Though the feasibility of these techniques were evaluated, further *in vitro* and *in vivo* investigation of the benefit of drug delivery system needs to be characterized.

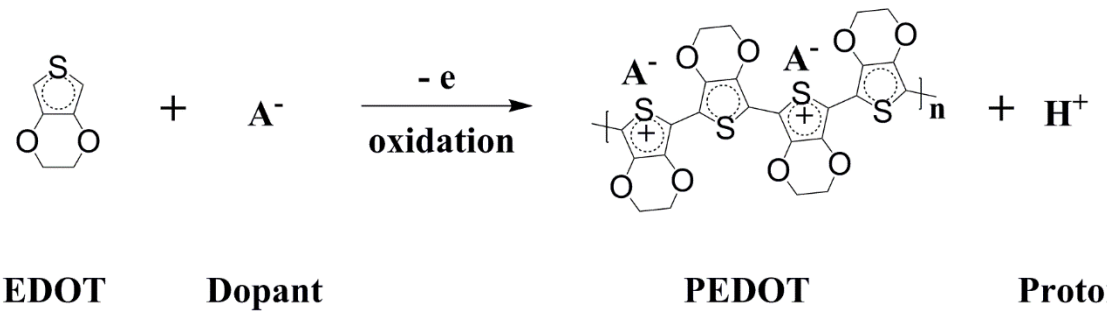

Figure 3-1 Polymerization of EDOT monomer. When oxidation voltage is applied to the electropolymerization solution, the EDOT monomer in the solution will be oxidized and form PEDOT polymer. The conjugated polymer exhibit positive charge on the backbone, allowing the electrostatic interaction between PEDOT

and the anionic dopant molecule A. Only a portion of the monomeric subunit on the polymer chain is positively charged and the ratio of these charged monomeric subunit is termed doping level. High doping level correlate with more drug molecules to incorporate due to increase in net charge. In the process of this reaction protons are generated so the solution pH is affected by the quantity of reaction. GABA molecules in the aqueous solution are utilized as the dopant molecule A.

Neuronal activities on various scales, from synaptic transmission to network oscillation and plasticity, are mediated by various types of receptors that can be specifically activated, inhibited or modulated by endogenous and exogenous molecules. For example, GABA is a major inhibitory neurotransmitter that plays critical roles in neural network activity and function[191, 192]. GABA is also important for developmental plasticity of neuronal circuits [193, 194] and the GABA system abnormality is associated with many types of neural disorders. The study of different receptors involved in neural network activity requires pharmacological manipulations of these target receptors[56].

However, electrochemically controlled released of GABA molecule is difficult because of the zwitterionic property of GABA. During electropolymerization of conducting polymer, the quantity of zwitterionic molecule to incorporate is low. And GABA molecule reduce the conductivity of the polymer, thus only very small amount of polymer with GABA can be synthesized before the film become semi-conductive or even close insulative. Furthermore, no direct spectrometry measurement can quantify the concentration of GABA molecule in solution. To bypass these difficulties, we utilized CNT as dopant to facilitate the polymerization of PEDOT. Meanwhile, the interior cavity of CNT harbor high concentration GABA solution and function as reservoir of GABA molecule to remarkably increase the quantity of GABA loaded in the polymer film. Next, an optimized OPA fluorescent reaction for quantification of amine

groups on GABA was utilized to indirectly measure the precise concentration of releasable GABA molecules.

The proposed mechanism of GABA molecule delivery is based on the local polarization of small molecules and the acid deprotonation dynamics in the solution. When GABA molecule are present in water solution, the amine group can undergo protonation process and gain one positive charge while the carboxyl group can deprotonate and gain one negative charge to the molecule. So the process yields no net charge for the molecule. However due to the positive and negative charge on amine and carboxyl groups , respectively, the GABA molecule is polarized in aqueous solution. During the polymerization of the solution, we hypothesize the carboxyl end of GABA molecules with negative net charge can be incorporated into the conducting polymer film as dopant molecules. And another source of GABA molecules in the polymer is the interior of CNT reservoir because high concentration GABA solution was pre-loaded into the CNT and the CNT was immobilized and sealed with PEDOT. When GABA molecule on PEDOT backbone was released by electrochemical trigger, the CNT reservoir can replenish the polymer GABA molecule by concentration gradient[125].

The polymer and CNT film doped with GABA molecule can not only deliver GABA molecule on demand to modulate neural activity, the trophic effect of GABA can also facilitate NSC and neuron growth on the polymer surface. NSC and primary neuron culture was seeded onto four types of polymers: PEDOT/PBS, PEDOT/CNT, PEDOT/GABA and PEDOT/CNT/GABA. The NSC and neuron cell densities was quantified from immunohistochemistry images. The ratio of NSC differentiation into neurons was quantified by counting cells with neuron beta III tubulin marker and cells with glial marker. The neurite length extension was quantified from the immunohistochemistry of primary neuron culture and was

utilized to compare the beneficial effect of various polymers. The four experiment groups clearly demonstrate the benefit of CNT, GABA as well as the interaction between the two dopants for the performance of PEDOT polymer.

To demonstrate the GABA release from electrode, X-ray photoelectron spectroscopy (XPS) technique was utilized to analyze the surface element ratio change following electrochemical drug release triggers. The drug delivery stimulation reduced the surface ratio of GABA molecules, indicating the electrochemical reduction of polymer successfully delivered GABA molecules over trials.

Bioactivity of released GABA molecule was assessed to validate the system can successfully be utilized for delivery of GABA molecules to modulate neuronal firing. *In vitro* neuronal cell culture was utilized to verify the neurophysiological effect of the GABA release conducting polymer. Due to the low cost and large quantity of neuronal cell cultures compare to direct neurosurgical interrogation of *in vivo* neural networks, the method was developed as an excellent testbed for early phase pharmacological and toxicological assessment of various reagents. High throughput electrophysiological recording can be applied to the neural culture on the microelectrode array surface for the duration of the cell culture experiment. So we applied the released solution from macroelectrode to *in vitro* culture of neural networks on microelectrode array to suppress the neural activity in the network. The released GABA molecules produced a similar neurophysiological effect compared to a known GABA solution. This experiment clearly indicate the GABA molecules delivered by the electrochemical technique maintained their biological activity.

3.3 MATERIALS AND METHODS

3.3.1 Materials and Electrodes

3.3.1.1 Materials

The materials utilized to build microelectrode array using optical adhesives are described in chapter 1. The Pt/Ir wires were obtained from A-M systems (WA). The UV-curing epoxy (NOA 63) was purchased from Norland Products Inc. (NJ). Multi-walled carbon nanotubes (mwCNTs) were obtained from Nanoamore (TX) and functionalized with carboxyl groups using previously described method. Deionized water (DI H_2O) was processed by a Millipore Q water purification system (EMD Millipore, MA). All other chemicals are obtained from Sigma-Aldrich unless noted otherwise. The brief method for functionalizing CNT and manufacture the microelectrode arrays are described as follows: 200 mg CNTs were first sonicated in strong acid solution (33.3 mL HNO_3 and 100 mL H_2SO_4). With the heat generated by mix the two types of condensed acid, the solution was sonicated for two hours for chemical reaction and breaking the CNTs down from 10 μm to around 1 μm in length. Then the solution is placed on a hotplate (55 ^oC) for overnight. Afterwards the acid was gradually removed by repetitively wash the solution with DI H_2O and separate by ultracentrifuge at 12-19k rpm. The microelectrode array with Pt/Ir wires embedded in the optical adhesive was prepared as follows: first three micro wires were aligned in the optical adhesive solution, then UV light was shined onto the solution to cause the adhesive to cure. Then the array was sawed down to 1.5 cm in length and polished with 1um and 0.05 μm electrode polishing kit. After each time the array is coated with conducting polymer and used for drug delivery experiment, the electrode was polished again with the same method to a brand new state.

3.3.2 Electrochemical synthesis and characterization

3.3.2.1 Electrochemical deposition

The electrochemical deposition solution is prepared as follows: 1 mg CNT is mixed with 5 mg GABA in 1 mL DI H_2O to obtain high concentration drug solution with CNT suspension solutions. After sonicating for 5 minute with a probe sonicator (Q500, Qsonica, CT), 1.5 μL EDOT monomer was added to the solution to prepare for electrochemical deposition. 10 minutes of further sonication is applied to homogenize the solution for polymerization. On microelectrodes, the PEDOT/CNT/GABA and PEDOT/GABA polymer were synthesized by passing 0.95 V to the microelectrode surface in a three electrode setup. A platinum sheet electrode was used as counter and a AgCl coated Ag wire was utilized as reference electrode. After the polymerization, the electrode array was carefully removed from the electrochemical deposition solution, gently rinsed with DI H_2O and then stored in a container with high humidity but not direct contact with DI H_2O. The array was stored for up to one days before the electrochemical release quantification was carried out on the GABA release array. For cell culture experiments the conducting polymer was deposited onto gold sputtered plastic microscope coverslips (macroelectrode area: 0.38 cm^2) using a Gamry Potentiostat.

3.3.2.2 Characterization of polymer

The impedance spectrum from 10 Hz to 32 kHz and cyclic voltammetry measurements with a scan rate of 1 V/s and a scan range of -0.9 V to 0.6 V were measured by an Autolab N128 potentiostat/galvanostat unit (Metrohm Autolab B.V., The Netherlands) in 10 mM phosphate buffered solution (1X PBS). A three electrode electrochemical cell including a platinum sheet as

counter electrode and Ag/AgCl reference electrode was utilized to carry out the impedance and cyclic voltammetry measurement.

Microscopy images of the polished microelectrodes and polymer coated electrodes were examined under a Zeiss fluorescent microscope (Germany). The image brightness was adjusted for each situation due to the drastic difference in contrast for each type of polymer. Scanning electron microscopy (SEM) images of GABA polymer on microelectrodes were taken using a JSM 6330F SEM (Joel, Japan). A 5 nm layer of Pd was sputtered onto the electrode to improve the conductivity before the SEM and 5 kV accelerating voltage was utilized for the SEM imaging.

3.3.3 Evaluation of drug release and quantification of delivered GABA molecules

3.3.3.1 XPS analysis of drug release

XPS analysis of PEDOT/GABA films was performed with a K-Alpha XPS system (Thermo Scientific) equipped with a monochromated Al Kα source (1486.68 eV). The conducting polymer underwent up to 90 cyclic voltammetry stimulation to delivery GABA molecules. The structure of PEDOT and GABA are demonstrated in Fig. 3-2. One GABA molecule contains one nitrogen atom and no sulfur, while EDOT repeat unit in PEDOT molecules contains one sulfur atom but no nitrogen, therefore, N/S ratio can be utilized to quantify the molar ratio between GABA and EDOT unit in PEDOT and the N/S ratio decrease over stimulation trials would indicate the release of GABA from the polymer composite film. When GABA gets released, the phosphate ion in the PBS solution may be exchanged into the polymer film, which can be observed on XPS.

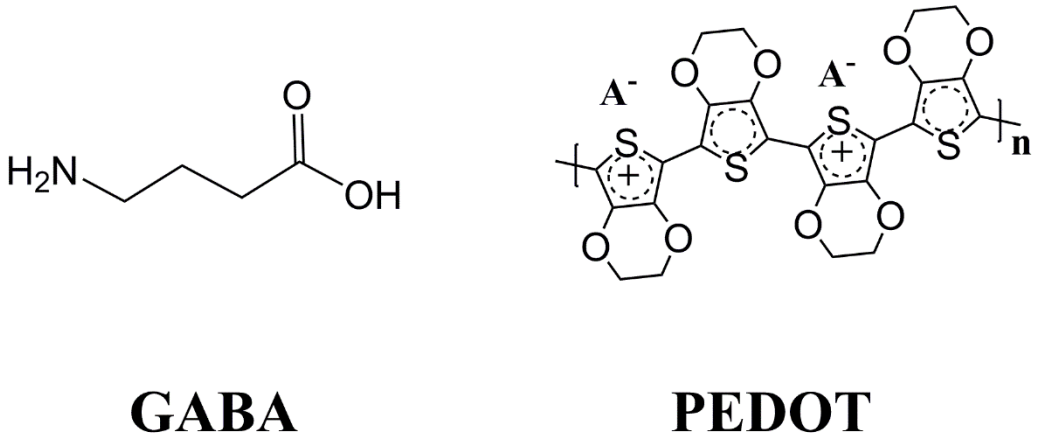

GABA **PEDOT**

Figure 3-2 The chemical structure of PEDOT and GABA molecules. GABA contains one nitrogen and no sulfur while PEDOT molecules have sulfur element but no nitrogen, therefore, nitrogen and sulfur element is utilized to quantify the molar ratio between GABA and EDOT unit in PEDOT.

3.3.3.2 OPA assay for quantification of amine group

The OPA reagent react with thiol group in 3-MPA and amine group in basic environment (pH 9-11) and form a fluorescent product. The excitation wavelength is 340 nm and the emission wavelength is 455 nm. This fluorescent emitting reaction is utilized as the main mechanism to quantitatively assess amines or amine containing compound in analytical chemistry. The selection of thiol reagent directly impact the stability of fluorescent signal over time due to the stability of fluorescent product molecule in Fig. 3-3. The OPA reaction duration was optimized to be 100 seconds in order to achieve a stable measurement. The concentration of OPA, 3-MPA and amine group of GABA follows the optimization of previously conducted HPLC experiments[195]. Mixture of 3 mM OPA and 9 mM of 3-MPA reagent in Borate Buffer Solution (BBS) at pH=9.3 was utilized. Preparation of OPA fluorescent reagent was fresh for each experiment and extra solution was stored in 4 ^{o}C for use up to three days. The spectrometry technique to detect drug delivery from epoxy microwire arrays was utilized to quantify the

GABA delivery from the microelectrodes. In brief, the microelectrode array was positioned carefully in 60 μL of PBS solution and stimulated with -1.5 V amplitude cosine waveform and 20 μL of the release solution was collected for OPA and moved to 96 well plates. The three microwire electrodes in each array were shorted together for increasing the quantity of GABA delivery. From trial 1 to trial 60 the release were accumulated each 15 trials, yielding 4 samples to quantify. From trial 61 to trial 150 the release were accumulated by 30 trials so the reduced GABA concentration can be quantified with better signal and less systemic error. After all GABA solution was collected, 200 μL of OPA reagent was immediately added to the solution and 100 seconds were allowed for the OPA to react with 3-MPA and GABA. The fluorescent intensity was sampled for 30 seconds at 5 seconds interval and the average intensity for each well was used as the final fluorescent intensity for calculating GABA concentration.

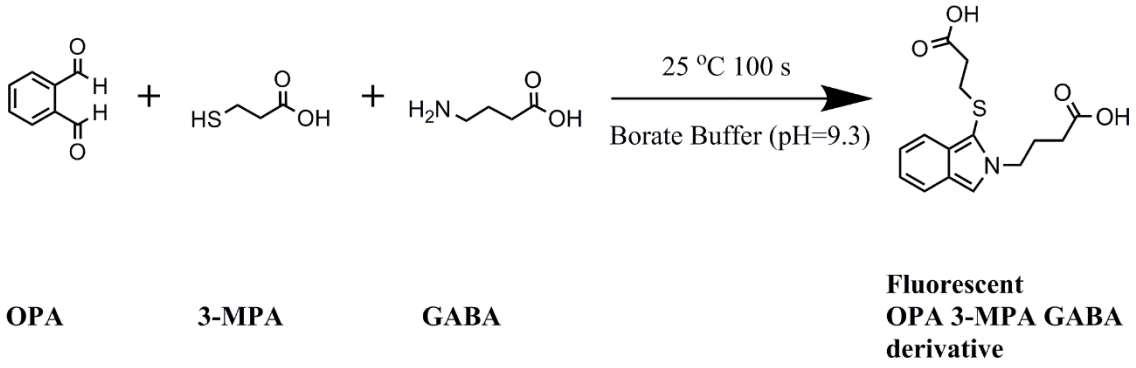

Figure 3-3 The chemical reaction to quantify amine groups in GABA. The OPA reagent react with thiol group on 3-MPA and the amine group in GABA molecule to form a stable fluorescent emitting derivative. The reaction serves as the basis to quantify amine groups in the solution.

3.3.4 Neural stem cell and neuron culture on GABA polymer

3.3.4.1 Neural stem cell culture

NSCs were isolated from the cortical tissue of E18 Sprague-Dawley rat embryos. The tissue was triturated in a Hank's Balanced Salt Solution (HBSS, Sigma-Aldrich) solution containing GlutaMAX (1%, Invitrogen) and Penicillin-Streptomycin (Pen-Strep; 1%, Invitrogen). The tissue was allowed to settle and the supernatant was centrifuged to pellet the cortical cells. After resuspension in NeuroCult NS-A proliferation medium (StemCell Technologies) with recombinant human epidermal growth factor (EGF; 20 ng mL-1, Invitrogen), recombinant human basic fibroblast growth factor (bFGF; 10 ng mL-1, Invitrogen), Heparin (2 mg mL-1; StemCell Technologies), and Pen-Strep (1%), the cortical cells were maintained at 37°C for 3 d or until the formation of neurospheres was detectable. The cells were then passaged as necessary every 3-4 d and were used for assays within passages 2 to 4.

For NSC experiments, the neurospheres were passaged to achieve a uniform suspension and seeded on prepared cell culture surfaces at a density of 150,000 cells cm^{-2}. The seeded cells were maintained at 37°C in NeuroCult NS-A Differentiation medium (StemCell Technologies) supplemented with Pen-Strep (1%) in the absence of growth factors in order to induce differentiation. The culture medium was exchanged every 3 to 4 d depend on the cell density and the culture medium indicator.

NSCs were seeded on the surface of the PEDOT films that were treated with PLO (20 μg ml-1in PBS, 1 h incubation) and fixed with paraformaldehyde (4%) at 7 d to assess differentiation. The samples were immunostained with markers for neurons (mouse monoclonal anti-β-III-tubulin, TuJ1; 1:500; Sigma-Aldrich), astrocytes (rabbit polyclonal anti-glial fibrillary

acidic protein, GFAP; 1:500; DAKO). The brief immunohistochemistry procedure is as follows: the cells were treated in blocking buffer (5% goat serum in PBS with Triton-X, 0.02%, for TuJ1 and GFAP) for 20 min, then incubated in primary antibody for 2 h at room temperature followed by fluorescent secondary antibody (Alexa Fluor 488 anti-mouse or Alexa Fluor 594 anti-rabbit; Molecular Probes) for 45 min at room temperature. The cells were counterstained for nuclei using Hoechst 33342 (Invitrogen).

TuJ1-immunoreactive cells and GFAP- immunoreactive cells were quantified to determine the extent of neuronal and astrocyte differentiation on each culture substrate (n = 3 for each). Each sample was imaged using a 20x objective and 10 random images were taken for quantification of neuronal differentiation ratio. Values were reported as the percent of differentiation by dividing the number of TuJ1 or GFAP cells by the total number of nuclei present in the image.

3.3.4.2 Primary neuron culture

PEDOT/PBS, PEDOT/CNT, PEDOT/GABA and PEDOT/CNT/GABA coated macroelectrodes were fixed to the surface of 24-well culture plates with Kwik-Sil (World Precision Instruments) and sterilized with UV light for 15 min. The polymer surfaces were washed with sterile PBS immediately afterwards. Cortical tissue was isolated from E18 Sprague-Dawley rat embryos and treated with 0.025% Trypsin in a buffer containing 137 mM NaCl, 5 mM KCl, 7 mM Na2HPO4, and 25 mM HEPES. Neurons were dissociated with gentle trituration and maintained in Neurobasal medium (Invitrogen, 21103-049) supplemented with B27 (Invitrogen, 17504-044), GlutaMAX (Invitrogen, 35050-061) and Antibiotic-Antimycotic (Invitrogen 15240-062). For neuron growth experiment, cells were seeded on GABA and control

polymer surfaces at a density of 100k cells per electrode and grown for 3 days. To measure the neurite length by preventing the formation of very long and interconnected neurites, neurons were seeded on the polymer surfaces at a density of 100k cells per electrode and grown for only 24 h before fixation and immunocytochemical analysis followed by quantification of neurite length.

3.3.4.3 Immunofluorescence staining and quantification

Neurons growing on the polymer surfaces were fixed in 4% paraformaldehyde in PBS for 15 min and washed with 2 minutes PBS soaking for several times. The cells were immersed in a blocking buffer (5% goat serum/0.2% triton-X in PBS) for 20 min followed by incubation in mouse monoclonal antibody against β-III-tubulin (TuJ1, 1:1000, Sigma) for 1 h. After washing in PBS, the cells were incubated in goat anti-mouse Alexa Fluor 488 (1:1000, Invitrogen) secondary antibody for 1 h, washed thoroughly in PBS several times.

TuJ1-positive neurons were imaged using a fluorescence microscope. For each group, 10 random 10x images were collected from each sample (n = 3). Neuron density was quantified by counting the number of TuJ1-immunoreactive cells that clearly display at least one neurite that measured longer than the width of the cell body. Neurite length analysis was performed using the NeuronJ plugin for ImageJ (http://rsbweb.nih.gov/ij/). Neurites extending from each neuron cell body were traced and measured, and the average neurite length was calculated and compared.

3.3.4.4 Statistical analysis

Statistical analyses of cell culture experiments were carried out in SPSS software. Student's t-tests were utilized for comparison of two experimental groups. Statistical significance was

considered for $p < 0.05$ (*) and $p < 0.01$ (**). All data is presented as the mean (± standard error of the mean).

3.4 RESULTS

3.4.1 Synthesis and characterization of GABA loaded coating

3.4.1.1 Electrochemical deposition and characterization

The microelectrode array was coated with conducting polymer PEDOT/CNT, PEDOT/CNT/GABA, PEDOT/PBS and PEDOT/GABA. The performance of PEDOT/GABA and PEDOT/CNT/GABA is compared to demonstrate the beneficial effect of CNT in facilitating the loading and release of zwitterionic molecules. Because the carboxyl group of GABA with negative charge acts as dopant for PEDOT polymers but the positive charge of amine groups will interfere with GABA incorporation, the use of GABA as dopant molecule is difficult and may yield very small quantity. Thus the addition of CNT is critical to increase the quantity of GABA molecules in the reservoir. In Fig. 3-4A, the coating current for PEDOT/GABA polymer with and without CNT were directly compared. The coating with CNT exhibited an increased current for the Chronoamperometry deposition at the same potential, 0.95 V. The curve also demonstrated two modes, the first mode is the general decreasing in current similar to PEDOT/GABA, the second mode was the slight convex of current around 5 seconds. The convex structure was because the newly synthesized conducting polymer could increase the surface area at high rate and partially overcome the increase in surface resistivity. Although the coating current and total charge density for PEDOT/GABA deposition shows significance difference

without the CNT, the final impedance of the electrodes demonstrated in Fig. 3-4B is very similar. The polymer with CNT demonstrated lowered conductivity at high frequency range and higher conductivity at low frequency range. This difference in impedance amplitude spectrum is typically considered very small thus indicate the electrodes has very similar performance. The cyclic voltammetry measurement of the polymers yield very similar performance. The PEDOT/CNT/GABA polymer exhibit slightly increased overall charge storage capacity while the PEDOT/GABA polymer displayed a more prominent reduction peak for drug delivery reaction at -0.35 V.

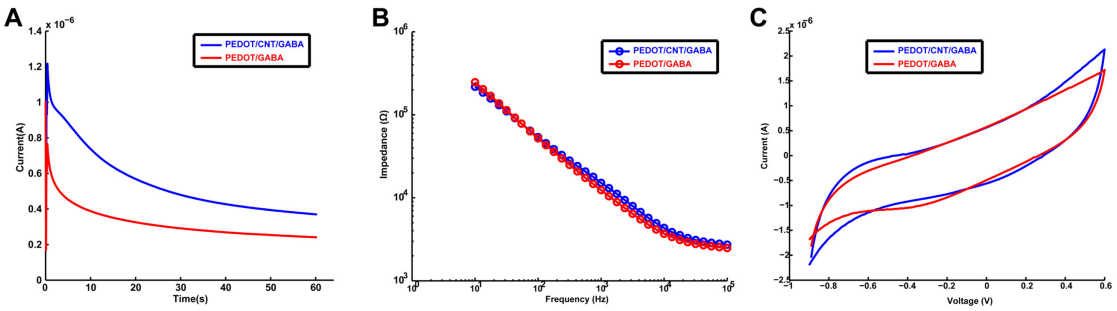

Figure 3-4 Morphology of GABA polymer with PEDOT and CNT. (A) The coating current comparison between PEDOT/CNT/GABA and PEDOT/GABA demonstrate the contribution of CNT to the electrochemical deposition of PEDOT polymers, the polymer including CNT exhibit much higher potentiostatic deposition current. Despite the downward trend of coating current for both types of conducting polymers, the deposition charge of both PEDOT/CNT/GABA and PEDOT/GABA reached sufficient amount to form a visible layer of conducting polymers and change the electrochemical characteristics of the electrode. (B) Impedance spectrum of PEDOT/CNT/GABA and PEDOT/GABA comparison between 10 Hz and 100000 Hz. The different between the polymer with and without CNT is very small. PEDOT/CNT/GABA polymer exhibit a slightly lower impedance value especially at low frequency range, this validate the CNT included polymer display less DC resistivity thus allow more coating current to form the polymer. (C) Cyclic voltammetry characterization of PEDOT/CNT/GABA polymer and PEDOT/GABA polymer between -0.9 V and 0.6 V. The scanning range was chosen to prevent water hydrolysis at large amount while maintain sufficiently low voltage to reveal the drug release reduction activity of the polymer.

The PEDOT/CNT/GABA polymer exhibit a slightly large current compare to PEDOT/GABA polymer while the PEDOT/GABA polymer displayed a more visible PEDOT reduction peak for drug delivery.

3.4.1.2 Morphology characterization of GABA polymer

The morphology of PEDOT/CNT/GABA and PEDOT/GABA was very different despite the similarity in the CV current and impedance spectrum. As demonstrated in Fig. 3-5B and E, the PEDOT/CNT/GABA film was thick and uniform, with a nanostructure feature size slightly larger than PEDOT/CNT compare to Fig. 3-5D. The polymer appears dark in color due to the absorption of light by CNT. Obvious deposition of PEDOT on the surface CNT was visible under SEM in Fig. 3-5E yet the hollow structure allowing ion mobility deep inside the polymer matrix maintained compare to PEDOT/CNT film. The polymer grew on the surface of the network of CNTs. This changes diameters of the nanotubes roughly 20-30 nm to around 50 nm. The hollow area in between individual CNTs are reduced as a consequence. In comparison, the PEDOT/GABA film in Fig. 3-5C lack the uniformity and thickness compare to PEDOT/CNT and PEDOT/CNT/GABA. The SEM morphology of PEDOT/GABA exhibited a cauliflower-like topography with spherical nanostructure on the surface. This less porous polymer matrix prevents the penetration of ions into the polymer film or the diffusion of deeply embedded drug molecules outwards. Due to the lack of CNTs in the PEDOT/GABA polymer to absorb light completely on the surface of electrode, the thinner polymer appears mostly clear with a different light refraction index. Thus the thickness difference of PEDOT/GABA across the surface of the microelectrode was clearly indicated by various darkness of the polymer coated regions. In both PEDOT/GABA and PEDOT/CNT/GABA cases the PEDOT polymer growth did not exceed the GSA of microelectrode itself, this addition of conducting polymer without impairment to the

electrode stimulation or recording spatial resolution is beneficial for interfacing with neural tissue.

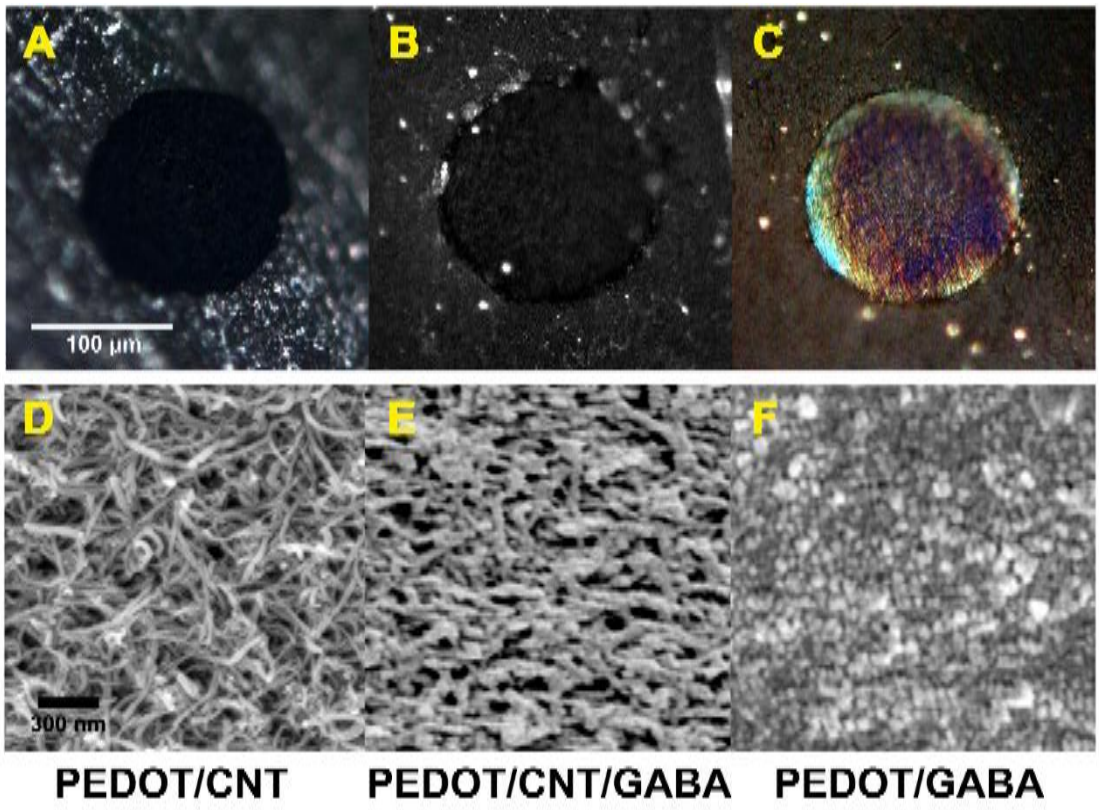

Figure 3-5 Morphology of GABA polymer with PEDOT and CNT. (A) Electrochemical deposition of PEDOT/CNT show a dark color appearance. The conducting polymer matrix expand slightly beyond the edge of the microelectrode. The difficulty for synthesizing PEDOT/CNT polymer is low so the PEDOT/CNT form a thick and uniform layer completely cover the surface of the microelectrode. (B) Incorporation of GABA into PEDOT/CNT polymer yield a very similar morphology compare to PEDOT/CNT only, the microelectrode was completely covered by a uniform layer of PEDOT/CNT/GABA polymer, allow the maximum amount of GABA molecules to be uniformly released from the surface of the electrode. (C) The PEDOT/GABA polymer without CNT demonstrated a completely different morphology due to the difficulty of electrochemical deposition. The uniformity of the polymer was undermined by the uneven distribution of charge deposition on the microelectrode surface. The center of microelectrode received more charge thus the polymer thickness and uniformity was superior compare to the edge of the microelectrode. (D) The microscopic texture of PEDOT/CNT under SEM examination. The polymer clearly

demonstrated an expanded structure with CNT visible on the surface of the matrix. Hollow area in between the CNT structure exist uniformly across the surface of the microelectrode, allowing the ionic exchange of the polymer matrix and solution penetrate to significant depth in the polymer. (E) SEM image of PEDOT/CNT/GABA polymer demonstrated a similar surface texture feature compare to PEDOT/CNT but the CNT polymer was clearly covered by PEDOT/GABA polymer. (F) Surface morphology of PEDOT/GABA observed under SEM illustrated a clearly different appearance. The morphology better resembles traditional conducting polymer such as PEDOT/PSS. The GABA molecules impede with the polymerization process so the polymer is only deposited as a thin layer on the electrode surface. The polymer exhibit a roughened surface than the bare metal electrode and shows cauliflower like surface patterns.

3.4.2 Electrochemically controlled GABA release

3.4.2.1 XPS characterization of GABA delivery on macroelectrodes

Fig. 3-6A shows the XPS of PEDOT/CNT/GABA film before and after 30 cyclic voltammetry (CV, cycles of ramping voltage, -0.9 to 0.5V, 100 mV/s) stimulation. Comparison of the two XPS spectrum reflect the dynamic change of GABA, PEDOT and phosphate quantity on the surface of the conducting polymer due to the exclusive existence of nitrogen, sulfur and phosphor in the three types of molecules, respectively. Due to the presence of chlorine in the PBS solution, a chlorine peak was also observed at 30 cycles of CV drug release stimulation. A drug delivery trigger is typically composed of two phases, one is the negative reductive phase to reduce the positive charge on the polymer in order to electrostatically repulse the anion dopant molecules into the surrounding environment, and the second phase was reversed to balance the charge in order to reduce the potential harmful effect of the polymer to biological tissues. Another important reason for charge balance phase is the conjugate polymer with more positive

charges demonstrate better conductivity than the reduced polymers, thus to allow further stimulation to cause drug delivery, the film is preferentially oxidized to partially recover the conductivity. During the re-oxidation of the polymer, limited quantity of drug molecules are re-absorbed into the surface due to the quick diffusion of the drug molecule, meanwhile the omnipresent PBS anions including phosphate and chlorine anions were incorporated into the film and was observed with XPS analysis. In Fig. 3-6B, N/S ratio was deduced from the XPS spectra indicating the molar ratio between GABA and the EDOT unit in the polymer matrix. After stimulated with 30, 60 and 90 CV cycles, the amount of GABA in the film consistently decreased, illustrated by the N/S ratio decreases in Fig. 3-6B. The reduction trend of N/S ratio follows a linear correlation indicated by the blue fitted curve in the plot. The linearity of the nitrogen content reduction reflect a rough trend for GABA molecule depletion in the polymer matrix.

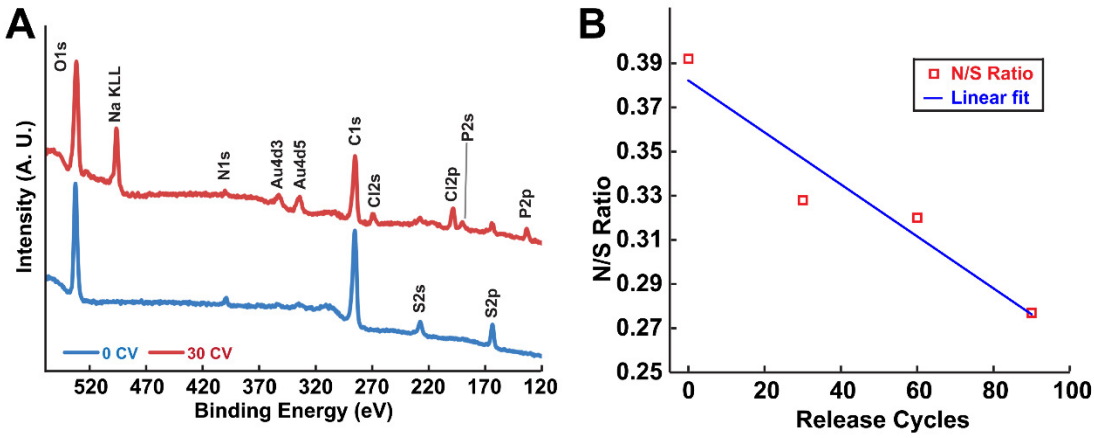

Figure 3-6 XPS characterization of PEDOT/CNT/GABA delivery. (A) The XPS characterization of PEDOT/CNT/GABA film. At CV cycle 0, the film exhibit prominent characteristic peaks for nitrogen and sulfur element. Due to the high surface ratio of GABA molecules when the film was first synthesized, the N/S ratio of the polymer is high according to (B). At 30 CV release cycles, the surface GABA molecules ratio is decreased, thus the

N/S ratio was decreased due to the exclusive presence of nitrogen in GABA molecule on the surface, while the phosphor characteristic peaks were present because the PBS anions exchange with the released drug molecules to balance the polymer backbone charge. (B) Quantitative N/S ratio characterized in various films following GABA delivery CV cycles. With the increase of CV cycles, the GABA quantity decrease gradually over trials, due to the consistency of sulfur in PEDOT backbone, the nitrogen atom is directly correlated with the total amount of GABA molecule on the surface of polymer. The N/S ratio of polymer film follows a decreasing trend demonstrated by the linear fit, with high linearity.

3.4.2.2 OPA fluorescent reagent quantification of released GABA

OPA reagent were prepared fresh before each GABA quantification experiment and is only used for up to 1 day after the initial mixture of the solution. The recipe was obtained from previously reported HPLC quantification method and was verified with known concentration GABA solutions. The selection of 3-MPA and the BBS buffer with pH=9.3 was optimized to yield a stable fluorescent derivative compound to quantify. The fluorescent intensity of OPA reagent reacting with GABA solution was very stable as indicated in Fig. 3-7A. The fluorescent intensity measured over 240 seconds was repetitive for each concentration. The result is depicted in Fig. 3-7B where the GABA concentration and the fluorescent intensity of OPA reagent was linearly correlated with very small variation across all concentrations. Fluorescence fluctuation of Fig. 3-7A also indicate the optimal technique for quantifying GABA concentration is to repetitively measure the kinetics of fluorescent intensity change over sufficient duration and calculate the average intensity of the solution, because the intensity variation of individual solution was obvious over time but only fluctuate around one stable value. Due to the stability of PBS blank control and 0.2 μM GABA solution, the quantification of lowest examined GABA solution can be precisely determined with time-lapse average of the fluorescent intensity.

Consequently, 30 seconds of measurement with 6 seconds interval between each value was utilized as the standard procedure to quantify the amine group concentration in the unknown drug delivery solution.

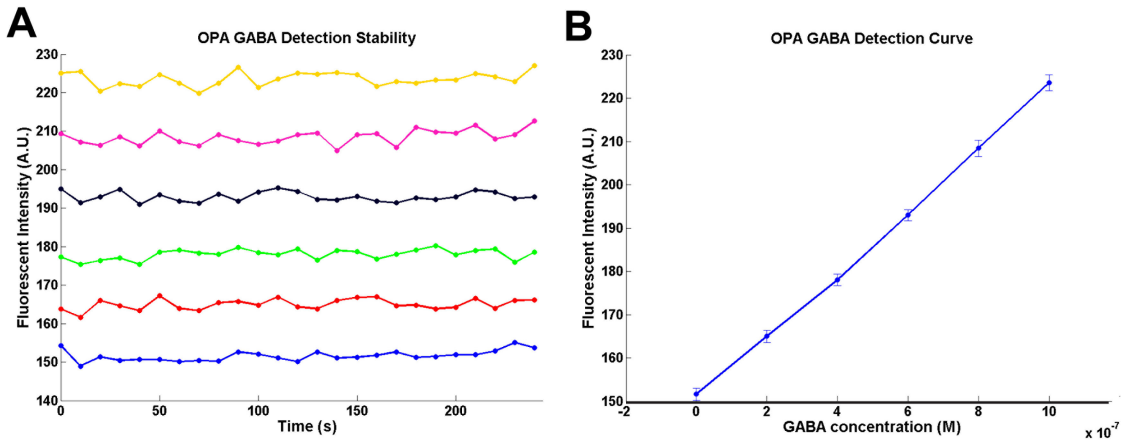

Figure 3-7 The functional curve of OPA reagent detection of amine group. (A) Kinetic measurement of fluorescent intensity following the OPA reagent reaction with GABA solution yield a very stable measurement of low concentration of GABA solution. The curves are samples at 10 seconds interval for 250 seconds, the fluorescent intensity of each solution remained stable. (B) The fluorescent intensity linearly correlate with the known concentration of GABA molecule in the solution. The error bars were derived from the repetitive kinetic measurement of 26 time points for each concentration of GABA solution. The blue line connects all the measurement values. Linear fit of the intensity function curve yield a fit quality factor of 0.9996.

The concentration of electrochemically released GABA from the conducting polymer film with and without CNT was quantified by the OPA reagent. Within the 60 µL of PBS for drug delivery experiment, 20 µL was sampled and relocated into 96 well plates to be mixed with 200 µL OPA reagent each. Mixture and reaction time of 100 seconds was selective and maintained across all trials due to the time-dependency of the fluorescent intensity. For each type of conducting polymer film, 15 trials of accumulative GABA release was executed for first 4

repeats of measurements and then the trial number was increased to 30 in order to accumulate more GABA molecule and reduce the systemic error during the measurement. The PEDOT/CNT/GABA solution denoted as “CNT release” yield the largest quantity of GABA molecules released. The release profile of PEDOT/CNT/GABA was close to linear and the variation across multiple electrode arrays was very small across all the measured trials. In comparison, the release profile of PEDOT/GABA polymer was sporadic, with very high GABA release at the beginning of the trials. The error for quantification of GABA concentration was accumulated to yield the final standard error value for the accumulative drug release quantity, thus the whole PEDOT/GABA release curve yield very large error across all measurements. The passive diffusion profile of GABA from PEDOT/CNT/GABA film indicates that a large quantity of GABA molecule can be released into the peripheral of the microelectrode without the electrical stimulation. This observation was consistent across all 4 electrode arrays measured in this group. The PEDOT/GABA film also spontaneously release GABA molecules indicated by the green line, with very good repeatability for measurement. Despite the spontaneous diffusion of GABA molecules from the conducting polymers after thorough PBS washing of the electrode, the electrical stimulation of conducting polymer still significantly increased the total quantity of GABA molecules released from the conducting polymers. Overall all types of conducting polymer film can release similar quantity of GABA molecule in both spontaneous diffusion trials and electrically stimulated trials. The electrical trigger boosted the release amount of GABA molecules in each type of conducting polymer. The incorporation of CNT into the conducting polymer matrix increased both the spontaneous diffusion of GABA and the electrically controlled release of GABA. The most beneficial property of including the CNTs into the conducting polymer film is the improvement in the repeatability and total quantity of GABA

delivered from the conducting polymer. The semi-linear release profile of GABA can be maintained for at least 150 trials when GABA is doped in the PEDOT/CNT/GABA film, while a clear decrease of GABA release quantity was observed in all other groups examined, especially the electrical release of GABA from PEDOT/GABA film.

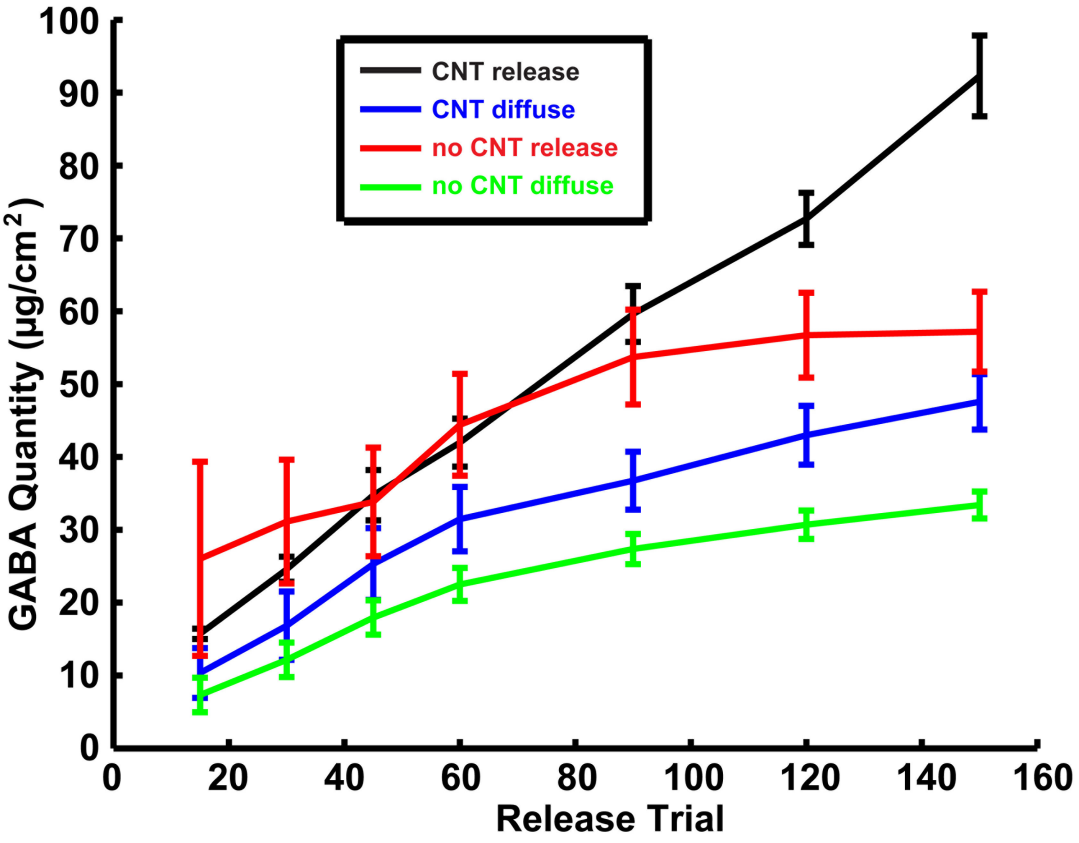

Figure 3-8 OPA quantification of GABA polymer release. Drug release from PEDOT/CNT/GABA polymer yield a more stable and largest accumulative quantity of GABA release over 150 trials (n=3). In comparison, the early accumulative diffusion GABA quantity (n=4) was lower than the electrochemically controlled release, but the quantity was similar to the active release of GABA from the PEDOT/CNT/GABA polymer. However, the quantity of GABA diffusion was lowered significantly during the later phase of release. The quantity of GABA release from PEDOT/GABA film (n=3) also demonstrated two different phases. The early drug release trials yield a very large quantity of GABA instantly delivered from the film, but significant errors were observed

across different electrodes. The later phase of drug release yield a more repeatable and lower quantity of GABA from the film. In comparison the diffusion of GABA from the PEDOT/GABA film (n=4) yield lower quantity and relatively stable profile across all electrodes. The accumulative quantity of GABA diffused from the PEDOT/GABA film was lowest among all groups, but the scale of diffused GABA quantity was similar to the electrochemically controlled release.

3.4.3 GABA conducting polymer film support NSC and neuron growth

3.4.3.1 GABA polymer improve the NSC survival and differentiation

The survival of NSC is critical for developing future treatment based on stem cell technologies and the differentiation of NSC into neurons is essential to recover the functional connectivity of damaged neural networks. On the four types of conducting polymers examined in Fig. 3-8A-D, PEDOT/GABA were the best compared to all other surfaces, with the highest NSC counts and highest neuronal differentiation (7.1%) indicated by the neuronal marker beta-III tubulin. The PEDOT/CNT film provide better support for the survival of NSC compared to PEDOT/PBS coating, with higher percentage of cells differentiating into neurons. While the incorporation of GABA into the PEDOT/CNT film enhanced the NSC attachment slightly, the ratio of cells differentiating into neurons was not improved over the film without GABA. The PEDOT/CNT/GABA film even demonstrated less overall NSC growth and lower neuron differentiation compared to the PEDOT/GABA without CNT. The phenomenon is possibly due to the change in surface morphology and GABA delivery capability of the conducting polymers. In the quantification result of Fig. 3-8E and F, ANOVA was applied to the results and the polymer with and without CNT incorporation demonstrated significant difference. Immobilized GABA in the conducting polymer matrix significantly increased the number of survived NSC on

the surface. But CNT incorporation in the polymer partially negated the benefit of immobilized GABA. In Fig. 3-8F, the neuron differentiation ratio on PEDOT/CNT did not show significance over the PEDOT/PBS film, due to the small number of cells available for quantification. However, the NSC culture experiment on PEDOT/PBS and PEDOT/CNT substantiated the safety and biocompatibility of both PEDOT and CNT material for NSC cultures.

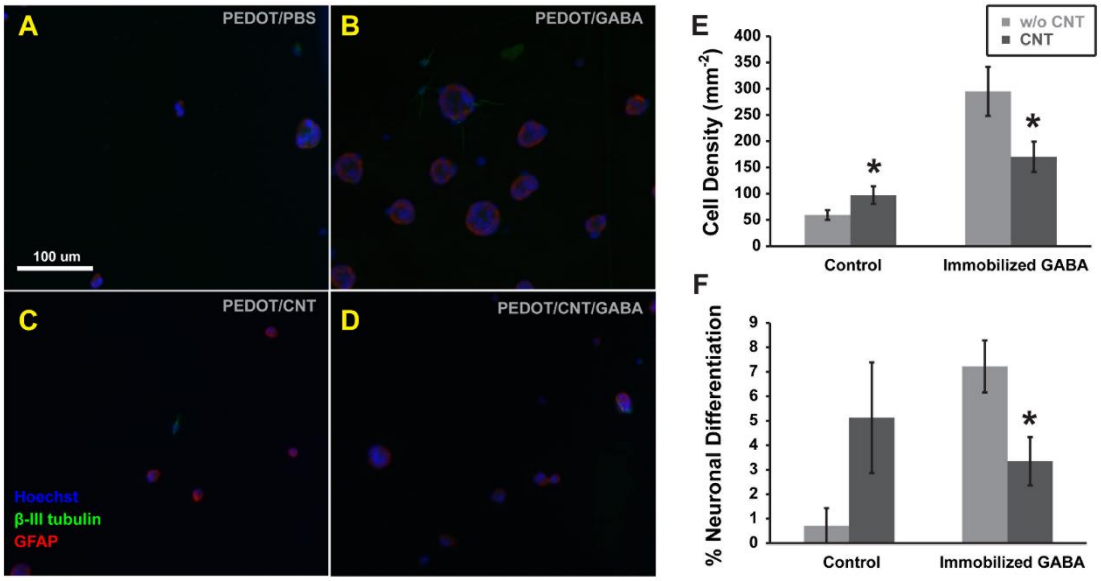

Figure 3-9 GABA polymer improve NSC growth and differentiation. (A) NSC culture was performed on polymer coated macroelectrode for cell toxicity and biocompatibility evaluation. Hoechst (blue) counter stain of cell nuclei, beta-III tubulin (green) staining for early differentiated neurons and GFAP (red) staining for astrocyte lineage cells were characterized. PEDOT/PBS polymer is non-toxic to NSC growth, but only limited number of NSC can adhere and grow, with a low ratio of beta-III tubulin expressing neurons. Scale bar=100 μm. (B) On PEDOT/GABA polymer, NSC can adhere to the surface well and a significant portion of NSC differentiate into neurons. (C) PEDOT/CNT support NSC growth and neural differentiation, slightly improved performance was observed compare to PEDOT/PBS. (D) NSC can adhere to surface of PEDOT/CNT/GABA and differentiate into neurons. The performance is much improved compare to the polymer without GABA. (E) Quantification of cell density following NSC culture, the PEDOT/CNT exhibit much better performance to support NSC growth compare to the polymer without CNT. The PEDOT/GABA coating demonstrate the best performance among the groups and

significantly improve over PEDOT/GABA/CNT coating. (F) Neuron differentiation ratio of NSC culture demonstrated similar trend compare to the polymer support for NSC growth, the ratio of beta-III tubulin positive cells were observed at highest frequency on PEDOT/GABA polymer, while PEDOT/GABA/CNT polymer shows similarly improved performance over non-GABA loaded polymer surface.

3.4.3.2 CNT and GABA facilitate neuron growth and neurite length

Compare to the NSC culture experiment, the primary neuron culture illustrated a very distinctive pattern of facilitation from the different conducting polymers. The best neuron survivability was observed on PEDOT/CNT polymer where large number of primary neurons maintained after the total duration of cell culture. The neuron count on the PEDOT/CNT was higher than both PEDOT/PBS and PEDOT/CNT/GABA condition. The neurite extension on the PEDOT/CNT film was also greatly improved over the PEDOT/PBS polymer. PEDOT/GABA polymer showed more neuron count compared to the PEDOT/CNT/GABA, but the mean neurite length was shorter than that on the PEDOT/CNT/GABA surface. This indicates that the PEDOT/GABA polymer created a beneficial environment to maintain a health population of neurons possibly by the unique surface morphology as well as leaching out GABA molecules into the culture medium, but did not promote neurite growth which is important for network formation. Meanwhile, the PEDOT/CNT/GABA film enhanced the extension of processes and promoted the formation of the network. Overall the CNT and GABA demonstrated synergistic beneficial effect on neurite extension but not the density of neurons.

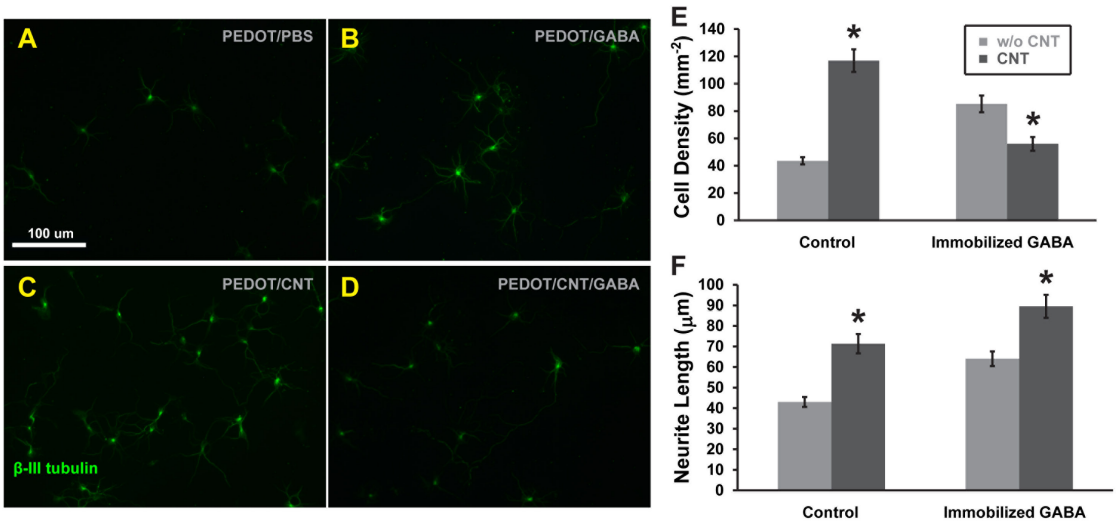

Figure 3-10 Conducting polymer improve neuron growth and neurite extension. (A) beta-III tubulin (green) staining for neurons was characterized and utilized as basis of measuring neurite outgrowth. PEDOT/PBS polymer supports neuron growth, but the neuron on the polymer surface was sparse, with only limited extension of neurites. Limited connection between neurons were observed in the culture. Scale bar=100 μm. (B) On PEDOT/GABA polymer, neurons can grow well on the polymer with density of 80 cells/mm2, each neuron extend a significant number of neurites with some of them extend far enough to form connection with other neurons. (C) PEDOT/CNT demonstrated outstanding performance to support neuron growth and neurite extension, the density of neurons reached 120 cells/mm2, significantly improved over the non-CNT modified PEDOT polymer. The interconnected neurites were frequently observed. (D) Neurons can adhere to PEDOT/CNT/GABA polymer and extend neurite distantly. The direct impact of polymer loaded with GABA is most prominent in neurite extension, with some very long neurites connecting distant neurons. (E) Quantification of neuron density on various polymer surface, the neuron density was highest on PEDOT/CNT polymer while the PEDOT/GABA polymer outperformed the PEDOT/CNT/GABA. (F) Neurite length quantification demonstrated different result comparing to the neuron cell density. The incorporation of CNT in the polymer matrix significantly improved the performance of conducting polymer for facilitating the elongation of neurites compare to the polymer without CNT. The inclusion of GABA molecule perform synergistically with the improvement of CNT, further extending the neurite length.

3.4.4 Electrochemically released GABA abolish *in vitro* neural network activity

In order to evaluate the bioactivity of the released GABA, an inhibitory neuro transmitter, *in vitro* hippocampal neuronal network cultured on MED was used. As illustrated by Fig. 3-11A-C, application of GABA solution released from the PEDOT/CNT/GABA film completely abolished the neural network firing, and the effect observed with released GABA solution was qualitatively similar to that obtained from direct addition of GABA solution at 10 mM concentration. The quantification of this process summarized in Fig. 3-11D validate the firing rate observed in the neural network after the washing of GABA solution was comparable to the firing rate before the GABA application in both released GABA and 10 mM GABA situation. Indicating the GABA solution from drug delivery did not generate long lasting irreversible effect on the firing rate of the neural networks. After washing off GABA solution from the cell culture, the network activity was recovered but also demonstrated a distinctive synchronized firing state. GABA neurons in a network can entrain excitatory neurons to fire synchronously and generate oscillatory patterns, so this phenomenon could be due to strong GABA neuron activity after recovery from activity reduction.

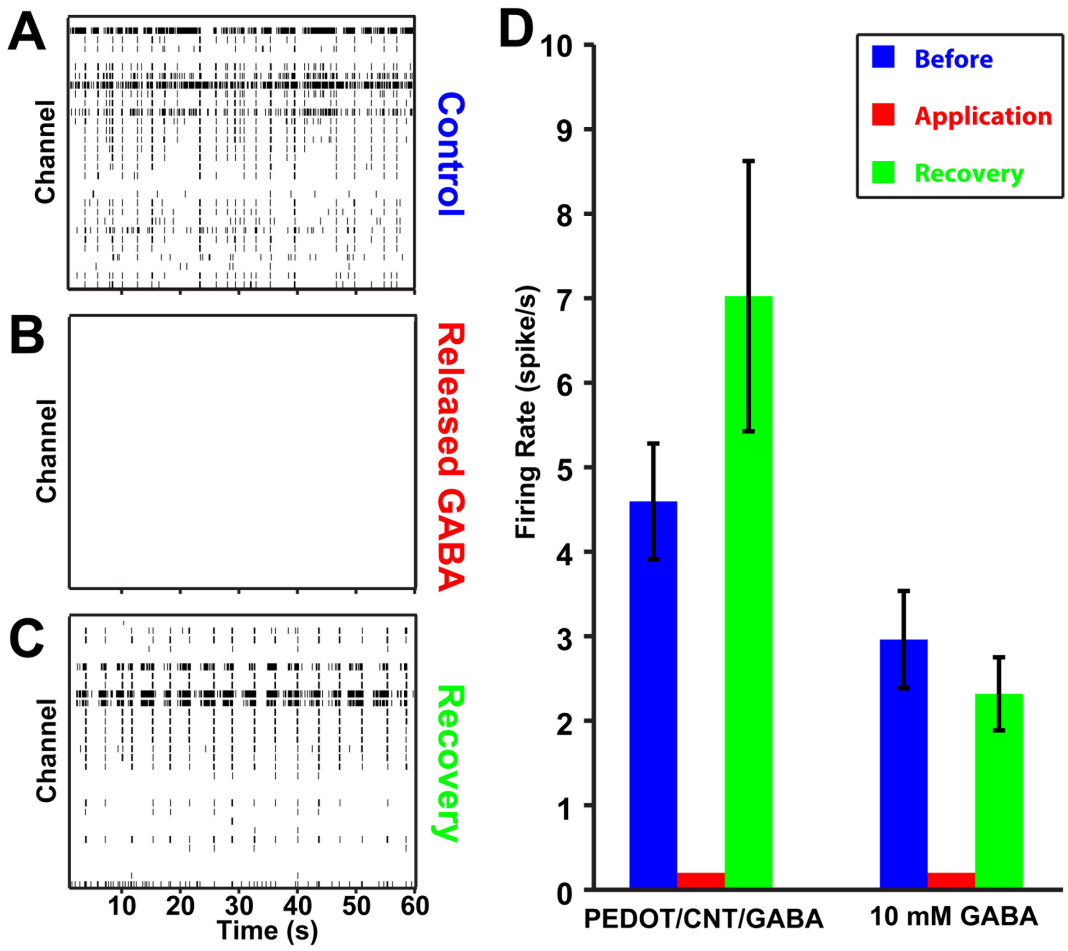

Figure 3-11 MED recording suppressed by electrochemically released GABA. (A) Raster plots of spike timings of action potentials recorded on different channels of MED is illustrated in Fig. A. The recorded channels demonstrated high firing rate as the baseline for spike number quantification. The network activity was recorded for 60 seconds, and both synchronous and asynchronous neural activity were observed over the recording period. (B) The application of released GABA solution from macroelectrode suppressed all spike generation in the cultured neural network. The result substantiate the bioactivity of GABA molecules after being released by the electrochemical triggers. (C) After replacing the drug release solution with regular culture medium for washing away the GABA molecules, the neural network activity was recovered. The neural network was entrained to generate more synchronous firing patterns in the culture medium free of released GABA molecules. (D) The spike number suppression effect of released GABA solution demonstrate similar biological effect compare to the GABA solution with known concentration. 10 μM GABA solution completely abolished the neural network action potential

generation while refreshing the medium can recover the neural network activity to the firing rate similar to before the application of GABA.

3.5 DISCUSSION

3.5.1 Synthesis and characteristics of GABA polymers

The inclusion of CNT as additive for conducting polymer drug delivery application had been proven to increase the quantity of total polymer, increase the mechanical stability and improve the electrical property of the film. The Chronoamperometry deposition in Fig. 3-4A substantiate the contribution of CNT for increasing the deposition current. Interestingly the deposition current was segmented into two fractions switched around 15 seconds. The second phase of deposition behaved very similarly to PEDOT/GABA, indicating the dominant mechanism for this deposition is the expansion of PEDOT/GABA polymer on the originally synthesized film. The first segment was marked by a slightly slower decrease in current, possibly due to the increase in surface area by the CNT deposition despite the increase in impedance caused by PEDOT/GABA. The overall competing effect was slower decrease in current. In the CV measurement for the polymers, the PEDOT/GABA polymer exhibit slightly smaller current but increased reduction peak, this may be due to the fact that the CNT films large surface area causing more capacitive current and consequently masking the redox peaks of PEDOT. . The morphology of PEDOT/CNT/GABA and PEDOT/GABA was examined to elucidate the effectiveness of Chronoamperometry synthesis process. The PEDOT/GABA film was very thin after polymerization due to a few reasons. First, part of the coating current of PEDOT/GABA

could be diverged to the non-faradic charge transfer mechanisms on the electrode surface. Second, the adherence of the conducting polymer film with PEDOT/GABA is poor compare to PEDOT/CNT/GABA blend. Although the electrochemical polymerization occur around working electrode, the synthesized polymers may not deposited on microelectrode surface. Examples of this scenario include conductive polymers with significant solubility in aqueous solutions. The microscope and SEM examination indicate both PEDOT/CNT/GABA and PEDOT/GABA were successfully deposited onto the surface of the Pt/Ir microelectrode. With a much improved performance for the PEDOT/CNT/GABA film. The porous structure of PEDOT/CNT/GABA resembles the morphology of PEDOT/CNT film but slightly expanded the diameter of individual nanofibers in the matrix. The high porosity on the surface of PEDOT/CNT/GABA polymer could greatly improve the surface area to volume ratio of the polymer thus increase the ionic delivery capability of the film. With the low porosity on the PEDOT/GABA polymer, only a thin layer of surface polymer could be utilized for the release of GABA molecules, thus the accumulative GABA release quantity may be impaired by the surface morphology.

3.5.2 GABA release quantification

The sensitivity of the optimized OPA fluorescent quantification of amine group was sufficient to quantify GABA concentration down to 0.2 μM and may even be further extended according to Fig. 3-7B. Carefully designed experiment to quantify the GABA delivery from various conducting polymer films elucidate very distinct pattern of GABA release in each condition. Low surface area to volume ratio was observed on PEDOT/GABA polymer, so the GABA molecules ready to be released are most likely aggregated on the outermost surface of the

polymer due to the low ionic mobility inside the polymer matrix. This result in a large quantity of GABA molecules being released at the very beginning of the experiment. The variation between multiple electrode arrays was also very pronounced, possibly due to the quantity of GABA molecules that are physically adsorbed with a binding force strong enough to withstand the PBS washing. Because the nodular morphology of PEDOT/GABA could form regions with very limited ionic mobility and possibly harbor a relatively high concentration of GABA molecules in a small volume. In comparison the PEDOT/CNT/GABA almost demonstrated a linear profile for the release of GABA molecules. The porous structure of the PEDOT/CNT/GABA polymer increased the penetration depth for solution significantly. But within the polymer CNT matrix, only limited mobility of ionic species is expected. Furthermore, the PEDOT reduction stimulation for triggering drug release was immediately followed by an oxidation process to maintain the conductivity and net charge on the electrode surface. Thus during the release triggers, the slowly diffused GABA molecules could be re-captured immediately, and only move slightly towards the outmost surface of the polymer. This creates a very controllable GABA concentration gradient over time, allowing the formation of almost linearized release profile of GABA molecules. The porosity of PEDOT/CNT/GABA also enabled more GABA molecules to diffuse out spontaneously when the electrode was positioned in PBS solution as demonstrated by the blue and green curves in Fig. 3-8.

3.5.3 GABA containing polymer benefits NSC and neuron growth

GABA acts as an excitatory transmitter during the early maturation stage of neurons instead of inhibitory neurotransmitter[196, 197] and the earliest formation of GABA-releasing synapse is before the formation of excitatory glutamatergic contacts in many different neural

developmental process. GABA provide important trophic actions and facilitate neuron outgrowth during development as well[198, 199]. The presence of GABA molecules from spontaneous diffusion of the conducting polymer matrix may improve the survival of NSC and differentiation into neurons through this mechanism. With GABA molecules incorporated in PEDOT polymer, a very pronounced effect on NSC density and neural differentiation ratio was observed on the polymer compared to the film without GABA. Because the lack of nanofiber structures on the PEDOT/GABA film, the polymer surface could in full contact with NSC membrane. In comparison, the PEDOT/CNT/GABA demonstrated very porous structure and hollow regions on the surface of the polymer. The morphology is beneficial for diffusion and release of GABA molecules in PBS solution, but the effective surface in direct contact with NSC membrane is significance limited by this nanofiber texture. The NSC growth and differentiation may benefit most from the direct contact with conducting polymer due to the gradual diffusion of GABA molecules through from the matrix, so the culture of NSC on PEDOT/GABA/CNT polymer only demonstrated limited beneficial effect.

The neurons however, demonstrated a different trend on various conducting polymer surfaces. The most beneficial surface for primary neuron culture was observed on PEDOT/CNT and PEDOT/CNT/GABA, with the highest density of neurons observed on PEDOT/CNT and the longest average neurite on PEDOT/CNT/GABA. As mentioned previously, GABA molecules could significantly accelerate the maturation of neurons due to the lack of glutamatergic transmission in early developmental stages, so the extensive neurite outgrowth could be an indication of more mature neurons ready to form interconnected networks. The PEDOT/CNT polymer exhibit the best conductivity among the various types of conducting polymers, the phenomenon could be relevant to the beneficial carbon nanotube substrate for increase the

neuron electrical signaling[200]. Furthermore, the nanofiber structure of the PEDOT/CNT polymer could possibly interact with surface structural proteins of cells and stimulate the adhesion and outgrowth of neurite due to the similarity of size between the nanowires and neurofilament proteins with specific molecular weights[201].

3.5.4 Electrochemically released GABA maintain bioactivity

The MED technique is developed as a high throughput and highly repeatable platform for *in vitro* assessment of experimental treatment to neural networks or other tissue with bioelectrical activities [202, 203]. The cultured neural network is suitable for evaluating the bioactivity of released GABA molecules from the polymer matrix. Due to the lack of complex input to the cultured neural network, the *in vitro* culture of neurons normally demonstrate a high firing rate at quiescent conditions[204]. The culture thus provide an exceptional experimental baseline condition for testing inhibitory effect of GABA solution. With the addition of GABA released from the PEDOT/CNT/GABA film, the network firing recorded on MED was completely abolished, indicating the GABA molecules remain bioactive after the electrochemical polymerization and electrically controlled release from the film.

3.5.5 Future works for GABA release.

The PEDOT/CNT/GABA film exhibit beneficial properties for many various types of applications to neural tissue in this study. The utilization of the conducting polymer film and drug delivery technique could benefit the neuroscience research and possibly treatment of neural disorders[156]. To further evaluate the system, the *in vivo* application of the drug delivery

experiment should be performed to verify the effectiveness of the technique. More detailed quantification of GABA release from various microelectrode surface could significant improve our understanding of the dynamical process of zwitterionic molecules being incorporated and released from conducting polymer matrix. The use of other nanomaterials such as Graphene Oxide (GO) as co-dopant could potentially provide other beneficial properties due to the high surface area ratio and the unique electrical and physical properties[205]. This neurotransmitter releasing conducting polymer films can be a promising candidate as for neural interface and neural regeneration research.

3.6 CONCLUSIONS

GABA molecules can be successfully incorporated during the synthesis of PEDOT polymer and the inclusion of CNT can facilitate the polymerization process as well as providing a more linear release profile. With carefully designed OPA fluorescent reaction, GABA molecules diffused and released from the conducting polymer film was precisely quantified. The result indicates GABA can be released up to 90 $\mu g/cm^2$ by 1.5 V cosine waveform. The released GABA solution retained bioactivity to suppress neuronal firing in an *in vitro* cultured neural network. NSC and neuron cultured on various GABA, CNT and PEDOT film demonstrated the facilitation effect of GABA for NSC survival and differentiation. The CNT facilitate NSC growth without incorporating GABA molecule but impaired the performance of GABA for enhancing NSC growth. However, CNT contribute significantly to the growth of neurons and extension of neurites while GABA demonstrated synergistic facilitation effect to a limited

extend. Overall the zwitterionic molecule GABA was successfully delivered with our electrochemically controlled drug release system based on PEDOT and CNT and the polymer surface demonstrated beneficial effect for NSC and neuron cultures.

3.7 ACKNOWLEDGEMENTS

This work was supported by the National Science Foundation Grants 0748001 and0729869, National Energy Technology Laboratory and Oak Ridge Institute for Science and Education.

4.0 MODULATION OF *IN VIVO* BARREL CORTEX NEURAL NETWORK ACTIVITIES WITH ELECTROCHEMICALLY CONTROLLED RELEASE OF 6,7-DINITROQUINOXALINE-2,3-DIONE (DNQX)

4.1 ABSTRACT

Conducting polymers can be electrochemically deposited on electrodes with negatively charged dopant molecules incorporated. When electrically stimulated, the dopant molecules can be released. This property of conducting polymer can be utilized to deliver various biological molecules into the body in controlled manner. Previously we have shown delivery of CNQX (6-cyano-7-nitroquinoxaline-2,3-dione), an AMPA (2-amino-3-(5-methyl-3-oxo-1,2- oxazol-4-yl)propanoic acid) receptor antagonist in hippocampal neuron culture diminished neurotransmission and reduced neuronal spiking. In this work the drug delivery technology is further developed and evaluated with DNQX (6,7-dinitroquinoxaline-2,3-dione) release in rat somatosensory (S1) barrel cortex. Barrel cortex neural activity reliably represents sensory stimulation from facial whiskers in a topographical manner. The repetitively quantifiable neural network in barrel cortex thus provides an excellent test bed for evaluating our local drug release system *in vivo*. Multi-whisker air puff stimulation is utilized to evoke repeatable neural firing in layer IV of barrel cortex. The recorded neural activity can be immediately suppressed by the delivery of DNQX for one to six seconds within the 300 μm, demonstrating the high spatial and

temporal selectivity of this novel drug delivery system. Furthermore, weaker neural activities after whisker stimulation can be nearly abolished by the released DNQX whilst stronger evoked activities were less affected, due to the sigmoidal activation function of neurons. This system demonstrates successful high precision modulation of neural network activity. With the ease of being incorporated in existing extracellular neural electrode devices without increasing the volume or complexity, this technology may advance basic neuroscience research as well as therapies for neurological disorders and injuries.

4.2 INTRODUCTION

Neural network activity on various scales underlies numerous neural functions such as cognition, learning, and memory [159, 160]. Many functional neural network abnormality accounts for neuronal diseases [206, 207]. To understand the *in vivo* neural network activities, Multielectrode Arrays (MEAs) with the capability of recording from ensembles of neurons or stimulate a small population of local neural networks have been developed to understand neural networks and correct abnormal activities [208, 209]. Neural modulation techniques are often required to dissect the function of neural networks in complicated neural processes. Such techniques include neural stimulation[135, 137], systemic injection[183], localized cannula injection[57], microdialysis[210, 211], iontophoresis[46, 212-214], and optogenetics[72, 74]. However, due to the already complicated *in vivo* MEA fabrication process and the required feature to integrate components into extremely small space[9, 10, 113, 215], the ideal neural interface systems with pharmaceutical modulation of recorded neural networks has yet to be realized. Because drawbacks were observed with each class of localized neural modulation

techniques, including the lack of spatial and temporal precision of the modulation effect. In some cases, the ongoing neural modulation treatment abolish the recording of MEAs from targeted neural tissue completely. The conventional techniques for cannula injection of neuroactive molecules cause neural tissue damage from the bulky size of device as well as the volume change during injection. The microfluidic device with pharmacological intervention capability requires additional complex steps of manufacturing thus raise the failure rate of device [216-218]. Furthermore, the addition of fluidic channels suffer from undesirable chemical leaking and clogging of channels when utilized for chronic applications. Optogenetics technique demonstrate outstanding performance for the modulation of specific genetically modified neurons[219-221], but the technique is restricted by the availability of genetic modified channels in target species, the positioning of fiber optics[75], the involvement of light source, as well as photoelectric artifact[222].

Conducting polymer coatings create an attractive means for localized pharmaceutical modulation of neural network activity directly from the neural microelectrodes. These polymers can be electropolymerized with oxidative current and deposited onto any electrodes from aqueous solution of monomers and electrolytes, resulting in positive charges on the backbone. During the polymerization, negatively charged species in the solution may be incorporated into the polymer coating as dopants. Negative electrical currents reduce the polymer in to a neutral form, release the dopants and electrostatically drive the drug molecules out. Based on this mechanism, the electrically controllable delivery of various reagent have been demonstrated, include anionic salicylate, adenosine triphosphate (ATP), 2-ethylhexylphosphate (EHP), and naproxen and dexamethasone [168-171].

Previously, electrically triggered release of CNQX (6-cyano-7-nitroquinoxaline-2,3-dione), an AMPA (2-amino-3-(5-methyl-3-oxo-1,2- oxazol-4-yl)propanoic acid) receptor antagonist based on this mechanism has been demonstrated to effectively reduce spike firing rate in hippocampal neural cultures in a manner [154]. Here we report the further development of this technology for *in vivo* use. The fast glutamate transmission mediated by AMPA receptor is a suitable target for pharmaceutical modulation of neural network activities due to the strong involvement of AMPA current in generating action potentials *in vivo*[223, 224]. Instead of CNQX, another AMPA receptor antagonist DNQX has been selected to demonstrate the effectiveness of this conducting polymer based technique *in vivo* [225-227].

Both molecules CNQX and DNQX are poor dopants, i.e. they significantly impair the electrical conductivity of the synthesized polymer film, thus only allow the formation of a very thin layer of conducting polymers with little drug loading capability. A bi-layer approach of incorporating PEDOT and functionalized carbon nanotubes (CNTs) has been developed to ameliorate this difficulty.

The incorporation of CNT into our drug delivery systems utilizes multiple unique features of this material. First, CNT has demonstrated excellent adherence and stability on electrode surface. Secondly incorporating CNTs can improve the conductivity of the conducing polymer matrix [94, 95, 110], which is critical when poor dopants such as CNQX and DNQX are used. The first layer of the coating consists of PEDOT/CNT, which provides a highly conductive and adherent substrate with high surface area topography that benefit the growth of the second layer[128], consisting of PPy/CNT/DNQX. PPy was selected due to increased drug incorporation quantity over other polymers and the low amplitude of reduction potential to switch the redox state of the polymer backbone. Incorporation of CNT in the PPy matrix allows

the formation of a more stable conducting polymer matrix to endure the repetitive application of drug release triggers, meanwhile the internal cavity of CNT serves as an excellent reservoir to increase the total amount of drug molecules can be released[125].

Rat somatosensory (SI) barrel cortex serves as an outstanding testbed to evaluate our drug delivery system due to the reliable action potential firing mechanism which is topographically evoked by stimulating specific facial whiskers[152, 228-230]. The barrel cortex input neural network in layer IV is selected as the target neural network for local modulation due to the high transient firing rate, high reliability, low spontaneous firing and low latency of the neurons[231]. In this work, the microelectrode array coated with bilayer PEDOT/CNT and PPy/CNT/DNQX conducting polymer was implanted into rat barrel cortex acutely. Air puff multi whisker stimulator was utilized to elicit strong and repeatable neuronal firing patterns[157]. The effect of electrically triggered DNQX release on sensory evoked neural response was characterized.

4.3 MATERIALS AND METHODS

4.3.1 Materials and Electrodes

4.3.1.1 Materials

DNQX disodium salt was acquired from Abcam (MA) or Alomone Labs (Israel), Multi-walled carbon nanotubes (CNT) was purchased from Nanoamor (TX) and was chemically functionalized with –COOH with previously reported method [125].

16 channel microelectrode arrays for *in vivo* neural recording and drug delivery was obtained from Neuronexus (MI). The GSA of electrode sites on the probe was 704 μm^2. The electrodes are arranged on 4 shanks with 4 electrodes on each shank. The site spacing on each shank is 100 μm and the shanks are 125 μm apart from each other. The sites expand a depth of 300 μm, allowing all recordings to be performed within layer IV of barrel cortex.

CNT were functionalized with carboxyl groups with acid treatment, the procedure is briefly described as follows: first CNTs were sonicated in acid solution (1:3 HNO_3 and H_2SO_4) for 2 hours rendering the inner and outer walls of CNTs hydrophilic. This treatment also opens the CNT ends and removes the heavy metal. Ultracentrifuge (Sorvall RC 6 plus, Thermo Scientific, PA) at 12k-19k rpm was employed to remove the residual acid from the CNT and DI H_2O was added to serially dilute the residual acid in the CNT. After the pH of CNT solution is neutral, the CNT were first completely dried at 50 ^oC.

4.3.2 Electrochemical synthesis and characterization

PEDOT/CNT films were electrochemically deposited onto microelectrodes in a solution of 0.015 M 3, 4-ethylenedioxythiophene (EDOT) monomer, 1.5 mg/mL CNT dissolved in DI H_2O. The deposition solution was sonicated with a probe sonicator for 10 minutes to create homogenized suspension solution. Chronoamperometry deposition of PEDOT was controlled by a FAS2 Femtostat (Gamry, PA) at 0.95 V for 20 seconds in a three electrode setup electrochemical chamber. A platinum sheet was utilized as counter electrode and a Ag/AgCl wire as reference electrode. The microelectrode array was carefully lowered into the deposition solution with a micromanipulator (WPI, FL). Custom built electrode holders and connector wires were used to switch the coating channel in sequence without moving the microelectrode array in

solution at all. The concentration of EDOT monomer was slightly increased than the solubility due to the extremely large surface area of CNT might absorb large amount of EDOT monomers and decrease the monomer content in the deposition solution. After synthesize of PEDOT/CNT the array was carefully lift out from deposition solution and immediately rinsed with DI H_2O to remove excess deposition solution and loosely attached particles. Then 1 mg/mL CNT is dissolved in 5 mg/mL DNQX high concentration solution. The process that H_2O enters the internal cavity of CNT requires great effort and is only ideal when the dry CNT is first dissociated in H_2O. So the high concentration DNQX solution can be easily carried into the inner cavity of CNT to serve as drug release reservoir. The solution was sonicated for 5 minutes until 0.45 M pyrrole monomer was added and additional 5 minutes of sonication homogenize the pyrrole, CNT and DNQX together. The same electrochemical setup was utilized to deposit the PPy/CNT/DNQX film on PEDOT/CNT pre-coated electrodes. The Chronoamperometry deposition was maintained at 0.75 V for 15 seconds. Electrical stimulation electrodes serve as control experiments with PPy/CNT on PEDOT/CNT coatings were prepared with same Chronoamperometry parameters while only Py monomer and CNT were sonicated in DI H_2O for deposition. Electrochemical Impedance Spectra (EIS) scan was performed on uncoated, PEDOT/CNT coated and double layer PPy/CNT/DNQX coated electrode sites. The data was imported into MATLAB (Mathworks) and analyzed for direct comparison.

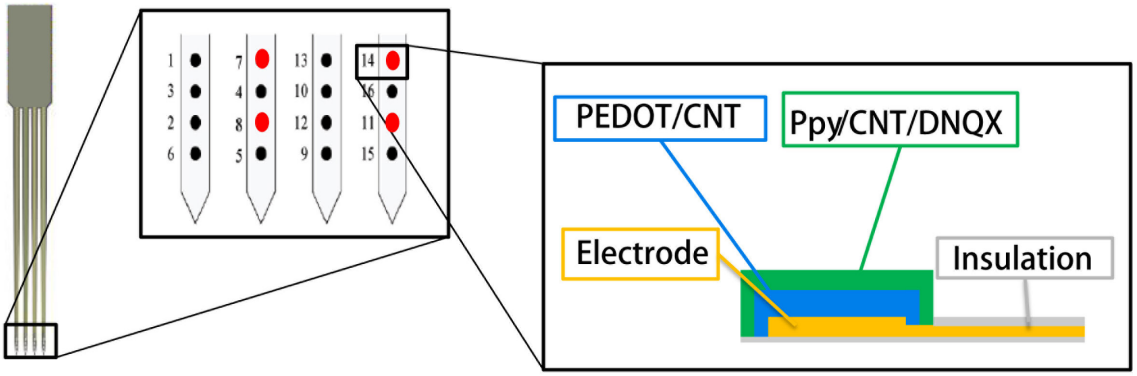

Figure 4-1 Illustration of drug release microelectrode array and double-layer coating. The microelectrode array obtained from Neuronexus has four shanks, with four microelectrodes on each shank. The site spacing on same shank is 100 μm and the shank spacing is 125 μm. Multiple drug coated microelectrodes are combined to maximize the effect of released DNQX into the barrel cortex. The drug releasing microelectrodes were separated by recording microelectrodes in order to obtain neural modulation on different concentration scales. On each microelectrode, the electrode material is composed of Iridium (Ir). Other metals utilized for fabrication of these microelectrode arrays include Gold (Au), Platinum (Pt) and Pt/Ir alloys. Selection of microelectrode materials is determined by the requirement for mechanical properties and conductivity as well as surface adhesion properties such as formation of Self-assembled monolayer (SAM) materials. On the electrode materials a layer of PEDOT/CNT was electrochemically deposited to expand the surface area of the electrode and decrease the surface impedance. Then the PPy/CNT/DNQX layer is synthesized to precisely delivery DNQX molecules to the neural networks adjacent to the implant and modulate the activity during recording sessions. The electrode traces and were insulated while the microelectrode sites were exposed, the conducting polymer matrix slightly grow over the region of microelectrode and extend onto the surface of insulations, rendering the effective electrode surface areas bigger than the original microelectrode.

4.3.3 *In vivo* DNQX release modulate barrel cortex activity

4.3.3.1 Air puff stimulator for evoking barrel cortex activity

A portable air compressor with compressed air tank was used to deliver 15 psi air puff stimulation to the rat facial whiskers. A custom built multi-channel manifold with solenoid valve receiving multi-channel TTL signal controlled the pattern of air puff stimulations. The digital I/O port on RX5 (TDT) recording processor was utilized as control signal for the on and off of air puff whisker stimulator. An externally powered custom built electrical circuit was utilized to ascertain the generation of 5 V TTL signals to precisely control the solenoid valve. A piezoelectric sensor directly held at the puffer nozzle generated electrical signal in order to measure the delay in the air puff sensory stimulation system. The electrical signal from piezoelectric sensor and the RX5 I/O port were both recorded on oscilloscope for direct comparison. The air puff system created 20 ms delay in the process of delivering compressed air to the rat facial whiskers.

4.3.3.2 Barrel cortex surgery for simultaneous recording and stimulation

All animal work was performed under the guidelines of the University of Pittsburgh Institutional Animal Care and Use Committee (IACUC). Sprague-Dawley (SD) rats were anesthetized under 3% isoflurane and head-fixed in a SR-6R stereotaxic frame (Narishige, NY). Two skull screws were carefully positioned above the right motor cortex and left visual cortex of the rat illustrated in Fig. 4-2A. The screws barely touch the surface of the brain to provide conductivity but without being affected by the slow oscillatory signals generated by the brain. A 3 mm by 3 mm semi-transparent window above the somatosensory barrel cortex (SI) of the right cortical hemisphere was created by thinning down the skull using a motorized drill. Saline was

repetitively applied to the skull surface during the drilling process to remove excessive heat generated in the process. The motorized drill speed was controlled by a foot unit to apply high speed drill at the beginning of the surgery but very carefully controlled low speed drill when approaching the brain surface. The center of barrel cortex coordination were of 2.5 mm posterior to Bregma and 5.5 mm lateral to the midline. After carefully examine the blood vessel patterns underneath the semi-transparent skull window, a 1 mm by 1 mm craniotomy was opened on the brain surface with forceps and surgical blade. The dura mater was recessed with a bent 30 Gauge needle and a spring loaded micro scissors. The neural probe was inserted into the cortex using a micromanipulator at a slow speed to 900 μm beneath the cortical surface where the layer IV of barrel cortex is located, as demonstrated in Fig. 4-2B. The recording performance of the implanted microelectrode array was carefully optimized once the principle whisker was discovered. A custom built electrode adapter was utilized to assign neural stimulation and recording functions to individual sites on microelectrode array. The adapter was specifically designed to completely segregate the neural recording and electrical stimulation circuit in order to ensure the safety of neural recording during simultaneous stimulation trials and reduce the impact of artefact on the neural recording quality. Multi-channel neural stimulation signal to trigger the release of DNQX embedded in the conducting polymer matrix was generated by an MS16 stimulator (TDT) controlled by an RX7 (TDT) stimulation based recording unit. The neural signal from microelectrode array was amplified using a 16 channel Medusa preamplifier and recorded using an RX5 processor at 25 kHz sampling rate (TDT, FL). Neural signal was subsequently imported into MATLAB with custom scripts for analysis. The synchronization of neural recording, drug release trigger and whisker air puff was controlled by RX 5 and RX 7 unit. Contralateral air puff to facial whisker was delivered by the whisker stimulator. The air puff

stimulator nozzle was made of a flat-end needle. The nozzle was carefully positioned around 1 cm above the top row of whiskers with a helping hand and repetitive air puff stimulations controlled by recording processor was delivered onto facial whiskers to confirm the principle whisker of the barrel that the neural electrode array was implanted into. The air puff stimulator was held about 1.5 cm above the principle whisker and 15 psi air puff reliably evoked strong neural activity in the layer IV of barrel cortex. Each air puff stimulation to the whisker lasts 100 ms in duration and was delivered at 4 Hz to evoke strong neural response. Once the principle whisker for the implant is optimized, the electrode depth was slowly adjusted with simultaneous whisker stimulations and audio amplitude representation of whisker evoked response. The probe is located at the depth in layer IV to evoke the strongest sensory response from the principle whisker.

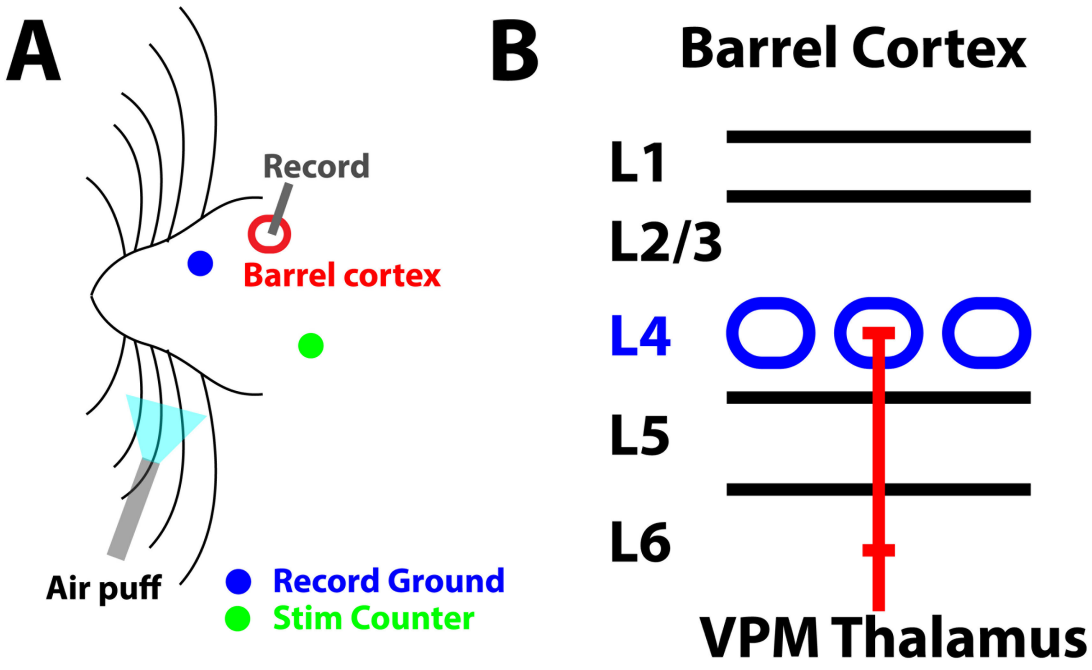

Figure 4-2 Neural surgery and experiment paradigm for whisker stimulation. (A) The schematics demonstrating the experiment setup. The craniotomy was opened in rat barrel cortex centered at -2.5 mm post

Bregma and 5.5 mm lateral to midline. Neural recording and drug delivery array was inserted slowly with a micromanipulator until layer IV of barrel cortex. Two ground screws were placed in the skull, one recording ground screw in right motor cortex and one stimulation counter screw in left visual cortex. The air puff stimulator was held above the principle whisker of the implanted barrel on the contralateral side of the face. (B) Illustration of cortical layers for neural recording. The layer IV is one of the major input layers of the barrel cortex with clear topographical segregation of neural networks representing different whiskers. Another low latency input to the cortical layers was observed in layer VI of barrel cortex. The layer IV of barrel cortex is typically 600-1000 μm from the surface of the brain. Optimal neural recording was usually achieved around 900 μm. In certain cased the probe might be inserted into the Septa region between barrel networks in layer IV, the evoked response in Septa region is weak so the probe is sometimes repositioned to achieve the highest firing rate from the principle whisker.

4.3.4 Experiment paradigms for evaluating the DNQX effect in barrel cortex

A cosine waveform with amplitude of -3 μA and duration of 100 ms was delivered to each microelectrode to trigger the release of DNQX from the microelectrode, as illustrated in Fig. 4-3A. The cosine waveform can deliver sufficient charge to the conducting polymer surface with a slow rate of increase in the current. Fast change in neural stimulation current can induce massive capacitive current on the membrane of neurons thus change the firing property of neurons. So the slow change of cosine waveform will cause faradaic reaction on polymer electrode and release drug without affecting the neural firing property on its own. The drug release current is followed by a reverse phase current with 1.5 μA amplitude and 200 ms duration in order to balance the change. The charge balance phase serves two functionalities: reduce the net charge delivered to local tissue in order to maintain the safety of the neurons adjacent to the probe, and partially reverse the reduction of PPy polymer so the conjugated polymer maintain

sufficient conductivity for the following drug release triggers. In Fig. 4-3B, the air puff stimulation to the whiskers is delivered in burst of three air puffs, at 4 Hz frequency. The duration of air puff is 100 ms and the interval between air puffs is 150 ms in order to control the air puff at 4 Hz. The spikes generated in this sensory stimulation pattern amounts to higher firing rate than single air puff stimulation. The intensity of each burst of air puff is sufficient to quantify the effectiveness of released DNQX molecules. In Fig. 4-3C the experiment time chart is briefly demonstrated, the beginning of the first air puff burst is designated as 0 second, five consecutive bursts of air puffs were first delivered before the drug release trigger to establish a stable baseline of neural response. The drug release trigger was applied at 29 seconds, one second before the 6^{th} burst of air puff. Then additional ten air puff bursts were delivered after the drug release trigger in order to quantitatively assess the effectiveness and duration of the delivered DNQX molecule. Each drug release session is 90 seconds in total duration. At least one additional minute was allowed before the next drug release trial begins in order to allow the wash away of previously released DNQX molecules and the recovery of AMPA receptors in the barrel cortex.

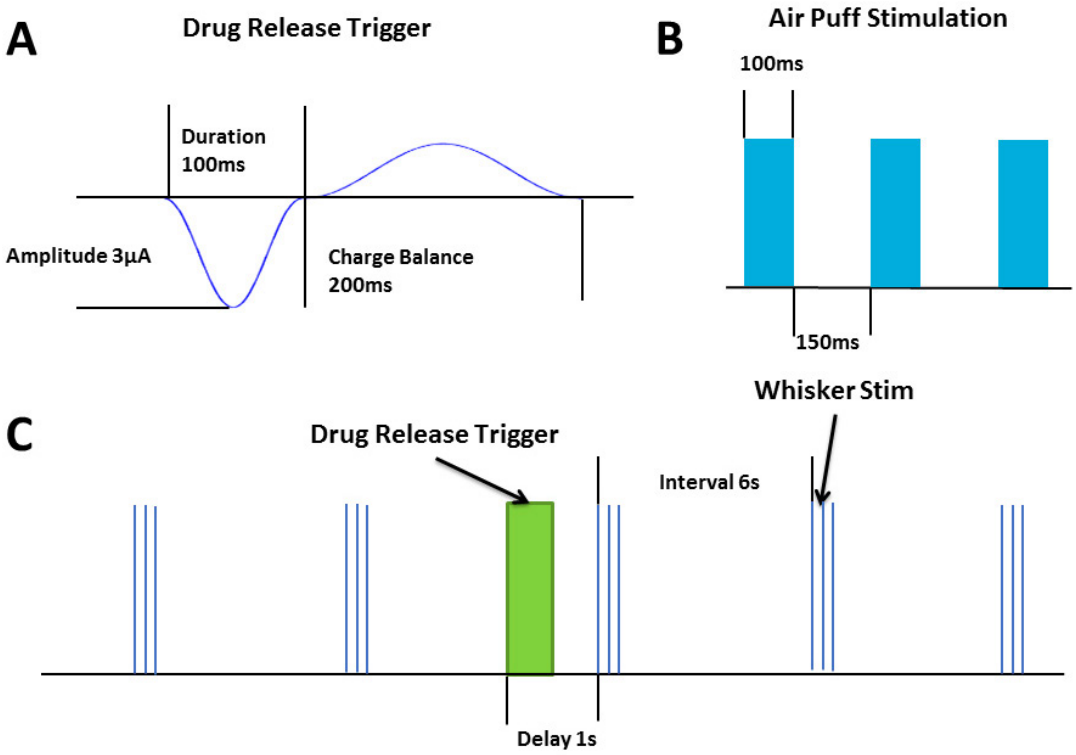

Figure 4-3 Experiment design to evaluate DNQX release in barrel cortex. (A) The cosine waveform to trigger drug release from microelectrode last 100 ms and is followed by 200 ms half amplitude charge balance phase. The release is represented by the green trigger in (C). (B) The air puff stimulation delivered to the principle whisker is 100 ms in duration and 4 Hz in frequency. The total duration of the air puff is 300 ms, with 450 ms following the air puff for quantification of spike numbers in the interval of sensory stimulations. (C) Five bursts of sensory stimulations were delivered to the principle whisker for establishing the baseline spike count before the drug release trigger was applied to the release electrodes. Each burst of whisker stimulation is delivered at 0.1667 Hz to allow sufficient time for receptors in the barrel cortex to recover from adaptation effect. The drug release trigger was applied one second before the 6th whisker stimulation burst. Ten additional whisker stimulation bursts were delivered to the principle whisker to evoke neural activities in order to observe the effective duration of the released DNQX molecules.

4.3.5 Neural data analysis and quantitative assessment of drug release

4.3.5.1 Neural data preprocessing

The raw data stream recorded at 25 kHz was imported into MATLAB and processed with custom scripts. The spike data stream was generated by band pass filter the raw data stream between 300 Hz and 3000 Hz, because the typical waveform frequency of extracellular action potentials is about 1000 Hz. 1 Hz to 300 Hz band pass filtered waveform represent the LFP (local field potential) of the data stream. After the filtering process, common average reference (CAR) technique was applied to all data streams on recordable neural electrodes, in order to calculate the common fluctuation in the data waveform to remove simultaneous artefacts and waveform deviation caused by the reference electrode. CAR component is then removed from each individual recorded waveform. The standard deviation (SD) of the spike data stream was calculated and 3.5 times SD was utilized to threshold the waveforms with amplitudes higher than the threshold. All threshold crossing waveforms with 0.4 ms before and 0.8 ms after the threshold crossing time point was removed from the spike data stream. Next the SD of data stream without threshold crossing waveforms was calculated and 3 times this SD is utilized as the final threshold for detecting threshold crossing extracellular action potential waveforms. The spiking time points of these multi-unit recording waveforms were utilized to calculate the firing rate and the drug release effect of the system.

4.3.5.2 Quantification of drug release on sensory input

During each burst of air puff stimulation, high firing rate was observed during the 100 ms period when air puff was turned on, and relatively low firing rate was observed during the 150 interval period between air puffs. After the third air puff, additional 150 ms was utilized to

calculate the firing rate of the neurons in this non-sensory response period. Because the air puff stimulator may generate oscillatory mechanical movement on the principle whiskers, and this effect of air puff could last after the solenoid is already switched off. Thus the non-sensory response period also demonstrate higher firing rate compare to the spontaneous baseline duration of the recording sessions. Each air puff stimulation in the three burst delivered at 4 Hz is characterized by one sensory response period and one non-sensory response period. The three consecutive sensory response period elicit weaker response towards the end due to the adaptation of the neural response. But the sensory response firing rate was still much higher than the non-sensory response firing rate. The sensory and non-sensory response of each period was calculated for the three air puff stimulations and the drug effect on each of these period was compared to the regular firing rate during the baseline recording to yield the drug release suppression ratio of these firing rates.

4.3.5.3 Effective drug delivery trials and distance

On 16 channel multielectrode array for recording and stimulation, four channels were utilized to deliver DNQX to the local neural network. During electrically evoked control experiments, another four microelectrodes with only PEDOT/CNT and PPy/CNT double layer polymer coating without DNQX molecules were utilized as electrical control stimulation to evaluate the effect of drug release trigger waveforms on the recorded neural networks. During control experiment another four recording channels were utilized for drug release triggers, so a maximum recording channel number of 12 is achieved during each drug release experiment. The sensory evoked firing rate response observed on the 12 recording channels were averaged together in order to evaluate the total impact of DNQX release on the local neural network during one single drug release trial. During different drug release experiments, the corresponding

release trial of DNQX from the first release after fresh polymer coating towards the end of the experiment was considered equivalent DNQX release trials and multiple recording channels were analyzed together to obtain the general trend of neural response suppression caused by DNQX release.

Furthermore, analysis was conducted to evaluate the spatial resolution of the released drug molecules. As demonstrated in Fig. 4-1, each of the four DNQX release sites was considered to generate a semi-sphere diffusion concentration gradient of DNQX following the drug release trigger. Due to the spatially restricted diffusion of molecules inside the brain, the semi-sphere estimation was a preliminary estimation of the drug release concentration pattern, but the effect of the drug release concentration variation during each experiment can be overcome by the high number of experiments to repeat the DNQX release because the spatial restraint on DNQX diffusion is considered randomly anisotropic. The summation result of the four semi-sphere DNQX concentration patterns following each drug delivery trigger cause the highest concentration of DNQX to occur on the center of the four release sites. In Fig. 4-1 the highest concentration of DNQX occur on electrode site 10, and the quantity of DNQX decrease as the recording electrode is further from site 10 as the DNQX release center. The distance effect of DNQX release is summarized by quantification of firing rate reduction correlating with the increase of distance from the highest concentration of DNQX release. A second order polynomial function was fitted to the distance-suppression effect plot, thus the distance at which the drug effect would vanish could be extrapolated from the fitting polynomial function despite the limited recording sites on the recording probe.

4.4 RESULTS

4.4.1 Synthesis and characterization of double layer DNQX release polymer

4.4.1.1 Electrochemical synthesis and property of double layer PPy/CNT/DNQX

Electrochemical synthesis of PPy/CNT/DNQX polymer was hindered by the incorporation of DNQX a in the polymer film. Typically PPy polymer with good dopants forms films with good conductivity and as the film grows thicker and rougher, the impedance drops, resulting in continuous increase in the deposition current. However the incorporation of DNQX molecule greatly increase the surface impedance of electrode and decrease the coating current (Fig. 4-4A), suggesting a low conductivity of the resulting film. The synthesis of first layer PEDOT/CNT polymer partially solve this problem by decreasing the initial impedance and increase the initial effective area for PPy/CNT/DNQX coating. The PPy/CNT/DNQX Chronoamperometry deposition current on top of the PEDOT/CNT film is illustrated as the blue curve in Fig 4-4A, while the PPy/CNT/DNQX Chronoamperometry current of PPy/CNT/DNQX on unmodified microelectrode was represented by the red curve in Fig 4-4A. The bilayer PPy/CNT/DNQX deposition current demonstrated much higher initial current and accumulated charge. The blue curve demonstrated two decreasing rate feature during different time period due to the fact that PPy/CNT/DNQX polymer can simultaneously increase coating current by increasing electrode surface area and decrease coating current due to poor polymer conductivity. The first period before 5 seconds demonstrated a faster decreasing rate of deposition current, due to the high rate of DNQX polymer synthesis completely dominant over increase of polymer surface area. However after 5 seconds, the resistivity increase by DNQX polymer already decrease the deposition current significantly, thus the effect of increased polymer surface area

roughly balance out the further decrease of polymer conductivity. This phase benefit from the high initial surface area of the PEDOT/CNT polymer and contribute to the major portion of increase in total deposition charge. In Fig. 4-4B, the EIS measurement of different electrode surface was compared to each other. The most emphasized impedance value for extracellular action potential is 1000 Hz because the characteristic frequency of recorded action potential waveforms correspond to this frequency. For the conductivity of polymer film and the capability to deposit polymers onto the electrode surface, the low frequency impedance near DC current is the major determine factor. For uncoated microelectrodes, the impedance value at 1000 Hz is the highest among the measured electrode surface. The impedance of typical electrode site for neural recording at 1000 Hz is between 500 kΩ and 1 MΩ. The deposition of PEDOT/CNT greatly decreased the impedance of the microelectrode to the green curve, with 1000 Hz impedance around 20 kΩ. After the synthesis of second layer PPy/CNT/DNQX polymer the electrode impedance ends around 200 kΩ at 1000 Hz. Due to the importance of 1000 Hz impedance value for extracellular action potential recording performance of microelectrodes, the double layer DNQX polymer can improve the recording quality of the coated microelectrode. The recording of double layer PPy/CNT/DNQX coated microelectrodes were utilized during electrical control trials where double layer PPy/CNT polymer coated electrodes were utilized for evaluation of electrical stimulation effect.

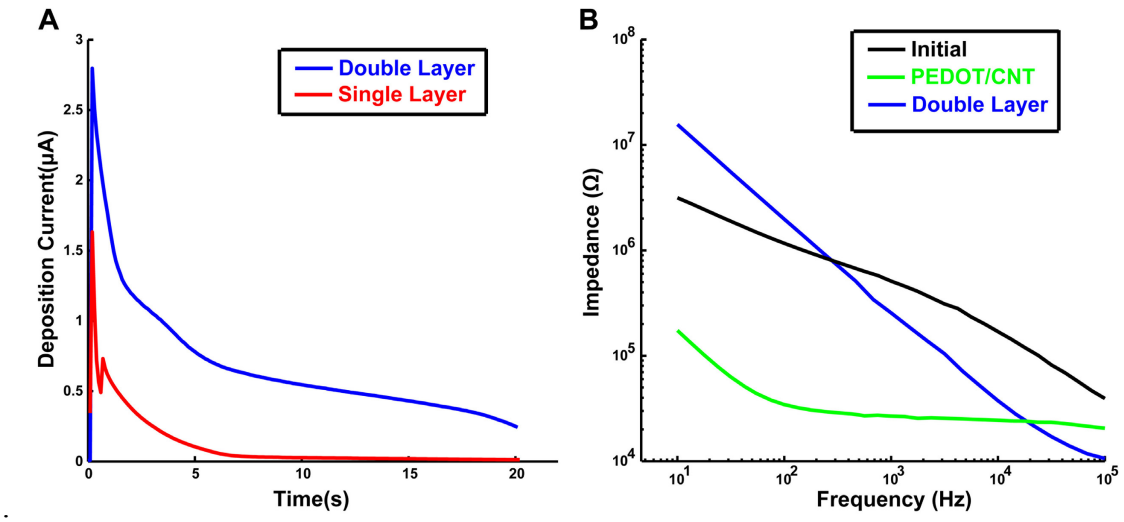

Figure 4-4 The electrochemical synthesis and EIS measurement of double layer DNQX polymer. (A) Electrodeposition current comparison between single layer PPy/CNT/DNQX polymer (example Chronoamperometry curve, n=3 electrodes demonstrated same curve) and double layer PPy/CNT/DNQX polymer as second layer polymer on PEDOT/CNT (n=3). The single layer coating current start at high amplitude about 1.5 μA but decrease rapidly over the duration of polymerization. The total charge for deposition is limited and the final impedance of the conducting polymer was high so the voltage for drug delivery trigger was high, causing severe redox side effects to the electrode and local tissue. With double layer PPy/CNT/DNQX on top of PEDOT/CNT polymer, the deposition current is greatly increased, the deposition charge increment benefit the total polymer with DNQX molecules and the higher ending current benefit the lower drug release trigger voltage caused by the control current. (B) EIS measurement of electrode sites with different modifications, the black curve demonstrate the initial microelectrode impedance value. The impedance was highest among the measured groups in the high frequency range but the increment rate of impedance towards low frequency range was moderate. The PEDOT/CNT film (n=3) greatly reduced the impedance in all frequency range compare to the uncoated microelectrodes (n=3). The double layer PPy/CNT/DNQX polymer (n=3) increased the impedance of the electrode in almost all frequency range, due to the low conductivity of the polymer with DNQX dopant. The increase in impedance was prominent at both 1000 Hz and the lowest frequency 10 Hz, corresponding to the performance of extracellular action potential recording and further electrochemical deposition, respectively.

The microscopic examination of PEDOT/CNT and PPy/CNT/DNQX polymer was performed under optical microscope. The PEDOT/CNT conducting polymer formed a uniform layer of polymer that appears dark in color due to the light absorption by CNT. The polymer coating increase the microelectrode surface area slightly, but does not significantly impact the regional specificity for neural recording or stimulation of the coated electrodes. The double layer PPy/CNT/DNQX coating does not change the appearance of the conducting polymer. Because the surface morphology of PEDOT/CNT polymer examined under SEM demonstrate nano features and large surface area to volume ratio in chapter 1, the PPy/CNT/DNQX coating slightly thickens the PEDOT/CNT polymer without horizontally expand the surface are of polymer coated microelectrodes. After the *in vivo* drug release experiment, microelectrode arrays were removed from the cortex and dipped in warm Trypsin solution for 10 minutes to remove the tissue on the electrode surface. The electrode array can be coated again with PPy/CNT/DNQX polymer and reused for DNQX delivery purposes. The morphology of microelectrodes showed no observable change under the microscope before and after *in vivo* use, demonstrating that the mechanical perturbation during probe insertion into the brain and the electrical stimulation during the drug delivery did not cause the double layer PPy/CNT/DNQX coating to delaminate under microscope.

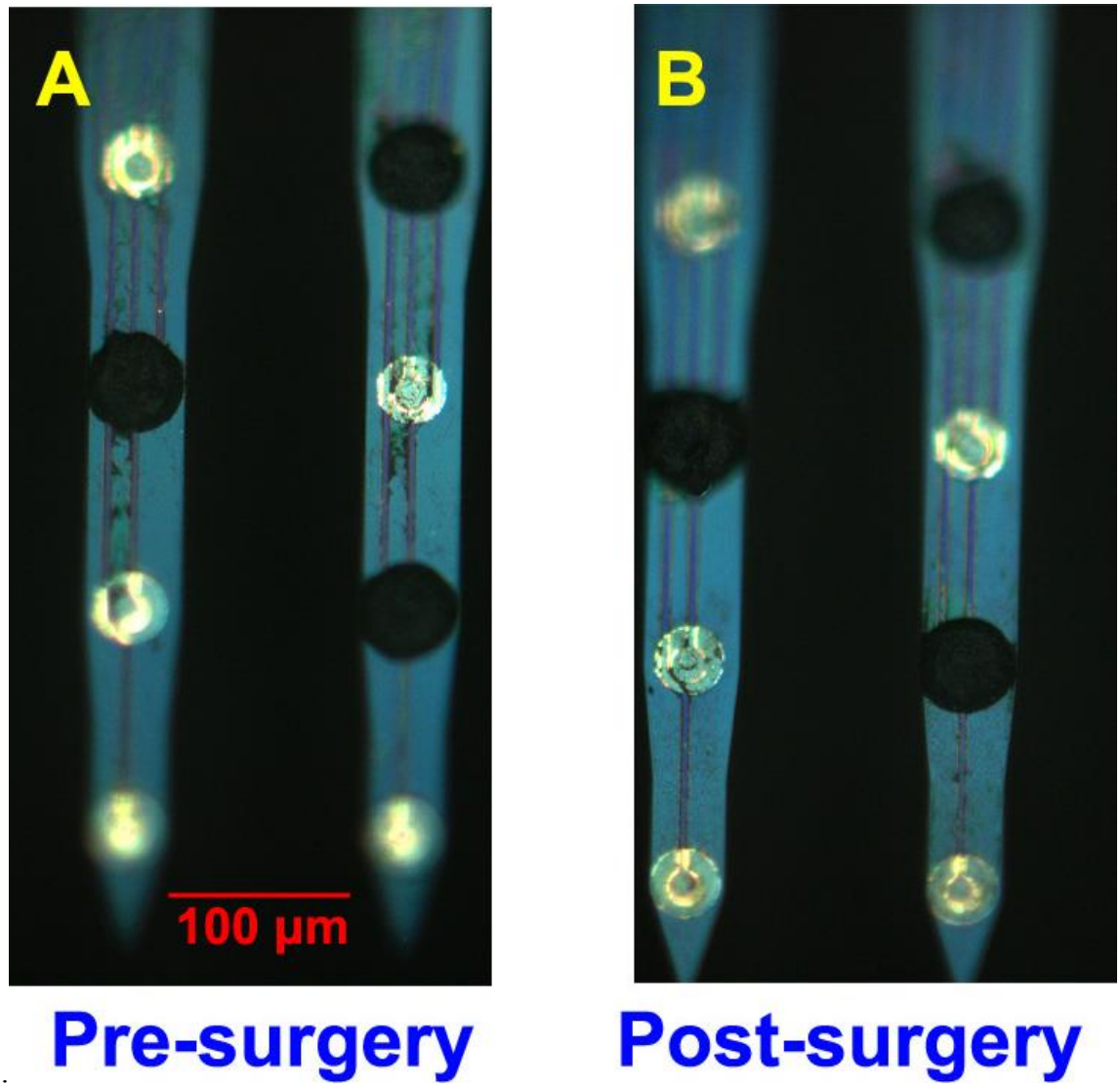

Figure 4-5 Microscopy examination of conducting polymer coated microelectrodes. (A) Representative images of double layer PPy/CNT/DNQX coated microelectrodes sites among the uncoated Iridium microelectrodes. The deposition of first layer PEDOT/CNT polymer significantly change the surface appearance of the electrode but only slightly increase the electrode surface area. The second layer PPy/CNT/DNQX coating does not increase the area of microelectrode at all. The deposition of polymer on microelectrode is uniform and covers the microelectrode completely. (B) After acute neural surgery for DNQX release, the microelectrode array was explanted from the brain and treated with trypsin to remove the tissue debris on the surface of microelectrodes for reuse. Representative images of the conducting polymer coating morphology indicate the polymer did not change at all during the drug release experiment.

4.4.2 *In vivo* DNQX release in barrel cortex

4.4.2.1 Neural recording in barrel cortex with sensory evoked activity

The raw neural signal filtered between 300 Hz and 3000 Hz were utilized to analyze the extracellular action potentials recorded in the barrel cortex as demonstrated in Fig. 4-6. The air puff stimulation evoked strong neural network activity during the period of stimulation and the interval between puffs. The firing pattern during the interval of air puffs could be result of repetitive firing of excitatory neural networks or the vibration of facial whiskers following the stimulation. The noise floor of the recording was roughly 15 uV and a large amount of multi-unit spikes cross the threshold for detecting spikes. The strongest and most reliable neuronal firing of layer IV in barrel cortex mostly occur during the air puff stimulation only but not the spontaneous recording after the third green vertical line indicating the end of whisker stimulation. The drug release trigger evoked electrical artifact recorded by the same microelectrode. The consequence of drug release trigger was very transient due to the procedure to carefully and completely separate the stimulation and recording circuit by utilization of separate counter electrodes. The recording counter and reference were shorted together to skull screw above the surface of ipsilateral motor cortex while the counter for the drug release trigger was a skull screw above the contralateral visual cortex. The artifact caused preamplifier saturation was only observed during the period of the trigger itself. Indicating the trigger was safe for further neural recordings. The same quantity of neural recording was observed across all DNQX release trials. The drug release effect was clearly observed. The air puff stimulation was delivered one second after the initiation of DNQX release trigger. The spike number during the

air puff as well as during the air puff interval were all decreased as a consequence of the DNQX release because high concentration of DNQX effectively block the fast AMPA receptor mediated glutamate transmission. Towards the end of the time frame demonstrated in this subfigure, the spike generation was already start to recover, because during the spontaneous recording, layer IV of barrel cortex usually generate limited quantity of spikes but the network already demonstrated firing rate higher than some of the previous drug affected sensory evoked spikes in the same plot. The recovered neural network activity seven seconds after the drug release trigger indicate the drug effect was completely washed away by seven seconds, the air puff stimulations and the intervals during the air puff all correspond to high firing rate. The firing pattern of the recorded channel was further analyzed by calculating the PSTH of sensory evoked multi-unit spikes.

4.4.2.2 Released DNQX suppresses sensory evoked PSTH

The evoked firing rate increase can be separated into direct air puff induced increase and indirect interval increase. The three air puff stimulation will be denoted as AP1, AP2 and AP3, with the sensory evoked and interval period designated as s (sensory) and i (interval). The six different period to quantify the firing rate is emphasized by the red and blue semitransparent box in Fig. 4-6A. Time 0 represent the start of the first air puff stimulation, during electrically evoked control trials without release, the raster plot indicate transient increase in firing rate immediately after the start of the air puff, towards the dnd of the AP1s period, the recorded neurons displayed increased firing rate compare to the baseline spontaneous firing, but the spike generation was evoked at different time points and less reliably compare to the spikes evoked at the starting of AP1s stimulation. The AP1i period exhibit very similar firing pattern in correspondance with the later pattern of AP1s. During the AP2s stimulation the evoked whisker response still maintain very high temporal precision and very low spiking latency after the stimulus started over the

quantified trials. However from the AP3s, the air puff evoked sensory spikes display less precision and slightly longer latency than the previous two stimuli. The effect was partially induced by the adaptation of neural activity due to high frequency strong sensory input. During all the interval period the generated spike numbers were similarly elevated compare to the spontaneous firing rate towards the end of the burst air puff stimulation, representaed by raster plot from 0.75 seconds to 1 second in Fig. 4-6A. The average spike counter was utilized to calculate Peri-Stimulus Time Histogram (PSTH) of the air puff burst stimulation in Fig. 4-6B. The sensory stimuli AP1s, AP2s and AP3s each evoked strong and instantaneous firing rate increase after the begininig of the stimuli, due to adaptation the firing rate quickly decreased from AP1s to AP3s, the average firing rate during the interval periods AP1i, AP2i and AP3i clearly revealed the spike generation after the air puff stimulation was affected by an oscillatory source but display less strength and consistency compare to the direct sensory air puff stimuli. The first sensory burst after drug release trials was compared directly to the electrically evoked firing pattern in Fig. 4-6A and B. In Fig. 4-6A, the DNQX release significantly decreased the spike generation probability during all the interval periods, the firing rate of AP2s and AP3s was also seriously affected by the DNQX release process, The firing pattern of AP2s after DNQX delviery resembles the AP3s firing during the control trials. The air puff evoked sensory spikes displayed less precision and more latency after the drug delivery. During AP3s the effect was more pronounced so the reliability of the sensory evoked spikes was partially impaired by the DNQX release effect. Less spikes were generated compare to the AP3s response of control trials. All the DNQX effect was clearly quantifiable in the PSTH of Fig. 4-6B. The most affected time period from the PSTH was the intervals. The spike numbers generated during the interval period was nearly abolished after the DNQX release and the oscillatory firng rate increase cannot be

observed during the DNQX release affected trials. The spike number of the AP3s period was also greatly decreased from the control trials.

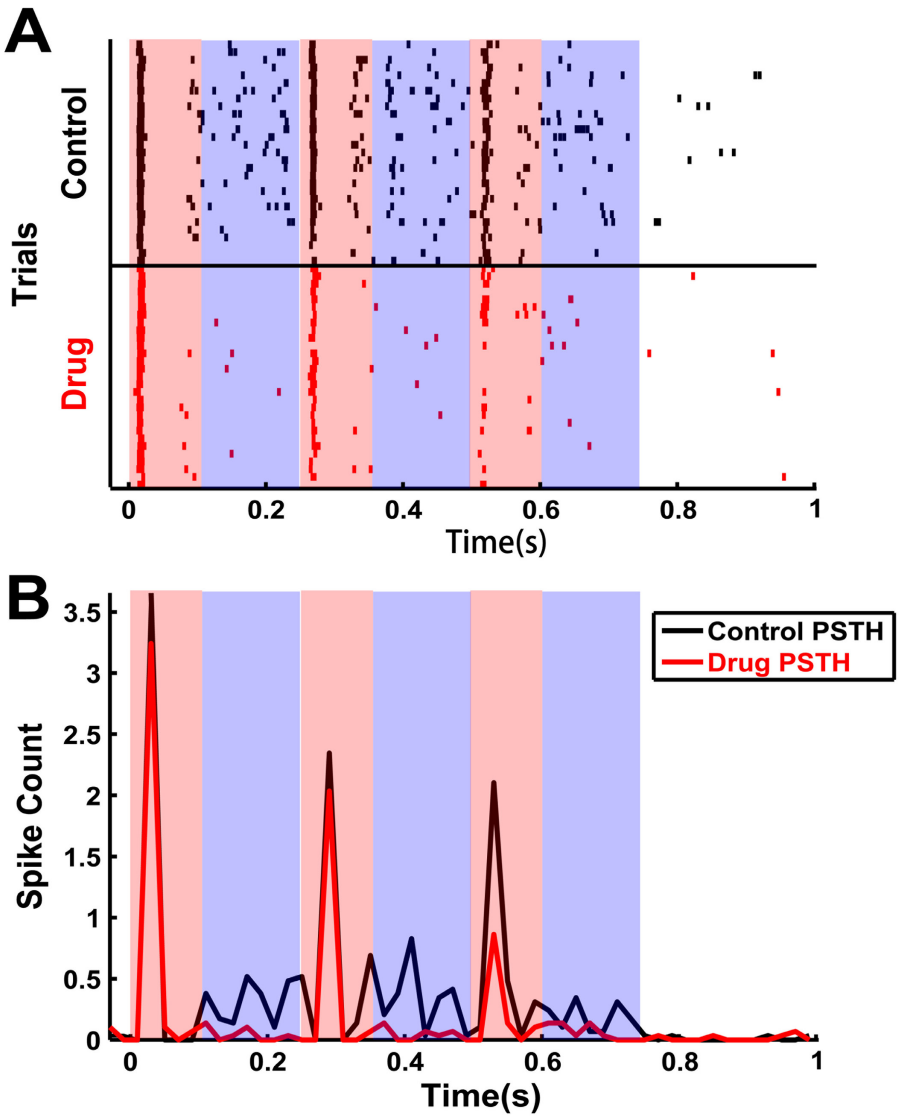

Figure 4-6 Spike time raster plot and PSTH of control and DNQX release trials. (A) The spike time of multi-unit action potentials were plotted as vertical bars following the air puff stimulation. The trials were re-aligned to the beginning of the first air puff. The black color trials on the top were the first sensory burst stimulus after the electrical trigger without DNQX. The red color denoted trials were the first sensory burst response after the DNQX release trials. During the control experiments, the third air puff evoked less precise and less consistent multi-unit activity compared to the AP1s and AP2s response. However the same reduction in precision and consistency was

observed in both AP2s and AP3s response following the DNQX release. Indicating the released DNQX can weaken the network response. (B) The average PSTH of air puff evoked sensory response following control and DNQX affected trials. During the control trials, higher number of spikes than the spontaneous firing was observed during all the sensory and interval periods, however during the DNQX release trials the firing rate during interval period was almost abolished and resembles the low firing rate pattern during spontaneous trials. The example multi-unit PSTH was averaged over 29 trials.

4.4.2.3 DNQX release change firing rate in barrel cortex

To quantitatively assess the effectiveness of released DNQX on the barrel cortex neural activity, the multi-unit spike numbers was accumulated in all sensory and interval periods to summarize the overall effect of the DNQX release. The starting time of air puff stimuli was realigned around the time of triggered DNQX released, denoted by 0 and the black vertical line. The dashed purple line indicate the first air puff evoked sensory response following the DNQX release or the control trials illustrated in Fig. 4-7. Both control spike number and the DNQX spike number displayed a slight decreasing trend at the beginning of the trials representing the effect of sensory adaptation on the neural network. Immediately follow the drug release or control trigger the sensory evoked spike number was greatly reduced after the DNQX release but not the control without DNQX. The effect was washed out by the second sensory stimulus occurred at 7 seconds after the drug release trigger. Steady spike number trend was observed after the DNQX and the control trigger for 10 additional air puff burst stimuli. The difference between the sensory evoked responses following the DNQX and control trigger was very small across the trials. Due to the observation of the early sensory spike adaptation effect, the spike number during the last seven air puff burst stimuli was averaged to serve as the baseline spike number for normalization.

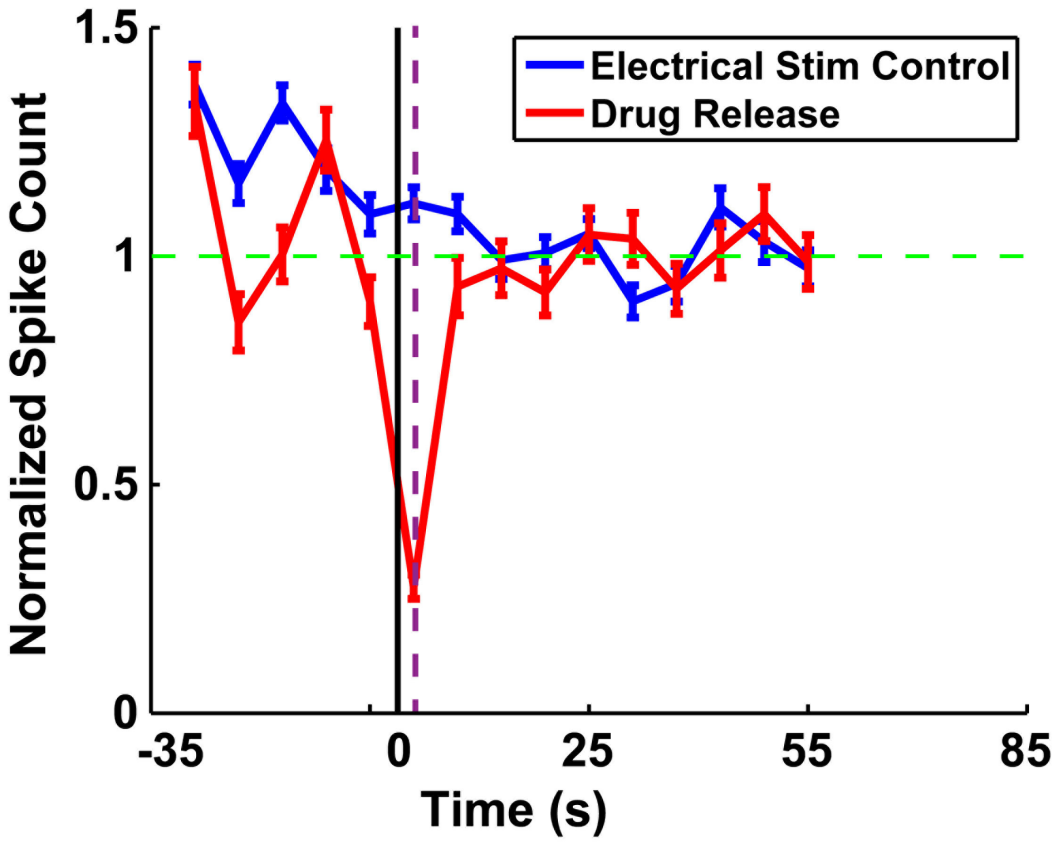

.

Figure 4-7 DNQX release reduce the spike number of sensory evoked activity. The total spike number from the beginning of air puff stimuli to the 0.75 seconds period in Fig. 4-7A was accumulated to represent the total neural activity evoked by the sensory input. During the control trials, the total spike number exhibit a smooth decreasing trend stabilized even after the release trigger without DNQX. The initial decrease in firing rate was caused by adaptation to the strong whisker stimulation. During the drug release trials, the spike number during the first air puff burst stimulus was discernibly different from the other consecutive air puff stimuli as well as the control trigger affected sensory response. The time 0 indicate the beginning of the DNQX release trigger, the purple vertical line indicate the first air puff stimulus following the DNQX release or control trigger. The second air puff stimulus evoked neural response was not affected by the released DNQX at all, indicating the neural network activity 7 seconds after the DNQX release was recovered to the baseline. Multi-unit recording on 20 channels (from 3 animals) was summarized in the figure.

4.4.2.4 Distinctive DNQX effect pattern on different network activity

In Fig. 4-6A and B the spike number generated during the different period of air puff burst stimuli was profoundly different in the control trials. The multi-unit spike count for sensory evoked spikes was remarkably higher than the interval spikes and displayed strong adaptation effect, so the spike count during AP3s was noticeably lower than AP1s. The effect of released DNQX was different on the various periods of air puff evoked spikes. During the stronger neural activity the DNQX exhibit less effectiveness as demonstrated by Fig. 4-8. The AP1s evoked spikes had the highest spike count during control trials and the DNQX affected trials generate negligible impact on the spike number in this period. In contrast, the AP1i spikes had very low spike number thus were noticeably reduced by the release of DNQX, the spike number generated during AP1i was nearly 25% of the number generated during the control trials. As the adaptation reduces the spike number during whisker stimulation, the spike number as well as the precision of the spikes noticeably reduced during AP2s and AP3s. Releasing of DNQX generated remarkably higher impact on the multi-unit spike numbers during these periods, 25% reduction and 45% reduction compare to the baseline, respectively. The spike numbers generated during the interval of air puff was denoted as non-Sensory spikes due to the lack of direct multi-whisker stimuli input. The lower spike numbers during the non-Sensory neural network activity was more severely impacted by the release of DNQX molecules.

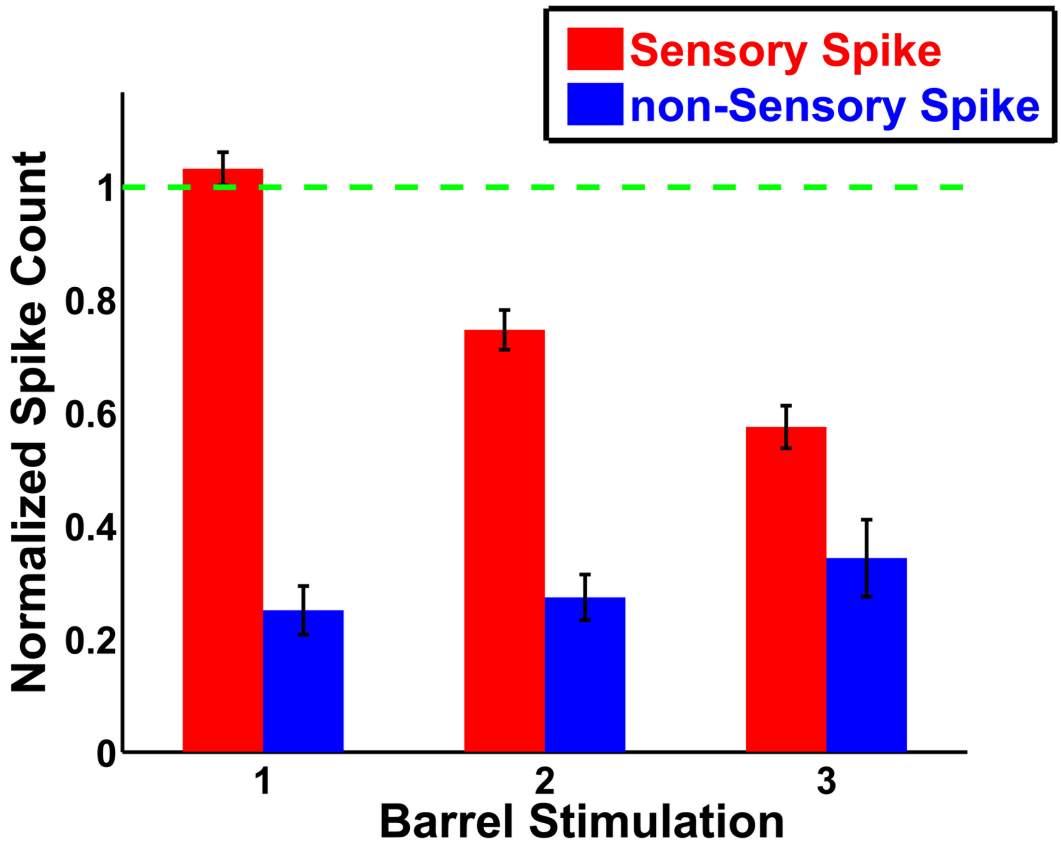

Figure 4-8 Distinctively affected sensory evoked response during air puff burst. The evoked neural response by the burst air puff stimuli exhibit remarkably different patterns. The sensory evoked firing rate increase display high amplitude, high precision, low latency and strong adaptation effect over the stimuli. The interval spike numbers exhibit the opposite characteristics with lower amplitude and lower reliability. Each of the neural response was normalized to the baseline firing rate during the same interval. During AP1s, the firing rate was highest, although the time of AP1s was the closest to the delivery of DNQX, the firing rate was not influenced by the released DNQX at all. With the adaptation gradually decrease the firing rate of sensory evoked spikes, the AP2s and AP3s response was affected more by the release of DNQX molecules. To a sharp contrast, the action potential elicit during the interval time of the air puff was profoundly less than the sensory evoked spikes and the DNQX effect on the interval spikes was remarkably higher than the effect on sensory spikes. Multi-unit recording on 20 channels (from 3 animals) was summarized in the figure.

4.4.3 Characterization of DNQX release system *in vivo*

4.4.3.1 DNQX effectiveness over trials

The DNQX release system generated noticeable difference in spike numbers over multiple trials. During each trial, the 8 to 12 recording microelectrodes displayed unanimous reduction in multi-unit spike number. The channels without stable sensory evoked baseline firing rate was removed from the analysis and the summary of DNQX release effect over trials is illustrated in Fig 4-9. Because the multi-unit spike number during AP1s, AP2s and AP3s period was less noticeably impacted by the release of DNQX, all the summary of DNQX impact was calculated from averaging the spike numbers generated during AP1i, AP2i and AP3i. This account for a more precise quantification of DNQX effect, because the sensory evoked spikes were possibly driven by over-saturated synaptic input onto the neural network in barrel cortex. Although the DNQX can partially antagonize the input synaptic transmission onto these neurons, the networks were still driven by almost saturated neural input. The phenomenon is represented by the sigmoidal activation function of the neurons. So the sensory evoked spikes cannot represent the effectiveness of the DNQX. In Fig 4-9, the first DNQX release exhibit the most substantial impact on the total spike number. 90% of the spike number was reduced during the first trial of DNQX release. During the later trials, each DNQX release induced noticeable spike number reduction compare to the baseline spike numbers denoted as the red horizontal dash line. The general trend of drug release effectiveness was continuously reduced over the period of the experiment. Thus linear regression was fitted to the spike number trend over trials to capture the decrease in DNQX effect. Over the trials sensory evoked spike numbers displayed fluctuation because of the random fluctuation of spike numbers *in vivo*. Despite the high consistency of the air puff induced spikes, the interval spike numbers quantified for the drug delivery effect

demonstrated less precision and lower repeatability, yet they account for a longer duration of the total air puff burst stimuli, thus sufficient time period was recorded to estimate the spike number during this process.

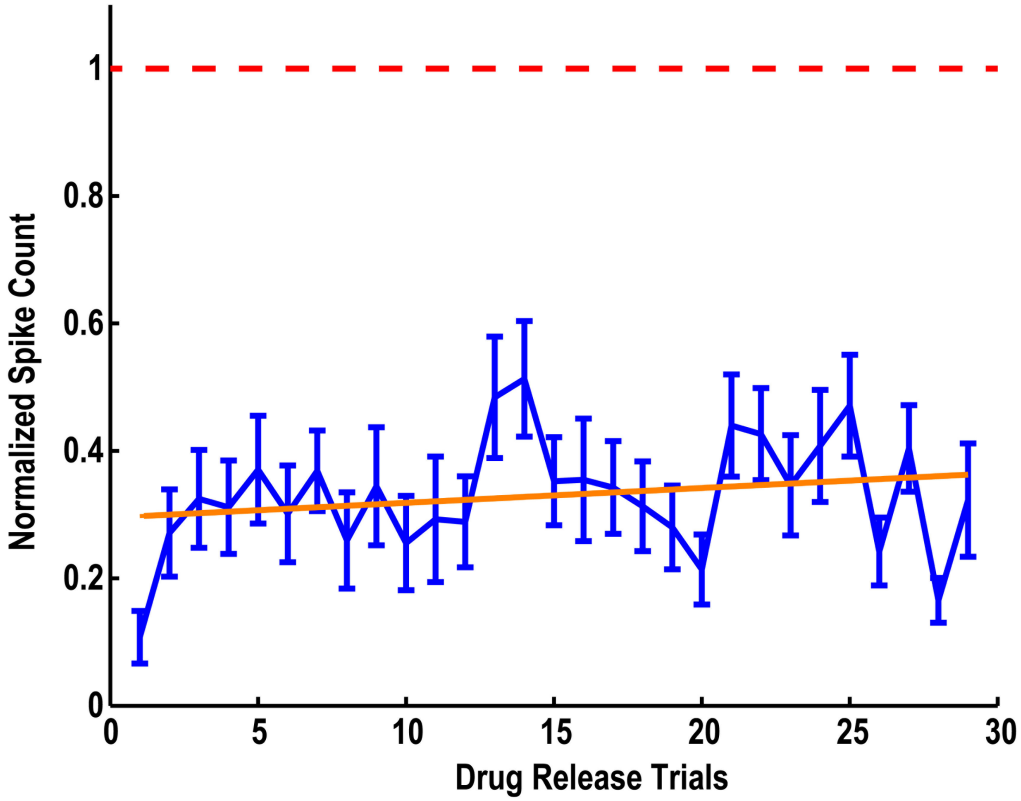

Figure 4-9 *In vivo* effect of DNQX release on barrel neural networks over trials. The average action potential suppression effect was summarized during multiple DNQX release trials during the *in vivo* experiment. The action potential suppression was derived from the normalized spike count during the air puff interval period. Normalization baseline was calculated as the stable neural response during sensory evoked spikes after the DNQX release effect completely diminished. The maximum DNQX effect was observed during the first release trial and a slight decrease trend of DNQX effect was observed over the 29 drug release trials. The trial number was determined by the minimum number of recordable trials for each animal, affected by the anesthesia state and animal survival during acute recording. A linear function was fitted to the DNQX effect over trials. Fit quality reached 0.217, indicating a relatively weak correlation between the trial number and the DNQX efficacy. Multi-unit recordings on 20 channels (from 3 animals) was illustrated in the figure.

4.4.3.2 The spatial resolution of DNQX release

The spatial extend of the DNQX effect was estimated by observing the drug effect on various recording channels. The effect of drug molecules were estimated by the normalized spike number reduction compare to the sensory evoked baseline firing rate. The center recording electrode demonstrated the strongest normalized spike number reduction. The drug release effect from 3 *in vivo* animal experiments were summarized together to generate an estimate for the drug effective range in Fig. 4-10. The furthest electrode to record the drug release efficacy was 325 μm away from the center of drug delivery. Although the result was affected by the random spike number fluctuation during the *in vivo* experiment and the change of brain state, a second order polynomial function was fitted to the reduction trend of the drug action with a quality factor of 0.658 in Fig. 4-10. The high fit quality of the polynomial function demonstrate the trend of DNQX action decrease over the distance. The extrapolation result from the fitted polynomial function indicate the drug was effective for up to 400 μm distance from the center of release. The *in vivo* drug efficacy gradually decrease as the distance from the center of release increased. This reflect the semi-sphere drug diffusion profile from the releasing electrode observed *in vitro*. Despite the influence of restricted diffusion in the tissue, the large number of trials of recording on various channels could account for the randomly distributed diffusion restriction patterns *in vivo*.

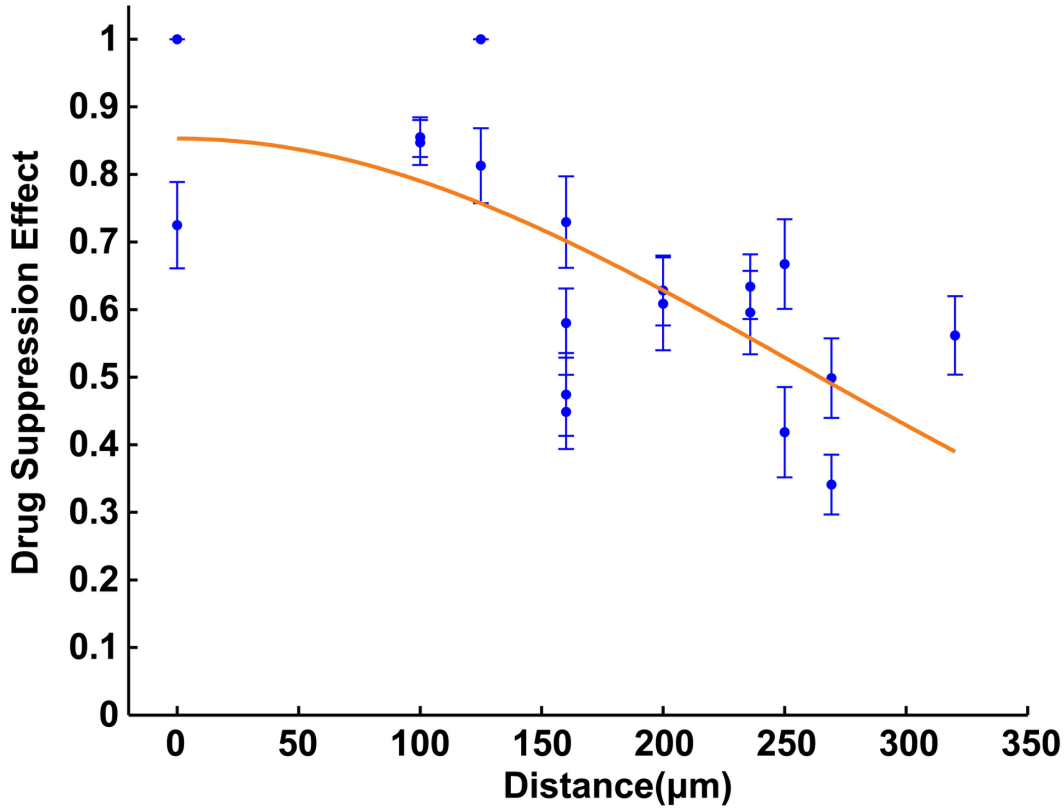

Figure 4-10 The spatial extent of DNQX effect. The normalized spike number generation during the air puff interval period of the drug release was quantified to estimate the effective range of the released DNQX. The maximum DNQX effect was observed in the center of delivery and the suppression efficacy decreased as the distance of the microelectrode from the center increased. A symmetric second order polynomial function describes the reduction trend of DNQX effect over a distance of 400 μm. The fitness reached quality factor of 0.658, indicating good trend for predicting the effectiveness of DNQX release. The released DNQX effectiveness was reduced to half efficacy by the distance of 310 μm as extrapolated by the fitted function. Multi-unit recording of 20 channels (from 3 animals) was summarized, 29 trials of each multi-unit was averaged in the experiment.

4.5 DISCUSSION

4.5.1 Benefit of double-layer DNQX conducting polymer

The single layer PPy/CNT/DNQX polymer only maintain very limited quantity of DNQX on the microelectrodes. Due to the high value in microelectrode array fabrication as well as the extreme importance to ensure the success of *in vivo* experiments, the microelectrodes with DNQX coating requires large quantity of drug loading capacity. Increasing the coating capacity of PPy/CNT/DNQX by double-layer approach can significantly broaden the range of application for the drug release technique, because the benefit of PEDOT/CNT polymer on promoting the second layer deposition of PPy film with drug molecule is not affected by the choice of molecules or the difficulty in electrochemical synthesis. The PEDOT/CNT polymer improve the deposition of PPy/CNT/DNQX film by decreasing the initial impedance and increasing the surface area of the substrate for deposition. The beneficial effect was characterized by the remarkably reduced impedance across a broad range of measured frequencies. The incorporation of CNT into the PEDOT/CNT polymer as well as the PPy/CNT/DNQX polymer not only enhance the overall conductivity and the mechanical stability of the polymer, but also serve as the reservoir to release drug. Because high concentration DNQX solution was initially utilized to wet the interior surface of CNT, the conducting polymer sealed CNT in the PPy/CNT/DNQX

embed large quantity of DNQX molecules that could be driven out during the drug release by the concentration gradient created in the polymer matrix.

4.5.2 Effectiveness of DNQX release in barrel cortex

4.5.2.1 Benefit of barrel cortex for evaluating the technique

The transient increase in action potential firing rate in the barrel cortex is strong and reliable. The topographical representation of facial whiskers by the barrel neural networks also enable the optimization of sensory evoked neural response by evoking neural activity on various facial whiskers and observe the quantity of generated multi-unit spikes. The quantifiable and repeatable spike number generated in the barrel cortex have been utilized to evaluate various neuromodulation techniques in the brain such as iontophoresis [47]. The barrel cortex neural network activity not only displayed the high precision high amplitude firing pattern directly evoked by the air puff stimuli, but also demonstrated relatively weak but still repeatable action potential firing patterns during the intervals of the air puff. The oscillatory neural networks activity observed during the intervals could be a result of network oscillation generated by interaction between excitatory and inhibitory neural networks [232], another possible mechanism for such neural activity is the residual mechanical vibration of the whisker after the air puff. The reliable quantity of the muti-unit activity in the barrel cortex represent one benefit of the barrel cortex as model system, the other benefit is the various techniques to evoke complex neural network activity patterns. For the further evaluation of the DNQX release technique, sequential stimulation to the principle whisker and adjacent whisker could possibly be utilized to elicit various patterns of neural network activity[231]. Furthermore, the non-barrel septa region of the layer IV of SI cortex neural networks may respond to axonal input from the POm nuclei of

thalamus [233]. Due the lack of detailed neural transmission mechanisms in the septa region and the more effective suppression of DNQX on relatively weak neural response. The drug delivery technique could find use in understanding the synaptic transmission in the septa region, with almost identical experiment preparation compare to the barrel cortex recording in this study.

4.5.2.2 DNQX release affect the neural network activity in barrel cortex

The optimal neural response to measure the DNQX release effect was the weaker neural network response during the interval of air puffs. Because of the spike activation function of the neuronal membrane potential [184], the overall input signal to the neurons during the air puff stimulation saturated the input of the neurons. So the released DNQX drive the membrane potential from oversaturated non-linear response range to the adaptive firing rate range of the neuron. Thus the effectiveness of the DNQX molecule was partially undetectable. However, during the relatively weaker neural activation period of the air puff interval, the neuronal membrane potential was near the threshold for firing action potentials, thus the DNQX release could effectively reduce the input to the neurons and subsequently noticeably reduce the firing probability of the neurons during this period. The spike numbers generated during the intervals of air puffs effectively represent the weaker neural transmission process in during the mechanical stimulation of whisker, because despite the low firing rate in this period, the baseline multi-unit spike numbers were still significantly higher than spontaneous spike numbers observed in layer IV of barrel cortex.

4.5.2.3 DNQX release system demonstrate high spatial and temporal resolution

The effect of the released DNQX molecule on the excitatory neural transmission was observed beyond one second from the trigger of the drug release. To prevent the strong

adaptation effect with frequent whisker stimulation, the drug effectiveness cannot be determined at very high temporal precision. Because the six seconds interval between each air puff burst allow the repetitive generation of multi-unit spikes with very stable baseline and little adaptation effect. The second air puff burst evoked sensory response was conducted 7 seconds following the release of DNQX and the observed DNQX effect was already washed out during this period. This high temporal resolution of pharmacological intervention technique allows the transient modulation of behavior neural states and prevent the occurrence of side effects caused by the drug molecules. The detailed temporal extent of the drug release system requires further investigation to improve the understanding of the drug release and diffusion dynamics during the process. The spatial extent of the DNQX release effect was examined by fitting second order polynomial function to the effective index of the specific channels. In the center of the neuromodulation, nearly complete abolish of neural activity was observed during the interval period of air puff, while on the electrode sites 300 μm away, the effectiveness reduced to nearly 40% of the maximum capability. The released drug molecule from a planar MEA electrode could form a semi-sphere diffusion concentration of neural molecules, but the *in vivo* restricted diffusion of substance may alter the detailed distribution of the drug molecules being released. At a certain distance away the drug molecule reduces below the effective concentration of the drug thus the neural suppression cannot be observed. The decay of drug concentration roughly follows a second order polynomial function, where in the center the drug demonstrate maximum effect and the effectiveness decay rapidly towards the edge of the diffusion range. The function was restricted by the symmetricity of the diffusion pattern and the maximum effectiveness in the center of the electrode. The fitted function demonstrated high fit quality factor of 0.658. Indicating the reduction trend for drug release effectiveness index could be described as a

symmetric second order polynomial function. The extrapolation of the fitted function indicate the drug effect will be zero around 435 μm from the center of release and the effectiveness of half the maximum drug action is observed near 310 μm. Thus the overall spatial resolution of the drug release modulation to neural network with the drug release parameters of this experiment is around 600-900 μm depending on the required drug modulation intensity for the purpose of the device. The effect is sufficient to affect roughly one excitatory barrel neural networks in the layer IV of S1 cortex. The drug delivery dosage and spatial resolution of drug modulation could be altered in future studies by varying the electrical drug release trigger amplitude or duration.

4.5.3 Drug release for therapeutic and behavior research device

In a recent study, Simon et al. utilized PEDOT/PSS polymers to successful delivery neural molecules such as glutamate (Glu), aspartate (Asp) and γ-amino butyric acid (GABA) to peripheral auditory environment. However the device requires complicated fabrication process and is not capable of simultaneous neural recording of the affected neural networks. The bulky size of the device also added great difficulties to integrate the device onto *in vivo* MEAs. The *in vivo* feasibility of simultaneous localized drug release and direct recording of modulated neural networks has not been demonstrated thus requires further investigation.

The drug release technique evaluated in this work demonstrated combination of multiple benefit towards implementing pharmaceutical modulation capability onto *in vivo* MEAs. The simple technique of coating conducting polymer directly onto specific sites of MEAs allow the incorporation of neuromolecules without additional device complexity such as microfluidic channels and cannulas or fiber optics for optogenetics. With the mechanical stability of the conducting polymer, the device could be implanted into the target neural tissue for long period

without losing the functionality. Any suitable neural stimulation device could be utilized to trigger the release of drug molecule from the conducting polymer coated microelectrodes. Additionally, different sites on the MEAs could incorporate various species of neuromolecules without interfering with each other. The neural modulation effect of multiple neuromolecules can be subsequently triggered simultaneously or in specifically designed spatial temporal patterns. The capability of the device to precisely deliver neuromolecules on demand also maximize the conservation of drug during the whole duration of the device implantation. For devices such as close-loop neural stimulation system for treating epilepsies based on the detection of abnormal neural activity, the drug delivery system can be easily adapted to maximize the suppression on neural activity without introducing additional complexity, and the drug release triggered by the detection of abnormal neural activity could provide long term effectiveness to the neural network intervention treatment with very small quantity of drug molecules incorporated in the conducting polymer film.

4.6 CONCLUSIONS

An electrochemically controlled DNQX release system was developed and evaluated in the somatosensory barrel cortex of the rats. Mechanical stimulation to the rat facial whisker evoked repetitive firing of action potentials in the barrel cortex neural network and this firing pattern was suppressed by the release of DNQX from implanted MEAs, evaluated by simultaneous neural recording and drug delivery. The effect of released DNQX lasted between one second and six seconds. The spatial extent of the drug release was estimated by observing the decay of DNQX effectiveness on distance recording microelectrodes. The range of DNQX

action was between 600 μm and 900 μm depending on the designated strength of drug action. Taken together, the system demonstrated successful *in vivo* neural network modulation capability with high spatial and temporal precision, the precisely controllable delivery of neuromolecules is promising for possible close-loop treatment device for neural disorders or *in vivo* functional neural network study in neuroscience research.

4.7 ACKNOWLEDGEMENTS

We acknowledge the financial support by NIH R01NS062019, 7R43DA035545-02, 1R43DA036264-01 and 1R43AA022030-01.

We thank the Center for Biological Imaging at the University of Pittsburgh and Dr. Simon Watkins, regarding the use of the facility to perform image analysis.

BIBLIOGRAPHY

1. Dunlop, J., et al., *High-throughput electrophysiology: an emerging paradigm for ion-channel screening and physiology.* Nature reviews Drug discovery, 2008. **7**(4): p. 358-368.

2. Van Pelt, J., et al., *Longterm stability and developmental changes in spontaneous network burst firing patterns in dissociated rat cerebral cortex cell cultures on multielectrode arrays.* Neuroscience letters, 2004. **361**(1): p. 86-89.

3. Wolpaw, J.R., et al., *Brain-computer interfaces for communication and control.* Clin Neurophysiol, 2002. **113**(6): p. 767-91.

4. Motta, P.S. and J.W. Judy, *Multielectrode microprobes for deep-brain stimulation fabricated with a customizable 3-D electroplating process.* Biomedical Engineering, IEEE Transactions on, 2005. **52**(5): p. 923-933.

5. Kozai, T.D. and D.R. Kipke, *Insertion shuttle with carboxyl terminated self-assembled monolayer coatings for implanting flexible polymer neural probes in the brain.* J Neurosci Methods, 2009. **184**(2): p. 199-205.

6. Kozai, T.D., et al., *In vivo two-photon microscopy reveals immediate microglial reaction to implantation of microelectrode through extension of processes.* J Neural Eng, 2012. **9**(6): p. 066001.

7. Williams, J.C., et al., *Complex impedance spectroscopy for monitoring tissue responses to inserted neural implants.* J Neural Eng, 2007. **4**(4): p. 410-23.

8. Williams, J.C., R.L. Rennaker, and D.R. Kipke, *Long-term neural recording characteristics of wire microelectrode arrays implanted in cerebral cortex.* Brain Res Brain Res Protoc, 1999. **4**(3): p. 303-13.

9. Campbell, P.K., et al., *A silicon-based, three-dimensional neural interface: manufacturing processes for an intracortical electrode array.* IEEE Trans Biomed Eng, 1991. **38**(8): p. 758-68.

10. Jackson, A. and E.E. Fetz, *Compact movable microwire array for long-term chronic unit recording in cerebral cortex of primates.* Journal of Neurophysiology, 2007. **98**(5): p. 3109-18.

11. Wise, K.D., et al., *Microelectrodes, Microelectronics, and Implantable Neural Microsystems.* Proceedings of the IEEE, 2008. **96**(7): p. 1184-1202.

12. Hodgkin, A.L. and A.F. Huxley, *The dual effect of membrane potential on sodium conductance in the giant axon of Loligo.* J Physiol, 1952. **116**(4): p. 497-506.

13. Hodgkin, A.L. and A.F. Huxley, *The components of membrane conductance in the giant axon of Loligo.* J Physiol, 1952. **116**(4): p. 473-96.

14. Hodgkin, A.L. and A.F. Huxley, *Currents carried by sodium and potassium ions through the membrane of the giant axon of Loligo.* J Physiol, 1952. **116**(4): p. 449-72.

15. Hodgkin, A.L., A.F. Huxley, and B. Katz, *Measurement of current-voltage relations in the membrane of the giant axon of Loligo.* J Physiol, 1952. **116**(4): p. 424-48.

16. Hodgkin, A.L. and A.F. Huxley, *A quantitative description of membrane current and its application to conduction and excitation in nerve.* J Physiol, 1952. **117**(4): p. 500-44.

17. Thomas, C., et al., *A miniature microelectrode array to monitor the bioelectric activity of cultured cells.* Experimental cell research, 1972. **74**(1): p. 61-66.

18. Wagenaar, D.A., J. Pine, and S.M. Potter, *Effective parameters for stimulation of dissociated cultures using multi-electrode arrays.* Journal of Neuroscience Methods, 2004. **138**(1-2): p. 27-37.

19. DeMarse, T.B., et al., *The neurally controlled animat: biological brains acting with simulated bodies.* Autonomous robots, 2001. **11**(3): p. 305-310.

20. Bakkum, D.J., et al. *Embodying cultured networks with a robotic drawing arm*. in *Engineering in Medicine and Biology Society, 2007. EMBS 2007. 29th Annual International Conference of the IEEE*. 2007. IEEE.

21. Clark, A., *Natural-born cyborgs: Minds, technologies, and the future of human intelligence*. 2004: Oxford University Press.

22. Schwartz, A.B., et al., *Brain-controlled interfaces: movement restoration with neural prosthetics.* Neuron, 2006. **52**(1): p. 205-20.

23. Shenoy, K.V., et al., *Neural prosthetic control signals from plan activity.* Neuroreport, 2003. **14**(4): p. 591-596.

24. Hochberg, L.R., et al., *Reach and grasp by people with tetraplegia using a neurally controlled robotic arm.* Nature, 2012. **485**(7398): p. 372-375.

25. Schwartz, A.B., D.M. Taylor, and S.I. Tillery, *Extraction algorithms for cortical control of arm prosthetics.* Curr Opin Neurobiol, 2001. **11**(6): p. 701-7.

26. Schwartz, A.B., *Cortical neural prosthetics.* Annu Rev Neurosci, 2004. **27**: p. 487-507.

27. Velliste, M., et al., *Cortical control of a prosthetic arm for self-feeding.* Nature, 2008. **453**(7198): p. 1098-101.

28. Schalk, G., et al., *BCI2000: a general-purpose brain-computer interface (BCI) system.* Biomedical Engineering, IEEE Transactions on, 2004. **51**(6): p. 1034-1043.

29. Wolpaw, J.R., et al., *An EEG-based brain-computer interface for cursor control.* Electroencephalography and clinical neurophysiology, 1991. **78**(3): p. 252-259.

30. Lebedev, M.A. and M.A.L. Nicolelis, *Brain–machine interfaces: past, present and future.* Trends in Neurosciences, 2006. **29**(9): p. 536-546.

31. Grill, W.M., S.E. Norman, and R.V. Bellamkonda, *Implanted Neural Interfaces: Biochallenges and Engineered Solutions.* Annual Review of Biomedical Engineering, 2009. **11**(1): p. 1-24.

32. Hatsopoulos, N.G. and J.P. Donoghue, *The science of neural interface systems.* Annu Rev Neurosci, 2009. **32**: p. 249-66.

33. Cogan, S.F., *Neural Stimulation and Recording Electrodes.* Annual Review of Biomedical Engineering, 2008. **10**(1): p. 275-309.

34. Leuthardt, E.C., et al., *A brain–computer interface using electrocorticographic signals in humans.* Journal of neural engineering, 2004. **1**(2): p. 63.

35. Nicolelis, M.A., et al., *Chronic, multisite, multielectrode recordings in macaque monkeys.* Proc Natl Acad Sci U S A, 2003. **100**(19): p. 11041-6.

36. Rousche, P.J. and R.A. Normann, *Chronic recording capability of the Utah Intracortical Electrode Array in cat sensory cortex.* J Neurosci Methods, 1998. **82**(1): p. 1-15.

37. Kipke, D.R., et al., *Silicon-substrate intracortical microelectrode arrays for long-term recording of neuronal spike activity in cerebral cortex.* IEEE Trans Neural Syst Rehabil Eng, 2003. **11**(2): p. 151-5.

38. Vetter, R.J., et al., *Chronic neural recording using silicon-substrate microelectrode arrays implanted in cerebral cortex.* IEEE Trans Biomed Eng, 2004. **51**(6): p. 896-904.

39. Barrese, J.C., et al., *Failure mode analysis of silicon-based intracortical microelectrode arrays in non-human primates.* J Neural Eng, 2013. **10**(6): p. 066014.

40. Chestek, C.A., et al., *Long-term stability of neural prosthetic control signals from silicon cortical arrays in rhesus macaque motor cortex.* J Neural Eng, 2011. **8**(4): p. 045005.

41. Polikov, V.S., P.A. Tresco, and W.M. Reichert, *Response of brain tissue to chronically implanted neural electrodes.* J Neurosci Methods, 2005. **148**(1): p. 1-18.

42. McConnell, G.C., et al., *Implanted neural electrodes cause chronic, local inflammation that is correlated with local neurodegeneration.* J Neural Eng, 2009. **6**(5): p. 056003.

43. Kozai, T.D., et al., *Mechanical failure modes of chronically implanted planar silicon-based neural probes for laminar recording.* Biomaterials, 2015. **37**: p. 25-39.

44. Arnsten, A., et al., *Dopamine D₁ receptor mechanisms in the cognitive performance of young adult and aged monkeys.* Psychopharmacology, 1994. **116**(2): p. 143-151.

45. Sawaguchi, T. and P.S. Goldman-Rakic, *The role of D1-dopamine receptor in working memory: local injections of dopamine antagonists into the prefrontal cortex of rhesus monkeys performing an oculomotor delayed-response task.* Journal of Neurophysiology, 1994. **71**(2): p. 515-28.

46. Armstrong-James, M., et al., *Quantitative ionophoresis of catecholamines using multibarrel carbon fibre microelectrodes.* Journal of Neuroscience Methods, 1981. **4**(4): p. 385-406.

47. Armstrong-James, M., E. Welker, and C.A. Callahan, *The contribution of NMDA and non-NMDA receptors to fast and slow transmission of sensory information in the rat SI barrel cortex.* Journal of Neuroscience, 1993. **13**(5): p. 2149-60.

48. Rouse, A.G., et al., *A chronic generalized bi-directional brain-machine interface.* J Neural Eng, 2011. **8**(3): p. 036018.

49. Osorio, I., et al., *An introduction to contingent (closed-loop) brain electrical stimulation for seizure blockage, to ultra-short-term clinical trials, and to multidimensional statistical analysis of therapeutic efficacy.* J Clin Neurophysiol, 2001. **18**(6): p. 533-44.

50. Berényi, A., et al., *Closed-loop control of epilepsy by transcranial electrical stimulation.* Science, 2012. **337**(6095): p. 735-737.

51. Tye, K.M. and K. Deisseroth, *Optogenetic investigation of neural circuits underlying brain disease in animal models.* Nature Reviews Neuroscience, 2012. **13**(4): p. 251-266.

52. Alivisatos, A.P., et al., *Nanotools for neuroscience and brain activity mapping.* ACS nano, 2013. **7**(3): p. 1850-1866.

53. Tzschentke, T., *Pharmacology and behavioral pharmacology of the mesocortical dopamine system.* Progress in neurobiology, 2001. **63**(3): p. 241-320.

54. Williams, G.V., S.G. Rao, and P.S. Goldman-Rakic, *The physiological role of 5-HT2A receptors in working memory.* Journal of Neuroscience, 2002. **22**(7): p. 2843-54.

55. Williams, G.V. and P.S. Goldman-Rakic, *Modulation of memory fields by dopamine Dl receptors in prefrontal cortex.* Nature, 1995. **376**(6541): p. 572-575.

56. Rao, S.G., G.V. Williams, and P.S. Goldman-Rakic, *Destruction and Creation of Spatial Tuning by Disinhibition: GABAA Blockade of Prefrontal Cortical Neurons Engaged by Working Memory.* The Journal of Neuroscience, 2000. **20**(1): p. 485-494.

57. Sawaguchi, T. and P.S. Goldman-Rakic, *D1 dopamine receptors in prefrontal cortex: involvement in working memory.* Science, 1991. **251**(4996): p. 947-50.

58. Gross, G.W., et al., *Odor, drug and toxin analysis with neuronal networks in vitro: extracellular array recording of network responses.* Biosensors and Bioelectronics, 1997. **12**(5): p. 373-393.

59. Dum, R.P. and P.L. Strick, *An unfolded map of the cerebellar dentate nucleus and its projections to the cerebral cortex.* Journal of neurophysiology, 2003. **89**(1): p. 634-639.

60. Kandler, K., L.C. Katz, and J.A. Kauer, *Focal photolysis of caged glutamate produces long-term depression of hippocampal glutamate receptors.* Nature neuroscience, 1998. **1**(2): p. 119-123.

61. Maalouf, M., R. Dykes, and A. Miasnikov, *Effects of D-AP5 and NMDA microiontophoresis on associative learning in the barrel cortex of awake rats.* Brain research, 1998. **793**(1): p. 149-168.

62. LESNIAK, M.S., et al., *Local delivery of doxorubicin for the treatment of malignant brain tumors in rats.* Anticancer research, 2005. **25**(6B): p. 3825-3831.

63. Hyland, B., et al., *Firing modes of midbrain dopamine cells in the freely moving rat.* Neuroscience, 2002. **114**(2): p. 475-492.

64. Barker, M., B. Billups, and M. Hamann, *Focal macromolecule delivery in neuronal tissue using simultaneous pressure ejection and local electroporation.* Journal of neuroscience methods, 2009. **177**(2): p. 273-284.

65. Gerhardt, G.A. and M.R. Palmer, *Characterization of the techniques of pressure ejection and microiontophoresis using in vivo electrochemistry.* Journal of neuroscience methods, 1987. **22**(2): p. 147-159.

66. Tamamaki, N. and Y. Nojyo, *Projection of the entorhinal layer II neurons in the rat as revealed by intracellular pressure-injection of neurobiotin.* Hippocampus, 1993. **3**(4): p. 471-480.

67. Hicks, T.P., *The history and development of microiontophoresis in experimental neurobiology.* Progress in neurobiology, 1984. **22**(3): p. 185-240.

68. Mourzina, Y., et al., *Patterning chemical stimulation of reconstructed neuronal networks.* Analytica chimica acta, 2006. **575**(2): p. 281-289.

69. Kaji, H., M. Nishizawa, and T. Matsue, *Localized chemical stimulation to micropatterned cells using multiple laminar fluid flows.* Lab Chip, 2003. **3**(3): p. 208-211.

70. Nagel, G., et al., *Channelrhodopsin-2, a directly light-gated cation-selective membrane channel.* Proc Natl Acad Sci U S A, 2003. **100**(24): p. 13940-5.

71. Cardin, J.A., et al., *Driving fast-spiking cells induces gamma rhythm and controls sensory responses.* Nature, 2009. **459**(7247): p. 663-667.

72. Zhang, F., et al., *Multimodal fast optical interrogation of neural circuitry.* Nature, 2007. **446**(7136): p. 633-639.

73. Sohal, V.S., et al., *Parvalbumin neurons and gamma rhythms enhance cortical circuit performance.* Nature, 2009. **459**(7247): p. 698-702.

74. Boyden, E.S., et al., *Millisecond-timescale, genetically targeted optical control of neural activity.* Nature neuroscience, 2005. **8**(9): p. 1263-1268.

75. Anikeeva, P., et al., *Optetrode: a multichannel readout for optogenetic control in freely moving mice.* Nature neuroscience, 2012. **15**(1): p. 163-170.

76. Lu, Y., et al., *Poly (3, 4-ethylenedioxythiophene)/poly (styrenesulfonate)-poly (vinyl alcohol)/poly (acrylic acid) interpenetrating polymer networks for improving optrode-neural tissue interface in optogenetics.* Biomaterials, 2012. **33**(2): p. 378-394.

77. Letheby, H., *XXIX.-On the production of a blue substance by the electrolysis of sulphate of aniline.* Journal of the Chemical Society, 1862. **15**(0): p. 161-163.

78. Angelopoulos, M., *Conducting polymers in microelectronics.* IBM Journal of Research and Development, 2001. **45**(1): p. 57-75.

79. Chen, J., et al., *Flexible, aligned carbon nanotube/conducting polymer electrodes for a lithium-ion battery.* Chemistry of Materials, 2007. **19**(15): p. 3595-3597.

80. Miasik, J.J., A. Hooper, and B.C. Tofield, *Conducting polymer gas sensors.* Journal of the Chemical Society, Faraday Transactions 1: Physical Chemistry in Condensed Phases, 1986. **82**(4): p. 1117-1126.

81. Ramanavičius, A., A. Ramanavičienė, and A. Malinauskas, *Electrochemical sensors based on conducting polymer—polypyrrole.* Electrochimica Acta, 2006. **51**(27): p. 6025-6037.

82. Gerard, M., A. Chaubey, and B. Malhotra, *Application of conducting polymers to biosensors.* Biosensors and Bioelectronics, 2002. **17**(5): p. 345-359.

83. Luo, S.-C., *Conducting polymers as biointerfaces and biomaterials: a perspective for a special issue of polymer reviews.* Polymer Reviews, 2013. **53**(3): p. 303-310.

84. Ateh, D., H. Navsaria, and P. Vadgama, *Polypyrrole-based conducting polymers and interactions with biological tissues.* Journal of the royal society interface, 2006. **3**(11): p. 741-752.

85. Green, R.A., et al., *Conducting polymers for neural interfaces: challenges in developing an effective long-term implant.* Biomaterials, 2008. **29**(24-25): p. 3393-9.

86. Ludwig, K.A., et al., *Poly(3,4-ethylenedioxythiophene) (PEDOT) polymer coatings facilitate smaller neural recording electrodes.* J Neural Eng, 2011. **8**(1): p. 014001.

87. Richardson-Burns, S.M., et al., *Polymerization of the conducting polymer poly(3,4-ethylenedioxythiophene) (PEDOT) around living neural cells.* Biomaterials, 2007. **28**(8): p. 1539-52.

88. Cui, X., et al., *Surface modification of neural recording electrodes with conducting polymer/biomolecule blends.* J Biomed Mater Res, 2001. **56**(2): p. 261-72.

89. Cui, X. and D.C. Martin, *Electrochemical deposition and characterization of poly(3,4-ethylenedioxythiophene) on neural microelectrode arrays.* Sensors and Actuators B: Chemical, 2003. **89**(1-2): p. 92-102.

90. Cui, X., et al., *In vivo studies of polypyrrole/peptide coated neural probes.* Biomaterials, 2003. **24**(5): p. 777-87.

91. Cui, X.T. and D.D. Zhou, *Poly (3,4-ethylenedioxythiophene) for chronic neural stimulation.* IEEE Trans Neural Syst Rehabil Eng, 2007. **15**(4): p. 502-8.

92. Cui, X.Y., et al., *Electrochemical deposition and characterization of conducting polymer polypyrrole/PSS on multichannel neural probes.* Sensors and Actuators a-Physical, 2001. **93**(1): p. 8-18.

93. Du, Z.J., et al., *Poly(3,4-ethylenedioxythiophene)-ionic liquid coating improves neural recording and stimulation functionality of MEAs.* Journal of Materials Chemistry C, 2015.

94. Kolarcik, C.L., et al., *Evaluation of poly(3,4-ethylenedioxythiophene)/carbon nanotube neural electrode coatings for stimulation in the dorsal root ganglion.* J Neural Eng, 2015. **12**(1): p. 016008.

95. Kozai, T., et al., *Chronic in vivo evaluation of PEDOT/CNT for stable neural recordings.* IEEE Trans Biomed Eng, 2015.

96. Luo, X. and X.T. Cui, *Electrochemically controlled release based on nanoporous conducting polymers.* Electrochemistry Communications, 2009. **11**(2): p. 402-404.

97. Barbey, R., et al., *Polymer brushes via surface-initiated controlled radical polymerization: synthesis, characterization, properties, and applications.* Chem Rev, 2009. **109**(11): p. 5437-527.

98. Skotheim, T.A., *Handbook of conducting polymers*. 1997: CRC press.

99. McCullough, R.D., et al., *Design, synthesis, and control of conducting polymer architectures: structurally homogeneous poly (3-alkylthiophenes).* The Journal of Organic Chemistry, 1993. **58**(4): p. 904-912.

100. Luo, X. and X.T. Cui, *Sponge-like nanostructured conducting polymers for electrically controlled drug release.* Electrochem commun, 2009. **11**(10): p. 1956.

101. Wallace, G.G., et al., *Conductive electroactive polymers: intelligent polymer systems*. 2008: CRC press.

102. Wadhwa, R., C.F. Lagenaur, and X.T. Cui, *Electrochemically controlled release of dexamethasone from conducting polymer polypyrrole coated electrode.* J Control Release, 2006. **110**(3): p. 531-41.

103. Leprince, L., et al., *Dexamethasone electrically controlled release from polypyrrole-coated nanostructured electrodes.* J Mater Sci Mater Med, 2010. **21**(3): p. 925-30.

104. Thompson, B.C., et al., *Effect of the dopant anion in polypyrrole on nerve growth and release of a neurotrophic protein.* Biomaterials, 2011. **32**(15): p. 3822-31.

105. Thompson, B.C., et al., *Optimising the incorporation and release of a neurotrophic factor using conducting polypyrrole.* Journal of Controlled Release, 2006. **116**(3): p. 285-294.

106. Richardson, R.T., et al., *The effect of polypyrrole with incorporated neurotrophin-3 on the promotion of neurite outgrowth from auditory neurons.* Biomaterials, 2007. **28**(3): p. 513-523.

107. Thompson, B.C., et al., *Conducting polymers, dual neurotrophins and pulsed electrical stimulation -- Dramatic effects on neurite outgrowth.* Journal of Controlled Release, 2010. **141**(2): p. 161-167.

108. Paul, N., et al., *Molecularly imprinted conductive polymers for controlled trafficking of neurotransmitters at solid-liquid interfaces.* Soft Matter, 2013. **9**(4): p. 1364-1371.

109. Cui, X.Y. and D.C. Martin, *Electrochemical deposition and characterization of poly(3,4-ethylenedioxythiophene) on neural microelectrode arrays.* Sensors and Actuators B-Chemical, 2003. **89**(1-2): p. 92-102.

110. Du, Z.J., et al., *Poly(3,4-ethylenedioxythiophene)-ionic liquid coating improves neural recording and stimulation functionality of MEAs.* Journal of Materials Chemistry C, 2015. **3**(25): p. 6515-6524.

111. Stauffer, W.R. and X.T. Cui, *Polypyrrole doped with 2 peptide sequences from laminin.* Biomaterials, 2006. **27**(11): p. 2405-13.

112. Luo, X., et al., *Carbon nanotube nanoreservior for controlled release of anti-inflammatory dexamethasone.* Biomaterials, 2011. **32**(26): p. 6316-23.

113. Skousen, J.L., et al., *Reducing surface area while maintaining implant penetrating profile lowers the brain foreign body response to chronically implanted planar silicon microelectrode arrays.* Plasticity in the Adult Brain: From Genes to Neurotherapy, 2011. **194**: p. 167-80.

114. Kozai, T.D., et al., *Ultrasmall implantable composite microelectrodes with bioactive surfaces for chronic neural interfaces.* Nat Mater, 2012. **11**(12): p. 1065-73.

115. Rebrik, S.P., et al., *Cross-channel correlations in tetrode recordings: implications for spike-sorting.* Neurocomputing, 1999. **26–27**(0): p. 1033-1038.

116. Ludwig, K.A., et al., *Chronic neural recordings using silicon microelectrode arrays electrochemically deposited with a poly(3,4-ethylenedioxythiophene) (PEDOT) film.* J Neural Eng, 2006. **3**(1): p. 59-70.

117. Ajayan, P.M. and O.Z. Zhou, *Applications of carbon nanotubes*, in *Carbon nanotubes*. 2001, Springer. p. 391-425.

118. Geim, A.K. and K.S. Novoselov, *The rise of graphene.* Nature materials, 2007. **6**(3): p. 183-191.

119. Kosynkin, D.V., et al., *Longitudinal unzipping of carbon nanotubes to form graphene nanoribbons.* Nature, 2009. **458**(7240): p. 872-876.

120. Lu, F., et al., *Advances in bioapplications of carbon nanotubes.* Advanced Materials, 2009. **21**(2): p. 139-152.

121. Keefer, E.W., et al., *Carbon nanotube coating improves neuronal recordings.* Nat Nanotechnol, 2008. **3**(7): p. 434-9.

122. Lu, Y., et al., *Electrodeposited polypyrrole/carbon nanotubes composite films electrodes for neural interfaces.* Biomaterials, 2010. **31**(19): p. 5169-5181.

123. Chen, G.Z., et al., *Carbon nanotube and polypyrrole composites: coating and doping.* Advanced Materials, 2000. **12**(7): p. 522-526.

124. Lee, Y.-K., et al., *Polypyrrole-carbon nanotube composite films synthesized through gas-phase polymerization.* Synthetic Metals, 2010. **160**(7): p. 814-818.

125. Luo, X., et al., *Carbon nanotube nanoreservior for controlled release of anti-inflammatory dexamethasone.* Biomaterials, 2011. **32**(26): p. 6316-6323.

126. Zou, J., et al., *TRANSPARENT CARBON NANOTUBE/POLY (3, 4-ETHYLENEDIOXYTHIOPHENE) COMPOSITE ELECTRICAL CONDUCTORS.* Soft Materials, 2009. **7**(4): p. 355-365.

127. Bhandari, S., et al., *Poly (3, 4-ethylenedioxythiophene)− Multiwalled Carbon Nanotube Composite Films: Structure-Directed Amplified Electrochromic Response and Improved Redox Activity.* The Journal of Physical Chemistry B, 2009. **113**(28): p. 9416-9428.

128. Luo, X., et al., *Highly stable carbon nanotube doped poly(3,4-ethylenedioxythiophene) for chronic neural stimulation.* Biomaterials, 2011. **32**(24): p. 5551-5557.

129. Matsumoto, K., et al., *Stimulation of neuronal neurite outgrowth using functionalized carbon nanotubes.* Nanotechnology, 2010. **21**(11): p. 115101.

130. Chao, T.-I., et al., *Carbon nanotubes promote neuron differentiation from human embryonic stem cells.* Biochemical and biophysical research communications, 2009. **384**(4): p. 426-430.

131. Mattson, M.P., R.C. Haddon, and A.M. Rao, *Molecular functionalization of carbon nanotubes and use as substrates for neuronal growth.* Journal of Molecular Neuroscience, 2000. **14**(3): p. 175-182.

132. Hu, H., et al., *Polyethyleneimine functionalized single-walled carbon nanotubes as a substrate for neuronal growth.* The Journal of Physical Chemistry B, 2005. **109**(10): p. 4285-4289.

133. Gut, N.K. and P. Winn, *Deep brain stimulation of different pedunculopontine targets in a novel rodent model of parkinsonism.* J Neurosci, 2015. **35**(12): p. 4792-803.

134. Santaniello, S., et al., *Therapeutic mechanisms of high-frequency stimulation in Parkinson's disease and neural restoration via loop-based reinforcement.* Proc Natl Acad Sci U S A, 2015. **112**(6): p. E586-95.

135. Obeso, J.A., et al., *Deep-brain stimulation of the subthalamic nucleus or the pars Interna of the globus pallidus in Parkinson's disease.* The New England Journal of Medicine, 2001. **345**(13): p. 956-963.

136. Limousin, P., et al., *Electrical Stimulation of the Subthalamic Nucleus in Advanced Parkinson's Disease.* New England Journal of Medicine, 1998. **339**(16): p. 1105-1111.

137. Loddenkemper, T., et al., *Deep brain stimulation in epilepsy.* J Clin Neurophysiol, 2001. **18**(6): p. 514-32.

138. Theodore, W.H. and R. Fisher, *Brain stimulation for epilepsy.* Acta Neurochir Suppl, 2007. **97**(Pt 2): p. 261-72.

139. Elble, R.J., *Mechanisms of deep brain stimulation for essential tremor.* Brain, 2014. **137**(1): p. 4-6.

140. Sandvik, U., et al., *Thalamic and subthalamic deep brain stimulation for essential tremor: where is the optimal target?* Neurosurgery, 2012. **70**(4): p. 840-846.

141. Ostrem, J., et al., *Subthalamic nucleus deep brain stimulation in primary cervical dystonia.* Neurology, 2011. **76**(10): p. 870-878.

142. Volkmann, J., et al., *Pallidal deep brain stimulation in patients with primary generalised or segmental dystonia: 5-year follow-up of a randomised trial.* The Lancet Neurology, 2012. **11**(12): p. 1029-1038.

143. Mayberg, H.S., et al., *Deep brain stimulation for treatment-resistant depression.* Neuron, 2005. **45**(5): p. 651-660.

144. Lozano, A.M., et al., *Subcallosal cingulate gyrus deep brain stimulation for treatment-resistant depression.* Biological psychiatry, 2008. **64**(6): p. 461-467.

145. Greenberg, B.D., et al., *Three-year outcomes in deep brain stimulation for highly resistant obsessive–compulsive disorder.* Neuropsychopharmacology, 2006. **31**(11): p. 2384-2393.

146. Sturm, V., et al., *The nucleus accumbens: a target for deep brain stimulation in obsessive–compulsive-and anxiety-disorders.* Journal of chemical neuroanatomy, 2003. **26**(4): p. 293-299.

147. Histed, M.H., V. Bonin, and R.C. Reid, *Direct activation of sparse, distributed populations of cortical neurons by electrical microstimulation.* Neuron, 2009. **63**(4): p. 508-22.

148. Nowak, L. and J. Bullier, *Axons, but not cell bodies, are activated by electrical stimulation in cortical gray matter I. Evidence from chronaxie measurements.* Experimental Brain Research, 1998. **118**(4): p. 477-488.

149. Hofmann, L., et al., *Modified pulse shapes for effective neural stimulation.* Frontiers in Neuroengineering, 2011. **4**.

150. Wagenaar, D.A. and S.M. Potter, *Real-time multi-channel stimulus artifact suppression by local curve fitting.* J Neurosci Methods, 2002. **120**(2): p. 113-20.

151. Simons, D.J. and G.E. Carvell, *Thalamocortical response transformation in the rat vibrissa/barrel system.* Journal of Neurophysiology, 1989. **61**(2): p. 311-30.

152. Simons, D.J., *Temporal and spatial integration in the rat SI vibrissa cortex.* Journal of Neurophysiology, 1985. **54**(3): p. 615-35.

153. de Kock, C.P., et al., *Layer- and cell-type-specific suprathreshold stimulus representation in rat primary somatosensory cortex.* J Physiol, 2007. **581**(Pt 1): p. 139-54.

154. Stauffer, W.R., et al., *Rapid modulation of local neural activity by controlled drug release from polymer-coated recording microelectrodes.* Journal of Neural Engineering, 2011. **8**(4): p. 044001.

155. Lewis, D.A. and G. Gonzalez-Burgos, *Pathophysiologically based treatment interventions in schizophrenia.* Nat Med, 2006. **12**(9): p. 1016-22.

156. Lewis, D.A., T. Hashimoto, and D.W. Volk, *Cortical inhibitory neurons and schizophrenia.* Nat Rev Neurosci, 2005. **6**(4): p. 312-24.

157. Ahissar, E., R. Sosnik, and S. Haidarliu, *Transformation from temporal to rate coding in a somatosensory thalamocortical pathway.* Nature, 2000. **406**(6793): p. 302-306.

158. Simons, D.J., *Multi-whisker stimulation and its effects on vibrissa units in rat SmI barrel cortex.* Brain Res, 1983. **276**(1): p. 178-82.

159. Abeles, M., *Corticonics*. 1991, Cambridge: Cambridge University Press.

160. Salinas, E. and T.J. Sejnowski, *Correlated neuronal activity and the flow of neural information.* Nat Rev Neurosci, 2001. **2**(8): p. 539-50.

161. Wise, K.D., et al., *Wireless implantable microsystems: High-density electronic interfaces to the nervous system.* Proceedings of the Ieee, 2004. **92**(1): p. 76-97.

162. Ono, T., et al., *Brain-computer interface with somatosensory feedback improves functional recovery from severe hemiplegia due to chronic stroke.* Frontiers in neuroengineering, 2014. **7**.

163. Simon, D.T., et al., *Organic electronics for precise delivery of neurotransmitters to modulate mammalian sensory function.* Nat Mater, 2009. **8**(9): p. 742-6.

164. Isaksson, J., et al., *Electronic control of Ca2+ signalling in neuronal cells using an organic electronic ion pump.* Nat Mater, 2007. **6**(9): p. 673-9.

165. Cui, X., et al., *In vivo studies of polypyrrole/peptide coated neural probes.* Biomaterials, 2003. **24**(5): p. 777-787.

166. Stauffer, W.R. and X.Y. Cui, *Effect of Biomolecules Immobilized on Polypyrrole Surfaces on Electronic Properties and Neuronal Cell Attachment, Differentiation and Growth.* NIH Neural Interface Workshop, 2004.

167. Wadhwa, R., C.F. Lagenaur, and X.T. Cui, *Electrochemically controlled release of dexamethasone from conducting polymer polypyrrole coated electrode.* Journal of Controlled Release, 2006. **110**(3): p. 531-541.

168. Pernaut, J.M. and J.R. Reynolds, *Use of conducting electroactive polymers for drug delivery and sensing of bioactive molecules. A redox chemistry approach.* Journal of Physical Chemistry B, 2000. **104**(17): p. 4080-4090.

169. Miller, L.L. and X.U. Zhou, *Poly(N-methylpyrrolylium) Poly(styrenesu1fonate). A Conductive, Electrically Switchable Cation Exchanger That Cathodically Binds and Anodically Releases Dopamine.* Macromolecules, 1987. **20**(7): p. 1594-1597.

170. Kontturi, K., P. Pentti, and G. Sundholm, *Polypyrrole as a model membrane for drug delivery.* Journal of Electroanalytical Chemistry, 1998. **453**(1–2): p. 231-238.

171. Massoumi, B. and A.A. Entezami, *Electrochemically stimulated 2-ethylhexyl phosphate (EHP) release through redox switching of conducting polypyrrole film and polypyrrole/poly (N-methylpyrrole) or self-doped polyaniline bilayers.* Polymer International, 2002. **51**(6): p. 555-560.

172. Chen, G.Z., et al., *Carbon nanotube and polypyrrole composites: Coating and doping.* Advanced Materials, 2000. **12**(7): p. 522-+.

173. Cui, X.T. and D.D. Zhou, *Poly (3,4-ethylenedioxythiophene) for chronic neural stimulation.* Ieee Transactions on Neural Systems and Rehabilitation Engineering, 2007. **15**(4): p. 502-508.

174. Kyotani, T., et al., *Chemical modification of the inner walls of carbon nanotubes by HNO3 oxidation.* Carbon, 2001. **39**(5): p. 782-785.

175. Tessonnier, J.P., et al., *Selective deposition of metal nanoparticles inside or outside multiwalled carbon nanotubes.* ACS Nano, 2009. **3**(8): p. 2081-9.

176. Ajayan, P.M., et al., *Single-walled carbon nanotube–polymer composites: strength and weakness.* Advanced Materials, 2000. **12**(10): p. 750-753.

177. Abidian, M.R., D.H. Kim, and D.C. Martin, *Conducting-polymer nanotubes for controlled drug release.* Advanced Materials, 2006. **18**(4): p. 405-409.

178. Hartings, J.A. and D.J. Simons, *Inhibition suppresses transmission of tonic vibrissa-evoked activity in the rat ventrobasal thalamus.* J Neurosci, 2000. **20**(19): p. RC100.

179. Vijayraghavan, S., et al., *Inverted-U dopamine D1 receptor actions on prefrontal neurons engaged in working memory.* Nat Neurosci, 2007. **10**(3): p. 376-84.

180. Robbins, T.W. and A.F. Arnsten, *The neuropsychopharmacology of fronto-executive function: monoaminergic modulation.* Annu Rev Neurosci, 2009. **32**: p. 267-87.

181. Papageorgiou, D.P., et al., *A shuttered neural probe with on-chip flowmeters for chronic in vivo drug delivery.* Microelectromechanical Systems, Journal of, 2006. **15**(4): p. 1025-1033.

182. Chen, J., et al., *A multichannel neural probe for selective chemical delivery at the cellular level.* Biomedical Engineering, IEEE Transactions on, 1997. **44**(8): p. 760-769.

183. Purcell, E.K., et al., *Flavopiridol reduces the impedance of neural prostheses in vivo without affecting recording quality.* J Neurosci Methods, 2009. **183**(2): p. 149-57.

184. Kyriazi, H.T., et al., *Quantitative effects of GABA and bicuculline methiodide on receptive field properties of neurons in real and simulated whisker barrels.* J Neurophysiol, 1996. **75**(2): p. 547-60.

185. Chen, J., et al., *A multichannel neural probe for selective chemical delivery at the cellular level.* IEEE Trans Biomed Eng, 1997. **44**(8): p. 760-9.

186. Rathnasingham, R., et al., *Characterization of implantable microfabricated fluid delivery devices.* IEEE Trans Biomed Eng, 2004. **51**(1): p. 138-45.

187. Lau, A.N. and L.L. Miller, *Electrochemical behavior of a dopamine polymer. Dopamine release as a primitive analog of a synapse.* Journal of the American Chemical Society, 1983. **105**(16): p. 5271-5277.

188. Miller, L.L. and X. Zhou, *Poly (N-methylpyrrolylium) poly (styrenesulfonate)-a conductive, electrically switchable cation exchanger that cathodically binds and anodically releases dopamine.* Macromolecules, 1987. **20**(7): p. 1594-1597.

189. Zhou, Q.-X., L.L. Miller, and J.R. Valentine, *Electrochemically controlled binding and release of protonated dimethyldopamine and other cations from poly (N-methyl-pyrrole)/polyanion composite redox polymers.* Journal of electroanalytical chemistry and interfacial electrochemistry, 1989. **261**(1): p. 147-164.

190. Miller, L.L., et al., *Electrochemically controlled release.* Journal of Controlled Release, 1987. **6**(1): p. 293-296.

191. Shabel, S.J., et al., *GABA/glutamate co-release controls habenula output and is modified by antidepressant treatment.* Science, 2014. **345**(6203): p. 1494-1498.

192. Yu, X., et al., *Wakefulness Is Governed by GABA and Histamine Cotransmission.* Neuron, 2015. **87**(1): p. 164-78.

193. Akerman, C.J. and H.T. Cline, *Refining the roles of GABAergic signaling during neural circuit formation.* Trends Neurosci, 2007. **30**(8): p. 382-9.

194. Hensch, T.K., *Critical period plasticity in local cortical circuits.* Nat Rev Neurosci, 2005. **6**(11): p. 877-88.

195. Kutlán, D. and I. Molnár-Perl, *Characteristics and stability of the OPA/3-mercaptopropionic acid and OPA/N-acetyl-L-cysteine derivatives of amino acids.* Chromatographia, 2001. **53**(1): p. S188-S198.

196. Van Eden, C., et al., *Prenatal development of GABA-ergic neurons in the neocortex of the rat.* Journal of Comparative Neurology, 1989. **289**(2): p. 213-227.

197. Ben-Ari, Y., *Excitatory actions of GABA during development: the nature of the nurture.* Nature Reviews Neuroscience, 2002. **3**(9): p. 728-739.

198. Represa, A. and Y. Ben-Ari, *Trophic actions of GABA on neuronal development.* Trends in neurosciences, 2005. **28**(6): p. 278-283.

199. Barbin, G., et al., *Involvement of GABA A receptors in the outgrowth of cultured hippocampal neurons.* Neuroscience letters, 1993. **152**(1): p. 150-154.

200. Lovat, V., et al., *Carbon nanotube substrates boost neuronal electrical signaling.* Nano letters, 2005. **5**(6): p. 1107-1110.

201. Jin, G.-Z., et al., *Neurite outgrowth of dorsal root ganglia neurons is enhanced on aligned nanofibrous biopolymer scaffold with carbon nanotube coating.* Neuroscience letters, 2011. **501**(1): p. 10-14.

202. Heuschkel, M.O., et al., *A three-dimensional multi-electrode array for multi-site stimulation and recording in acute brain slices.* J Neurosci Methods, 2002. **114**(2): p. 135-48.

203. Feinerman, O., A. Rotem, and E. Moses, *Reliable neuronal logic devices from patterned hippocampal cultures.* Nature Physics, 2008. **4**(12): p. 967-973.

204. Wagenaar, D.A., et al., *Controlling bursting in cortical cultures with closed-loop multi-electrode stimulation.* J Neurosci, 2005. **25**(3): p. 680-8.

205. Weaver, C.L., et al., *Electrically controlled drug delivery from graphene oxide nanocomposite films.* ACS Nano, 2014. **8**(2): p. 1834-43.

206. Tye, K.M., et al., *Dopamine neurons modulate neural encoding and expression of depression-related behaviour.* Nature, 2013. **493**(7433): p. 537-41.

207. Russo, S.J. and E.J. Nestler, *The brain reward circuitry in mood disorders.* Nat Rev Neurosci, 2013. **14**(9): p. 609-25.

208. Hales, C.M., J.D. Rolston, and S.M. Potter, *How to Culture, Record and Stimulate Neuronal Networks on Micro-electrode Arrays (MEAs).* J Vis Exp, 2010(39): p. e2056.

209. Berdondini, L., et al., *Extracellular recordings from locally dense microelectrode arrays coupled to dissociated cortical cultures.* J Neurosci Methods, 2009. **177**(2): p. 386-96.

210. Rowley, H.L., et al., *Differences in the neurochemical and behavioural profiles of lisdexamfetamine methylphenidate and modafinil revealed by simultaneous dual-probe microdialysis and locomotor activity measurements in freely-moving rats.* J Psychopharmacol, 2014. **28**(3): p. 254-69.

211. Bradberry, C.W., et al., *Cocaine and cocaethylene: microdialysis comparison of brain drug levels and effects on dopamine and serotonin.* J Neurochem, 1993. **60**(4): p. 1429-35.

212. Lalley, P.M., *Microiontophoresis and Pressure Ejection.*

213. Belle, A.M., et al., *Controlled Iontophoresis Coupled with Fast-Scan Cyclic Voltammetry/Electrophysiology in Awake, Freely Moving Animals.* ACS Chemical Neuroscience, 2013. **4**(5): p. 761-771.

214. Rogawski, M.A. and G.K. Aghajanian, *Modulation of lateral geniculate neurone excitability by noradrenaline microiontophoresis or locus coeruleus stimulation.* Nature, 1980. **287**(5784): p. 731-4.

215. Seymour, J.P. and D.R. Kipke, *Neural probe design for reduced tissue encapsulation in CNS.* Biomaterials, 2007. **28**(25): p. 3594-607.

216. Metz, S., et al., *Flexible polyimide probes with microelectrodes and embedded microfluidic channels for simultaneous drug delivery and multi-channel monitoring of bioelectric activity.* Biosensors and bioelectronics, 2004. **19**(10): p. 1309-1318.

217. Berdichevsky, Y., et al., *Microfluidics and multielectrode array-compatible organotypic slice culture method.* Journal of neuroscience methods, 2009. **178**(1): p. 59-64.

218. Andersson, H. and A. Van Den Berg, *Microfabrication and microfluidics for tissue engineering: state of the art and future opportunities.* Lab Chip, 2004. **4**(2): p. 98-103.

219. Yizhar, O., et al., *Optogenetics in neural systems.* Neuron, 2011. **71**(1): p. 9-34.

220. Fenno, L., O. Yizhar, and K. Deisseroth, *The development and application of optogenetics.* Annual review of neuroscience, 2011. **34**: p. 389-412.

221. Deisseroth, K., *Optogenetics.* Nature methods, 2011. **8**(1): p. 26-29.

222. Kozai, T.D. and A.L. Vazquez, *Photoelectric artefact from optogenetics and imaging on microelectrodes and bioelectronics: new challenges and opportunities.* Journal of Materials Chemistry B, 2015.

223. Ben-Ari, Y., et al., *GABA A, NMDA and AMPA receptors: a developmentally regulatedmenage a trois'.* Trends in neurosciences, 1997. **20**(11): p. 523-529.

224. Ruel, J., et al., *The selective AMPA receptor antagonist GYKI 53784 blocks action potential generation and excitotoxicity in the guinea pig cochlea.* Neuropharmacology, 2000. **39**(11): p. 1959-1973.

225. Lee, S.H., G. Govindaiah, and C.L. Cox, *Selective excitatory actions of DNQX and CNQX in rat thalamic neurons.* Journal of Neurophysiology, 2010. **103**(4): p. 1728-34.

226. Dalia, A., N.J. Uretsky, and L.J. Wallace, *Induction of locomotor activity by the glutamate antagonist DNQX injected into the ventral tegmental area.* Brain Res, 1996. **728**(2): p. 209-14.

227. Martin, A., M. Recasens, and J. Guiramand, *DNQX-induced toxicity in cultured rat hippocampal neurons: an apparent AMPA receptor-independent effect?* Neurochem Int, 2003. **42**(3): p. 251-60.

228. Wang, Q., et al., *Voltage-sensitive dye imaging reveals improved topographic activation of cortex in response to manipulation of thalamic microstimulation parameters.* J Neural Eng, 2012. **9**(2): p. 026008.

229. Beltramo, R., et al., *Layer-specific excitatory circuits differentially control recurrent network dynamics in the neocortex.* Nat Neurosci, 2013. **16**(2): p. 227-34.

230. Hooks, B.M., et al., *Laminar Analysis of Excitatory Local Circuits in Vibrissal Motor and Sensory Cortical Areas.* PLoS Biol, 2011. **9**(1): p. e1000572.

231. Simons, D.J., et al., *Responses of barrel cortex neurons in awake rats and effects of urethane anesthesia.* Exp Brain Res, 1992. **91**(2): p. 259-72.

232. Cardin, J.A., et al., *Driving fast-spiking cells induces gamma rhythm and controls sensory responses.* Nature, 2009. **459**(7247): p. 663-7.

233. Brecht, M. and B. Sakmann, *Dynamic representation of whisker deflection by synaptic potentials in spiny stellate and pyramidal cells in the barrels and septa of layer 4 rat somatosensory cortex.* J Physiol, 2002. **543**(Pt 1): p. 49-70.